BRAGG INTERACTIONS IN PERIODIC MEDIA

Thesis by

Dwight L. Jaggard

In Partial Fulfillment of the Requirements

For the Degree of

Doctor of Philosophy

California Institute of Technology

Pasadena, California

1977

(Submitted July 29, 1976)

To Vangie

ACKNOWLEDGEMENTS

Professor Charles Papas has provided fresh insights and constant encouragement during the course of this work at the California Institute of Technology (Caltech). Discussions and work with Dr. Charles Elachi of the Jet Propulsion Laboratory generated new ideas. Professor S. R. Seshadri of the University of Wisconsin-Madison provided hospitality, helpful criticism and stimulating discussions during a recent visit. Dr. Gary Evans of R & D Associates, Professor Cavour Yeh of the University of California-Los Angeles and Professor John Pierce of Caltech have been available for consultation. I thank these people and many others for their help.

A pleasant work environment and computing time were provided by the Jet Propulsion Laboratory through the Physics Section. The expert typing was performed by Mrs. Virginia Conner.

At various times I was supported by Caltech, the National Science Foundation and the Jet Propulsion Laboratory.

ABSTRACT

The interaction of electromagnetic waves of wavelength λ with periodic structures of spatial period Λ are studied. The emphasis of the work is on Bragg interactions where $\lambda \simeq 2\Lambda/N$ and the Bragg order N takes on the values $1, 2, \ldots$. An extended coupled waves (ECW) theory is developed for the case $N \geq 2$ and the results of the theory are found to compare favorably with the exact results of Floquet theory. Numerous numerical results are displayed as Brillouin diagrams for the first few Bragg orders. Moreover, explicit expressions for coupling coefficients, bandgap shifts and bandgap widths are derived for singly periodic media. Particular note is taken of phase speeding effects.

The effects of multiharmonic periodicities on the control of feedback strength are investigated. It is found that with proper phasing the feedback strength becomes zero and the bandgap disappears. Coupling parameters are calculated for typical multiharmonic periodicities for the first three Bragg orders.

For odd Bragg orders, inverted bandgaps and phase slowing occur when the gain or loss of the media is modulated. Also average gain or loss affects the bandgap shape and the spatial or temporal growth or decay. Absolute instabilities are observed and expressions are derived for the instability frequencies, thresholds and growth rates. Under certain conditions, instabilities occur for structures with average loss. The results for the first and second Bragg orders are archetypical of all odd and even orders respectively.

Applications of the ECW theory to higher-order DFB filters involve such phenomena as transient propagation, effects of periodicity profiles and the relative coupling due to boundaries and periodicities. The calculation of higher-order DFB laser parameters shows that the mode spectrum is asymmetrically shifted and the threshold gain is greatly dependent upon the periodicity profile. Approximate threshold parameters are calculated for high and low gain and for all Bragg orders. In addition, application of the ECW theory to holographic gratings and beam propagation is made.

TABLE OF CONTENTS

Table of Contents (Cont'd)

Table of Contents (Cont'd)

Table of Contents (Cont'd)

CHAPTER I

INTRODUCTION

This report investigates Bragg interactions in periodic media by using the example of electromagnetic waves propagating in spatially periodic dielectrics. The main purposes of this report are to develop physically meaningful approximate methods for higher-order Bragg interactions, to show the mathematical foundations of the coupled waves theory and to give physically meaningful explanations for several previously unexplained mathematical results. Exact and approximate theories are compared numerically and applications are made to both bounded and unbounded media, to lossless and lossy media and to both passive and active media. Examples are given which correspond both to wave-packets in space and time and to the steady-state response of plane waves.

The history of wave propagation in periodic media started with Mathieu's equation[1] in 1868 and subsequent generalizations by Floquet[2] and Hill[3] in the 1880's. Although Mathieu's equation had its origin in problems associated with elliptical boundaries, we will also show its connection to wave propagation in periodic media. This latter problem was first considered by Lord Rayleigh[4] in 1887. He considered the effect of periodic density variations upon the propagation of waves on a string. In the early 1900's a different, more physical, approach was taken by Sir William Bragg. He derived the necessary spatial period for constructive reflection of X-rays by crystals. These ideas were formalized for quantum mechanical applications by Bloch[44] in 1928. Two books in the 1940's, one by McLachlan[5] and the other by Brillouin,[6] summarized previous work with Mathieu functions and

with waves in periodic media. The books also provide useful bibliographies.

While most of the above work was concerned with exact solutions of differential equations, a second, independent approach was taken in the late 1940's and early 1950's. This approach stressed the physical concept of wave coupling by periodic perturbations. A mechanical device demonstrated this effect in 1949 by coupling torsional energy between two bicycle wheels which were periodically loaded with magnets.[7] In 1953 Pierce[9] used energy considerations to formulate what is now known as the coupled waves approach or the coupled mode theory. This approach has been popular because of its simplicity and intuitive appeal. Summaries of the coupled waves approach are given in texts by Pierce[10] and others.[14, 18, 26] Within the last twenty years the coupled waves approach has been successfully used in such diverse areas as hologram diffraction,[15, 22, 68, 69, 81, 82, 83, 84, 85] waveguide coupling,[12, 14, 16, 19, 20] traveling-wave tubes,[17, 74] parametric devices,[13, 14, 18, 56] X-ray diffraction,[21] distributed feedback (DFB) lasers,[14, 23, 24, 25, 30, 35, 36, 58, 70] and others.[10, 14, 22, 26, 27, 28, 29, 37] Extensive bibliographies on recent applications in optics and electromagnetics are given in the references.[12, 14, 20, 87] We note that the telegrapher's equations which were developed before the coupled waves theory are of the coupled waves form. These equations are not approximations, however, since they exactly describe one-dimensional transmission line problems.

The Floquet theory, which originated in the study of ordinary differential equations with periodic coefficients, has also been useful in the study of electromagnetic waves in periodic media. Although this theory is more cumbersome than the coupled waves approach, it provides an exact numerical solution. Extensions of the theory to include partial differential equations and finite length media have also been made.[44, 45] Applications of Floquet theory to electromagnetic waves have been made in the areas of traveling-wave antennas,[48] space-time periodic media,[11, 43, 56] integrated optics,[32, 58, 63, 64] corrugated structures,[8, 60] and others.[11, 22, 40, 57, 61, 62, 75]

Other exact methods that are used in plane-stratified material, such as the matrix method[78] or the method of invariant imbedding,[88, 89] will not be used here.

The second chapter of this report contains the derivation of the first Bragg order coupled waves equations and the Floquet solution for electromagnetic waves in longitudinally periodic media. A simple explanation for phase speeding is given and the connection between the Floquet and coupled waves theory is explained. The dispersion relation is found as well as all pertinent coupling parameters. Several Brillouin diagrams illustrate physical principles and compare the approximate and exact theories.

The primary purpose of the third chapter is to extend the coupled waves concept to higher Bragg orders. The resulting extended coupled waves (ECW) equations provide explicit dispersion and coupling information for every Bragg interaction. Numerical

examples again illustrate the results of both approximate and exact theories. A section is devoted to effects caused by perturbations of several frequencies and the resulting disappearance of bandgaps.

Periodic media with loss or gain is covered in chapter four. Inverting and non-inverting bandgaps are found which depend upon Bragg order and coupling type. Index and gain/loss coupling are both considered. The effect of the periodicity upon average gain or loss near Bragg resonance is noted.

The fifth chapter discusses the stability of active periodic media and gives explicit values for instability frequencies and thresholds at all Bragg orders. The stability criterion also specifies the correct root of the dispersion relation.

Several applications of the ECW theory are given in successive sections of chapter six. The reflection and transmission of transients are discussed and demonstrated with detailed numerical examples. The extension of previous work to higher order DFB lasers is briefly covered. Diffraction efficiencies can be found when the ECW theory is applied to holographic gratings. Finally, the case of beam propagation in longitudinally and transversely periodic media is outlined.

Conclusions of this report are given in chapter seven.

CHAPTER II

COUPLED WAVES AND FLOQUET THEORY

A. Bragg Reflections

In order to gain physical insight into the problem of waves in periodic media, we consider a plane wave incident upon a periodic structure as shown in Figure 2.1. It is apparent that the reflecting waves will constructively interfere if the reflections from successive layers differ by an integral number of wave lengths, $N\lambda$ ($N = 1, 2, 3, \ldots$). This result is usually stated as Bragg's Law,

$$N\lambda = 2\Lambda \sin\theta \qquad (N = 1, 2, \ldots) \qquad (2A.1)$$

where $\lambda = 2\pi/k$ = wavelength of plane wave

$\Lambda = 2\pi/K$ = spatial period of structure

N = Bragg order

and where the velocity is assumed to be that of free space. The cases $N \geq 2$ are referred to as higher-order Bragg interactions. For media with relative dielectric constant ϵ, we restate the result as

$$k\epsilon^{\frac{1}{2}}/K = N/2 \quad (N = 1, 2, \ldots) \qquad (2A.2)$$

for normally incident waves. Note that Bragg's Law does not account for the reflected wave amplitude, for the type of periodicity present or for the effect of slight variations of the wavenumber k from the value given by Bragg's Law.

The latter effect is called phase mismatch and can be considered in a semi-quantitative way by the use of Fig. 2.2. This figure shows an incident wave I which is reflected from a three layer

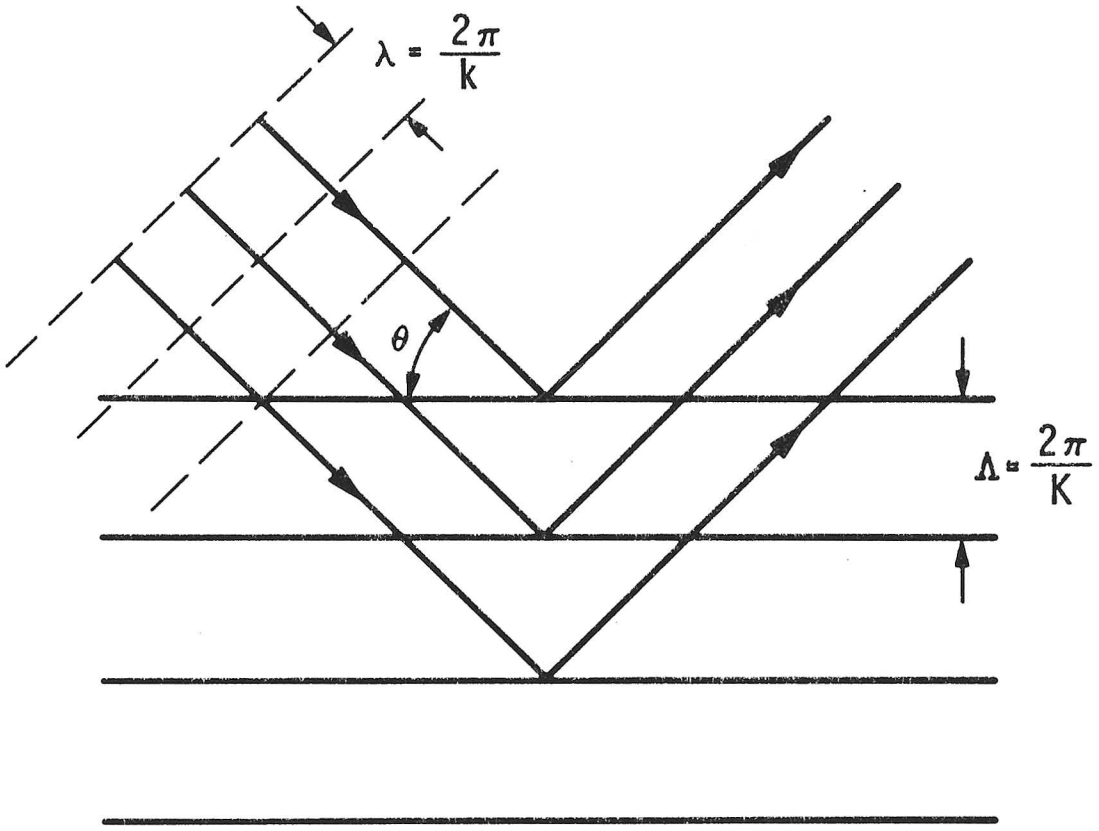

Fig. 2.1 Bragg scattering of plane wave from periodic media.

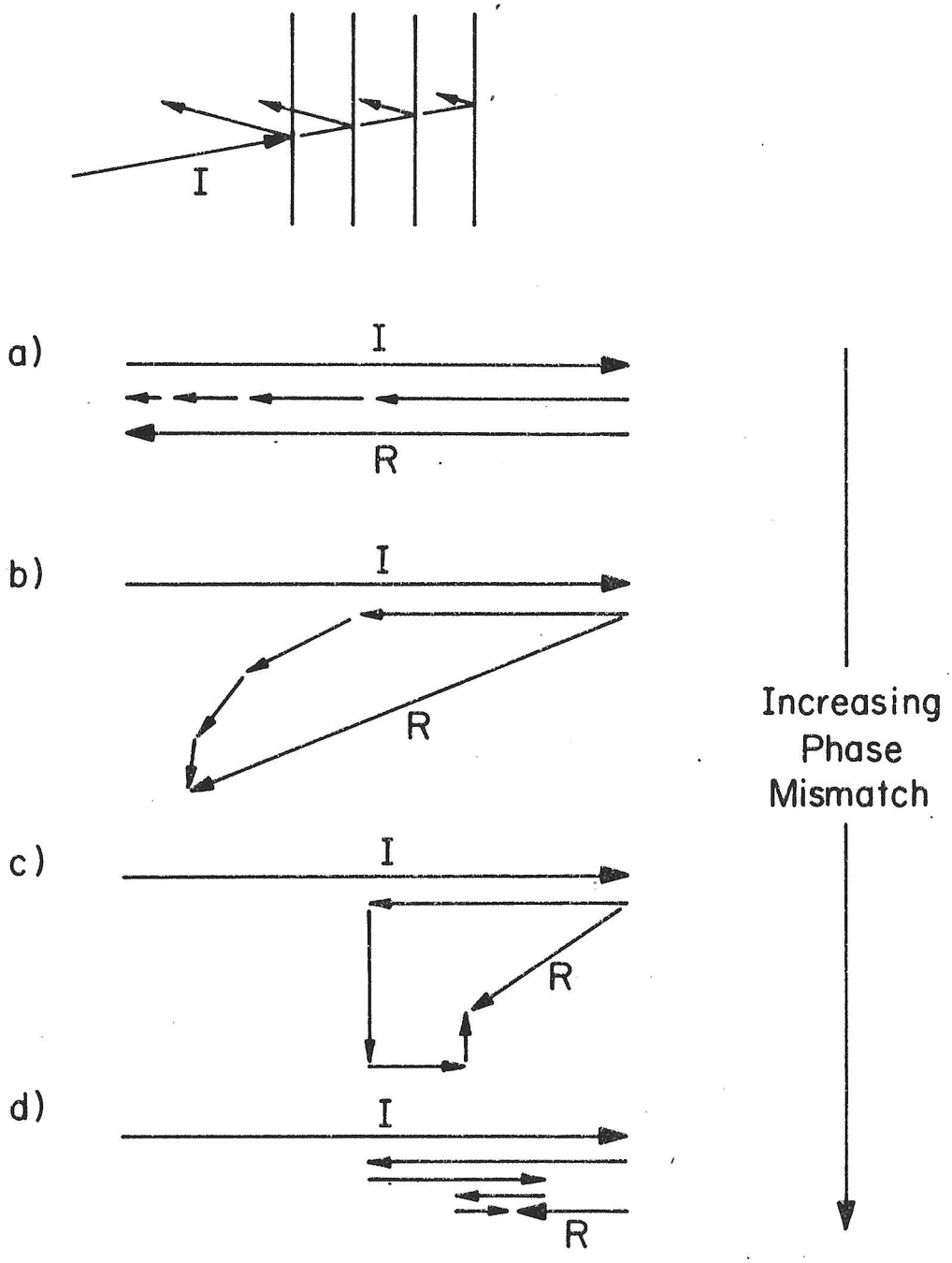

Fig. 2.2 The effect of phase mismatch upon the reflected wave. Zero phase mismatch a) indicates $k\epsilon^{\frac{1}{2}}/K = N/2$.

periodic medium to form a total reflected wave R. The wave R is a phasor sum of four sub-reflections each of which has phases relative to the first sub-reflection at the incident phase. Multiple reflections are ignored in this simple model. Parts a)-d) of Fig. 2.2 show the relation of the strength of the reflected wave R to the phase mismatch. Fig. 2.2a shows the constructive interference at the exact Bragg condition (i.e. zero phase mismatch) that produces large R. It is apparent that there is a considerable reflected wave R for slight phase mismatch (Fig. 2.2b) whereas large phase mismatch will produce small R (Fig. 2.2d).

Therefore, from simple wave interference arguments, one can deduce Bragg's Law and the qualitative effects of phase mismatch. Other theories are needed, however, to account for wave amplitudes and the effect of the form of the periodicity.

B. Coupled Waves Approach

1. TEM Waves in Passive Unbounded Media

Consider the case of a plane transverse electromagnetic (TEM) wave that propagates in a longitudinally periodic unbounded medium as shown in Fig. 2.3. Assume a time variation of the form $e^{-i\omega t}$. Starting with Maxwell's equations[67] in a source-free, linear, isotropic region, we find in the frequency domain that

$$\nabla \times \underline{E}(z, \omega) = i\omega \mu_o \underline{H}(z, \omega) \qquad (2.B1)$$

$$\nabla \times \underline{H}(z, \omega) = -i\omega \epsilon_o \epsilon(z) \underline{E}(z, \omega) \qquad (2.B2)$$

$$\nabla \cdot \underline{E}(z, \omega) = 0 \qquad (2.B3)$$

$$\nabla \cdot \underline{H}(z, \omega) = 0 \qquad (2.B4)$$

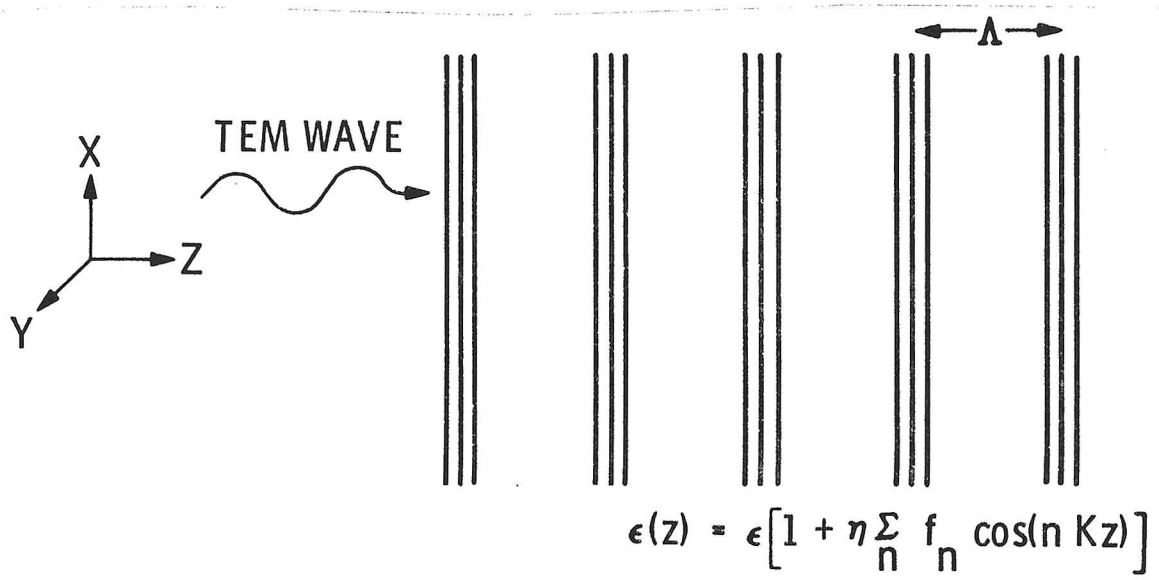

Fig. 2.3 TEM wave propagating in unbounded periodic media.

where ω = radian frequency

μ_o = free-space permeability

ϵ_o = free-space permittivity

$\epsilon(z)$ = relative permittivity or relative dielectric constant

and where $\underline{E}$ and $\underline{H}$ are the electric and magnetic field vectors. By combining (2. B1), (2. B2) and (2. B3) we find the wave equation for no transverse variation

$$\frac{d^2 E(z)}{dz^2} + k^2 \epsilon(z) E(z) = 0 \qquad (2.\text{B5})$$

where $E(z, \omega) = E(z)e^{-i\omega t}$ = transverse component of $E(z, \omega)$

$k = \omega/c = 2\pi/\lambda$ = free-space wave number

$\epsilon(z) = \epsilon\left[1 + \eta \sum_{p=0}^{\infty} f_p \cos(pKz)\right]$, $f_0 \equiv 0$, $f_1 \equiv 1$

$\eta \leq 1$ is the perturbation.

The periodic dielectric constant has been expanded in a Fourier cosine series. Assume that the electric field can be represented by just two waves,[10, 12, 15, 19] a forward wave $\tilde{F}(z)$ and a backward wave $\tilde{B}(z)$ which travel with positive and negative phase velocity along z. This assumption is intuitively appealing for $\eta << 1$ since these are the only two possible waves in the unperturbed case. Thus, we consider the transverse electric field

$$E(z) = \tilde{F}(z)\, e^{i\beta z} + \tilde{B}(z)\, e^{-i\beta z} \qquad (2.\text{B6})$$

where β is the longitudinal wavenumber. For first-order Bragg interactions, $\beta/K \simeq 1/2$. Then let

$$\beta \rightarrow \beta_o + \Delta\beta = K/2 + \Delta\beta \tag{2.B7}$$

$$F(z) = \tilde{F}(z)\, e^{i\Delta\beta z}, \quad B(z) = \tilde{B}(z) e^{-i\Delta\beta z} \tag{2.B8}$$

Use equations (2.B5) - (2.B8) and the slowly varying approximation $\left|\begin{matrix} F'' \\ B'' \end{matrix}\right| \ll \left|2\beta_o \begin{pmatrix} F' \\ B' \end{pmatrix}\right|$ and $\left|\begin{pmatrix} F'' \\ B'' \end{pmatrix}\right| \ll \left|\beta_o^2 \begin{pmatrix} F \\ B \end{pmatrix}\right|$, where primes denote differentiation with respect to z, to find

$$\begin{aligned}
&\left[-\beta_o^2 F + 2i\beta_o F' + k^2\epsilon F + \frac{k^2\epsilon\eta}{2} B\right] e^{i\beta_o z} \\
&\quad + \left[-\beta_o^2 B - 2i\beta_o B' + k^2\epsilon B + \frac{k^2\epsilon\eta}{2} F\right] e^{-i\beta_o z} \\
&\quad + \left[\frac{k^2\epsilon\eta}{2} F\right] e^{i3\beta_o} + \left[\frac{k^2\epsilon\eta}{2} B\right] e^{-i3\beta_o z} \\
&= -\frac{k^2\epsilon\eta}{2} \sum_{p=2}^{\infty} f_p \left[e^{i2p\beta_o z} + e^{-i2p\beta_o z}\right]\left[F e^{i\beta_o z} + B e^{-i\beta_o z}\right]
\end{aligned} \tag{2.B9}$$

where the arguments in z have been dropped. The coupled waves equations are found by equating the coefficients of $e^{\pm i\beta_o z}$ to zero.[15,19] The terms proportional to $e^{\pm ip\beta_o z}$ (p = 2, 3, . . .) are either ignored, termed non-synchronous or averaged over time and considered zero.[14] It will be shown later that these terms correspond to relatively unimportant coupling to other waves when $\beta/K \simeq 1/2$. The resulting coupled waves equations are,

$$F'(z) - i\,\delta\, F(z) = i\,\chi\, B(z) \tag{2.B10}$$

$$-B'(z) - i\,\delta\, B(z) = i\,\chi\, F(z) \tag{2.B11}$$

where

$$\delta = \frac{k^2\epsilon - \beta_o^2}{2\beta_o} = \text{phase mismatch} \tag{2.B12}$$

$$\chi = \frac{\eta}{4}\frac{k^2\epsilon}{\beta_o} = \text{coupling coefficient} \tag{2.B13}$$

These equations agree in form with those derived elsewhere.[10, 14, 15, 18, 20, 23, 30] The equations account for both the wave amplitudes and the phase mismatch as well as the interaction of the waves with the fundamental Fourier component of the dielectric periodicity. When $\delta = 0$, the waves F(z) and B(z) are coupled only through the perturbation η while the change in amplitude of one wave is proportional to the amplitude of the other wave. For zero perturbation, the wavenumber of F(z) and B(z) becomes equal to the phase mismatch.

2. Coupled Waves Dispersion Relation

By differentiating the coupled waves equations, a wave equation

$$\left[\frac{d^2}{dz^2} + (\delta^2 - \chi^2)\right]\begin{bmatrix} F(z) \\ B(z) \end{bmatrix} = 0 \qquad (2.B14)$$

is constructed. Assuming a solution of the form $e^{\pm i\Delta\beta z}$, the dispersion relation is found to be

$$\Delta\beta = \sqrt{\delta^2 - \chi^2} \qquad (2.B15)$$

The approximations for δ and χ are

$$\delta \simeq k\,\epsilon^{\frac{1}{2}} - \beta_o \equiv \Delta k\,\epsilon^{\frac{1}{2}} \qquad (2.B16)$$

$$\chi \simeq \chi\big|_{k=k_o} \equiv \eta\, K/8 \qquad (2.B17)$$

when $\Delta\beta \ll K$ and where $k_o\,\epsilon^{\frac{1}{2}}/K = \frac{1}{2}$ and $\beta_o = K/2$.
This produces the dispersion relation

$$\frac{\Delta\beta}{K} = \sqrt{\left(\frac{\Delta k\,\epsilon^{\frac{1}{2}}}{K}\right)^2 - \left(\frac{\eta}{8}\right)^2} \qquad (2.B18)$$

The following properties are evident for real ϵ and η.

1. Waves propagate without decay for $|\Delta k \epsilon^{\frac{1}{2}}/K| > |\eta/8|$ which correspond to passband regions.
2. Stopbands or bandgaps occur for imaginary $\Delta\beta/K$ or for $|\Delta k \epsilon^{\frac{1}{2}}/K| < |\eta/8|$. Here waves decay.
3. The coupling of waves is maximum at the bandgap center ($\Delta k\, \epsilon^{\frac{1}{2}}/K = 0$) where $\Delta\beta/K = i\eta/8$.

The dispersion relation (2. B18) is plotted as a Brillouin diagram in Fig. 2.4 which clearly shows the regions of interest, namely the stopbands (ellipse) and passbands (part of hyperbola).

Note that the coupled waves analysis gives much more information than Bragg's Law. However, the coupled waves approach is only valid around the first Bragg interaction and does not describe important wave interactions at higher Bragg orders.[41, 42] Furthermore, we have assumed a solution that is based on only two waves, F(z) and B(z). This is strictly valid only as $\eta \to 0$ when F(z) and B(z) are the two eigenmodes of the media.

C. Floquet Solution

1. TEM Waves in Passive Unbounded Media

An exact solution to the wave equation (2. B5) may be constructed through the application of Floquet's theorem. A form of this theorem is stated as follows: a linear differential equation with coefficients periodic in z with a period Λ has a solution E(z) with the property $E(z+\Lambda) = e^{i\beta\Lambda} E(z)$ where β is the fundamental wave number and Λ is the fundamental period; define $\phi(z)$ such that $E = e^{i\beta z}\, \phi(z)$; then $\phi(z)$ is periodic in z since $\phi(z+\Lambda) = \phi(z)$. A proof of the theorem

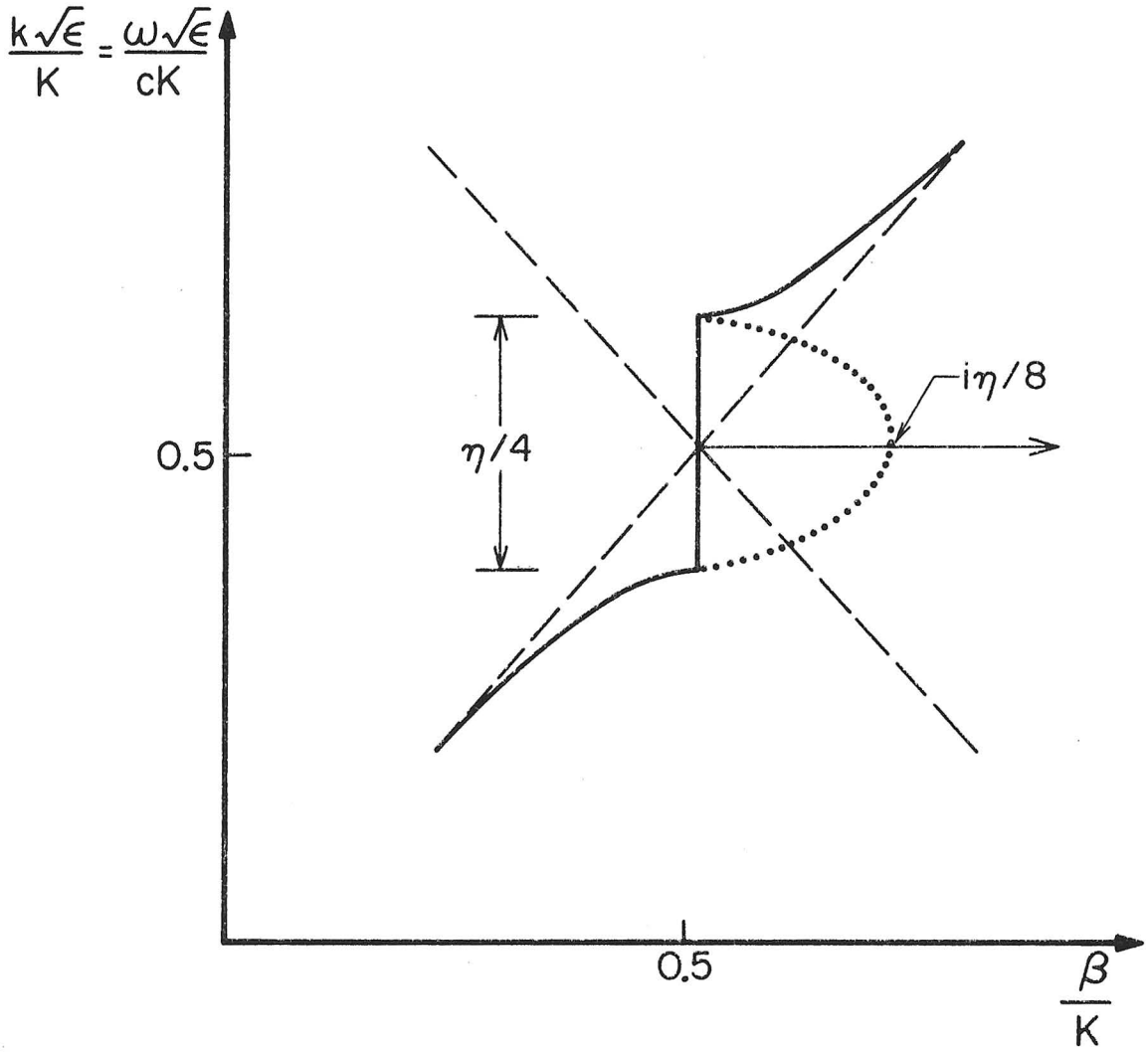

Fig. 2.4 Brillouin diagram near first Bragg interaction. Dotted line is imaginary part of β/K. Dashed lines are for unperturbed media where $\eta = 0$.

is given in several references.[2, 5, 46, 47]

We now expand the function $\phi(z)$, mentioned above, in a Fourier series.[3, 43-47] The resultant expansion for E(z) is

$$E(z) = \sum_{n=-\infty}^{\infty} a_n e^{i(\beta+nK)z} \tag{2. C1}$$

which is the constructed solution for the wave equation. This solution is made up of an infinite number of space harmonics, a_n, of order n, which propagate with longitudinal wave numbers $(\beta+nK)$ (see Fig. 2.6). Substitute the solution (2. C1) into the wave equation (2. B5) to find

$$\left\{[\epsilon k^2 - (\beta+nK)^2]\, a_n + \frac{k^2 \epsilon \eta}{2} \sum_{p=-\infty}^{\infty} f_p\, a_{n-p}\right\} e^{i(\beta+nK)z} = 0 \tag{2. C2}$$

$$(n = 0, \pm 1, \pm 2, \ldots)$$

where we have defined $f_p = f_{-p}$. Algebraic manipulations transform this result to

$$D_n a_n + \sum_{p=-\infty}^{\infty} a_{n-p} f_p = 0 \tag{2. C3}$$

where

$$D_n \equiv \frac{2}{\eta}\left[1 - \frac{(\beta+nK)^2}{k^2\epsilon}\right] \tag{2. C4}$$

In matrix form this can be rewritten as

$$\|D\| \cdot \underline{a} = 0 \tag{2. C5}$$

where

$$\underline{a} = \begin{pmatrix} \vdots \\ a_{-2} \\ a_{-1} \\ a_0 \\ a_1 \\ a_2 \\ \vdots \end{pmatrix} \tag{2. C6}$$

$$\|D\| = \begin{pmatrix} \ddots & \ddots & \ddots & \ddots & \ddots & \ddots \\ \ddots & D_{-2} & f_1 & f_2 & f_3 & f_4 & \ddots \\ \ddots & f_1 & D_{-1} & f_1 & f_2 & f_3 & \ddots \\ \ddots & f_2 & f_1 & D_0 & f_1 & f_2 & \ddots \\ \ddots & f_3 & f_2 & f_1 & D_1 & f_1 & \ddots \\ \ddots & f_4 & f_3 & f_2 & f_1 & D_2 & \ddots \\ \ddots & \ddots & \ddots & \ddots & \ddots & \ddots & \ddots \end{pmatrix} \tag{2.C7}$$

The non-triviality condition for the matrix equation requires

$$\det \|D\| = 0 \tag{2.C8}$$

which is the Floquet dispersion relation connecting β and k. For singly periodic media (i.e. $f_p = 0$ for $p \geq 2$) an expression for the space harmonic ratios and for the dispersion relation can be found in terms of a rapidly convergent continued fraction.[43]

2. Hill's Determinant

Hill[2,3,47] suggested an alternative form for the dispersion relation which is equivalent to (2.C8). The derivation for the case under consideration has been given in a previous report[42] with the following result.

$$\sin^2(\pi\beta/K) = \Delta(0) \sin^2(\pi k \varepsilon^{\frac{1}{2}}/K) \tag{2.C9}$$

where the elements of the Hill's determinant $\Delta(0) = \det \|\Delta\|$ are given by

$$\Delta_{pn} = \begin{cases} 1 & p = n \\ \dfrac{-k^2\epsilon}{p^2K^2 - k^2\epsilon} \dfrac{\eta f_{|n-p|}}{2} & p \neq n \end{cases} \qquad (2.C10)$$

Figure 2.5 shows the qualitative behavior of $\sin^2(\pi\beta/K)$ and the resulting bandgaps where β is complex.

Several authors[3-5] suggest an approximation for the infinite order determinant,

$$\Delta(0) \simeq 1 + \frac{\pi \cot(\pi k \epsilon^{\frac{1}{2}}/K)}{16\, k\, \epsilon^{\frac{1}{2}}/K} \left\{ \frac{[2k^2\epsilon\,\eta f_1/K^2]^2}{[1^2 - 4k^2\epsilon/K^2]} + \frac{[2k^2\epsilon\,\eta f_2/K^2]^2}{[2^2 - 4k^2\epsilon/K^2]} + \frac{[2k^2\epsilon\,\eta f_3/K^2]^2}{[3^2 - 4k^2\epsilon/K^2]} + \cdots \right\} \qquad (2.C11)$$

which is valid for $\eta f_p \ll 1$ $(p = 1, 2, 3, \ldots)$.

Note the following points about the dispersion relation (2.C8) and its approximation (2.C11).

1. This dispersion relation takes into account all Fourier components f_p of the perturbation and is valid for all k and β.
2. Away from the Bragg interaction regions $k\epsilon^{\frac{1}{2}}/K \simeq N/2$ $(N = 1, 2, \ldots)$, $\Delta(0) \simeq 1$ as $\eta \to 0$. Hence $k\,\epsilon^{\frac{1}{2}} \simeq \pm\beta$. Thus, the periodic medium has little effect upon wave propagation in the passbands as $\eta \to 0$. This was expected from Bragg's Law and the coupled waves approach.

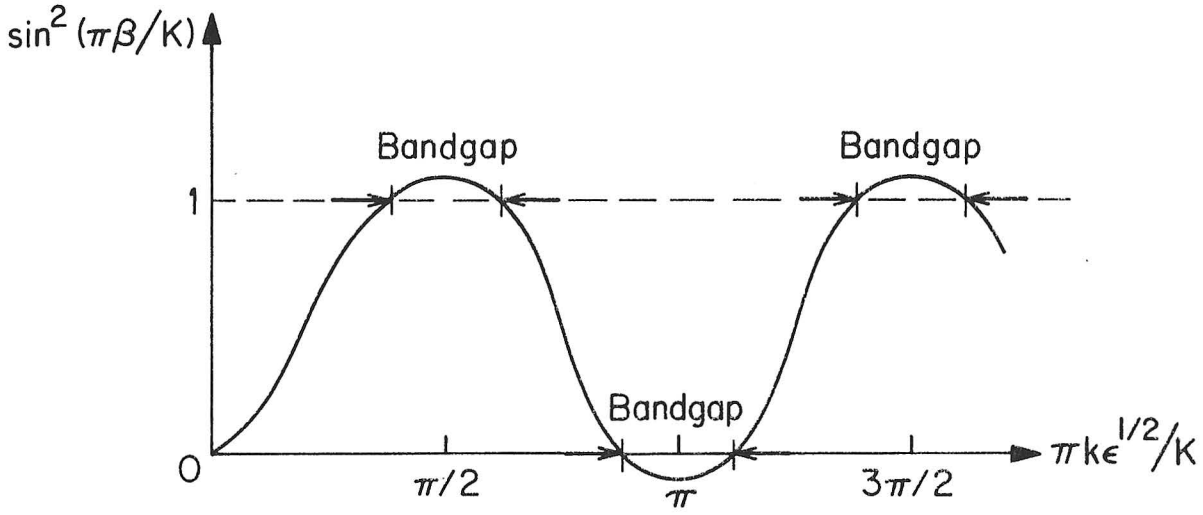

Fig. 2.5 A sketch of the behavior of the dispersion relation which shows the bandgap location for Bragg orders N = 1, 2, 3 whenever $\sin^2(\pi\beta/K) > 1$ or $\sin^2(\pi\beta/K) < 0$. It is assumed that f_1, f_2 and f_3 are significant in the perturbation.

3. When $\sin^2(\pi\beta/K) > 1$ or $\sin^2(\pi\beta/K) < 0$, β is complex. From (2.C9) and Figure 2.5, this occurs for $k\epsilon^{\frac{1}{2}}/K \simeq N/2$ ($N = 1, 2, 3, \ldots$). Hence, the dispersion relation agrees qualitatively with the position of the bandgaps predicted by both Bragg's Law and the coupled waves approach.

Note that the Floquet solution provides all of the information of the coupled waves equations with the additional advantage of being an exact solution that is valid for all β and k. However, the Floquet solution lacks the intuitive appeal and simplicity of the coupled waves approach. In particular, one has to use an approximation to find the approximate bandgap placement. In addition, a truncation of an infinite determinant must be performed.

D. Relation of Coupled Waves Solution and Floquet Solution

The recent interest[25, 51, 52] in the relation of the coupled waves solution and the Floquet solution is important for two reasons. First, it gives a more rigorous mathematical foundation for the coupled waves theory. Second, it can be used to expand the coupled waves approach to higher-order Bragg interactions.[53] This will be shown in Chapter III.

Consider equation (2.C3) for the case of cosinusoidal perturbations.

$$D_n a_n + a_{n+1} + a_{n-1} = 0 \qquad (2.D1)$$

$$D_n = \frac{2}{\eta}\left[1 - \frac{(\beta+nK)^2}{k^2\epsilon}\right] \quad (n = 0, \pm 1, \pm 2, \ldots) \qquad (2.D2)$$

For $\eta \ll 1$

$$k\,\epsilon^{\frac{1}{2}}/K \to \pm\,(\beta/K+n) \quad (n = 0,\ \pm1,\ \pm2,\ \ldots) \tag{2.D3}$$

The resulting Brillouin diagram is shown in Fig. 2.6 to consist of an infinite number of space harmonics $a_n^{\pm}$ which propagate as $e^{\pm i(\beta+nK)z}$.

From Bragg's Law, it is known that important interactions between F(z) and B(z) occur at $k\,\epsilon^{\frac{1}{2}}/K \simeq \beta/K \simeq \pm\frac{1}{2}$ where the $\pm$ sign comes from considering waves of both positive and negative phase velocities. Therefore, consider only the a_{-1}^{-}, a_o^{+}, a_o^{-} and a_{+1}^{+} space harmonics in the Floquet solution for the electric field

$$E(z) = a_{-1}^{-}\, e^{-i(\beta-K)z} + a_o^{+}\, e^{i\beta z} + a_o^{-}\, e^{-i\beta z} + a_{+1}^{+}\, e^{i(\beta+K)z} \tag{2.D4}$$

Let

$$\beta \to \beta_o + \Delta\beta = (\pm K/2 + \Delta\beta) \tag{2.D5}$$

where the $\pm$ sign holds for space harmonics that intersect each other at $\beta/K = \pm\frac{1}{2}$.

$$E(z) = \underbrace{(a_{-1}^{-}\, e^{-i\Delta\beta z} + a_o^{+}\, e^{i\Delta\beta z})}_{\triangleq F(z)} e^{i\beta_o z} + \underbrace{(a_o^{-}\, e^{-i\Delta\beta z} + a_{+1}^{+}\, e^{+i\Delta\beta z})}_{\triangleq B(z)} e^{-i\beta_o z} \tag{2.D6}$$

$$E(z) = F(z)e^{i\beta_o z} + B(z)e^{-i\beta_o z} \tag{2.D7}$$

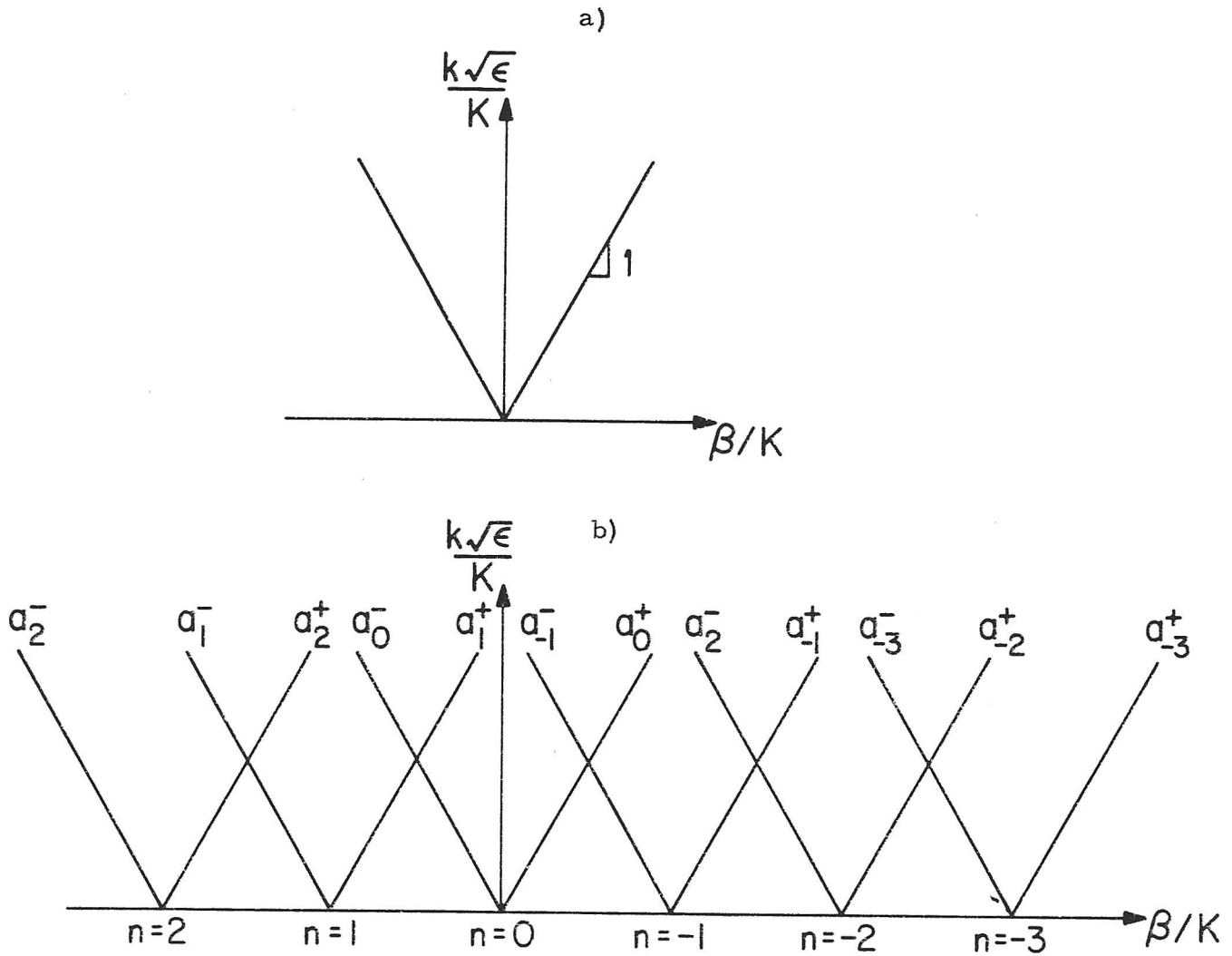

Fig. 2.6 a) Brillouin diagram for an unperturbed, homogeneous, infinite medium. b) Brillouin diagram for an infinite medium after introduction of a period perturbation. Part b) is derived from successive translation of a) along the β/K axis.

This is exactly equivalent to the assumed form of the electric field in the coupled waves approach. The waves F(z) and B(z) are each the sum of two space harmonics which are in agreement with previously derived results.[51] However, the terms $e^{\pm in\beta_o z}$ (n=3, 4, 5, ...) that were discarded in the coupled waves approach now have a clear meaning. These terms correspond to coupling to higher order space harmonics.[52] Explicitly, the terms $e^{\pm i3\beta_o z}$ correspond to space harmonics a^{+}_{+2} and a^{-}_{-2} which (along with a^{-}_{+1} and a^{+}_{-1}) couple to the adjacent Bragg intersections at $k\,\epsilon^{\frac{1}{2}}/K \simeq +\frac{1}{2}$, $\beta/K \simeq \pm\, 3/2$.

This truncated Floquet theory can also reproduce the coupled waves dispersion relation. Consider the first Bragg intersection at $\beta/K \simeq \frac{1}{2}$. Here only the a^{+}_{o} and a^{-}_{-1} space harmonics are important. If we truncate the relation $\underline{\underline{D}} \cdot \underline{a} = 0$ to include only these two space harmonics, we find the dispersion relation,

$$\det \begin{pmatrix} D_{-1} & 1 \\ 1 & D_0 \end{pmatrix} = 0 \qquad (2.D8)$$

where

$$D_{-1} = \frac{2}{\eta}\left[1 - \frac{(\beta_o+\Delta\beta - K)^2}{k^2\epsilon}\right] \simeq \frac{4}{\eta}\left[\frac{\Delta k\epsilon^{\frac{1}{2}}}{k_o\epsilon^{\frac{1}{2}}} + \frac{\Delta\beta}{\beta_o}\right]$$

$$D_0 = \frac{2}{\eta}\left[1 - \frac{(\beta_o+\Delta\beta)^2}{k^2\epsilon}\right] \simeq \frac{4}{\eta}\left[\frac{\Delta k\epsilon^{\frac{1}{2}}}{k_o\epsilon^{\frac{1}{2}}} - \frac{\Delta\beta}{\beta_o}\right]$$

$$k_o\epsilon^{\frac{1}{2}}/K = \tfrac{1}{2} = \beta_o/K$$

By evaluating the determinant we reproduce the results of the coupled waves theory, namely,

$$\frac{\Delta\beta}{K} = \sqrt{\left(\frac{\Delta k\epsilon^{\frac{1}{2}}}{K}\right)^2 - \left(\frac{\eta}{8}\right)^2} \qquad (2.D9)$$

Similar results are found at $\beta/K \simeq -\frac{1}{2}$ if we use the a_0^- and a_{+1}^+ space harmonics.

We note the following.

1. The coupled waves expressions for F(z) and B(z) are each the sum of two space harmonics.
2. The coupled waves approach can be viewed as a truncation of the Floquet solution. This shows that previously discarded terms correspond to coupling to higher-order space harmonics.
3. The coupled waves approach shows that wave coupling in periodic media can be viewed as coupling between the intersecting pairs of waves that make up F(z) and B(z).

E. Numerical Results

The dispersion relations are numerically compared by using the Hill's determinant and the coupled waves approach.

1. Limitations of Hill's Determinant

The Hill's determinant dispersion relation

$$\sin^2(\pi\beta/K) = \Delta(0)\sin^2(\pi k\epsilon^{\frac{1}{2}}/K) \qquad (2.E1)$$

is limited by the number of significant places used by the computer. In the case of the Univac 1108 this is 9 places for complex calculations. The smallest number that can be used which is larger than

unity is $1 + 10^{-8}$. Thus, if

$$\sin^2 (\pi\beta/K) \simeq 1 + 10^{-8} \qquad (2.E2)$$

at the first bragg order, then

$$\sin(\pi\beta_r/K)\cosh(\pi\beta_i/K) + i\cos(\pi\beta_r/K)\sinh(\pi\beta_i/K) \simeq 1 + 10^{-8} \qquad (2.E3)$$

where $\beta = \beta_r + \beta_i$.

For $\pi\beta_i/K \ll 1$ and $\pi\beta_r/K = \pi/2$, the above relation is approximated by

$$1 + (\pi\beta_i)^2/(2K^2) \simeq 1 + 10^{-8} \qquad (2.E4)$$

through trigonometric expansions. The maximum value of β_i/K is $\eta/8$ from equation (2.D9). Thus, the Floquet numerical calculations should be limited to $\eta > 10^{-4}$ at the first Bragg order. In this report, $\eta \geq 10^{-2}$ to account for this and any other computer errors. Similar arguments limit the numerical calculations at higher Bragg orders.

2. Brillouin Diagrams for Lossless Passive Media

Each Brillouin diagram is a plot of normalized frequency $[k\,\epsilon^{\frac{1}{2}}/K = \omega\,\epsilon^{\frac{1}{2}}/(cK)]$ versus normalized wavenumber $[\beta/K]$. In many of the cases the diagrams are expanded around the Bragg interaction region where Δk and $\Delta\beta$ replace k and β.

Figure 2.7 illustrates the main features of Floquet theory for a cosinusoidal perturbation (i.e. $f_p = 0$ for $p \neq 1$) with $\eta = 1$. The largest effect of the periodicity is in the vicinity of the Bragg wavenumbers $k\epsilon^{\frac{1}{2}}/K = N/2$

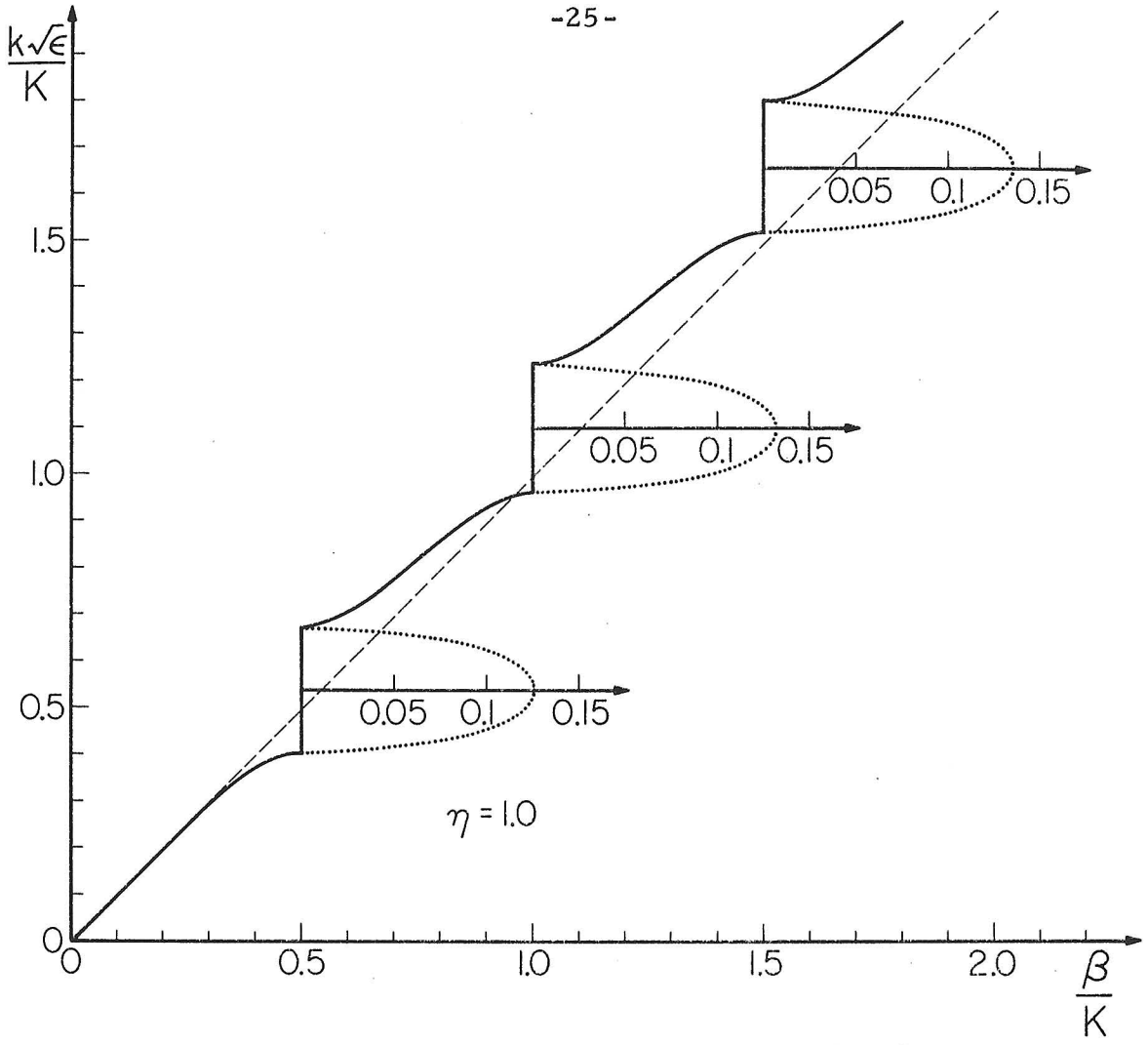

Fig. 2.7 Brillouin diagram for first three Bragg orders when $\eta = 1.0$ using Floquet theory. Dotted lines show imaginary parts of β/K on separate scales. Dashed line represents the unperturbed case. A cosinusoidal perturbation is assumed.

where the dispersion relation deviates from the unperturbed case (dashed line) and β becomes complex. Note that the bandgap is shifted towards the larger wavenumber and that this shift increases with Bragg order. This causes phase speeding[43] which is an increase in phase velocity ($= \omega/\beta$) due to an effective decrease in the dielectric constant. Physically, as the wave travels through the periodic medium, it speeds up and slows down with respect to the unperturbed velocity $c/\epsilon^{\frac{1}{2}}$. However, if we consider an average velocity $\langle v \rangle$ we find for singly periodic media

$$\langle v \rangle = \frac{1}{\Lambda} \int_0^{\Lambda} \frac{c}{\sqrt{\epsilon(1+\eta \cos Kz)}}\, dz \qquad (2.E5)$$

where $\Lambda = 2\pi/K$ = spatial period. For $\eta < 1$, expand the square root to find

$$\langle v \rangle = \frac{c}{\Lambda\, \epsilon^{\frac{1}{2}}} \int_0^{\Lambda} (1 - \frac{\eta}{2} \cos Kz + \frac{3}{8} \eta^2 \cos^2 Kz + \cdots) dz \qquad (2.E6)$$

$$\langle v \rangle = \frac{c}{\epsilon^{\frac{1}{2}}} [1+(3\pi/16)\eta^2 + O(\eta^4)] \qquad (2.E7)$$

Hence, the phase speeding is accounted for by effects $O(\eta^2)$ for $\eta < 1$.

Figure 2.8 is an expansion of the first-order Bragg interaction region of Figure 2.7. The coupled waves dispersion relation (2.B19) is superimposed. Even for $\eta = 1$, the coupled waves theory closely predicts the correct coupling coefficient as indicated by the maximum value of β in the bandgap. However, the coupled waves theory does not predict the bandgap shift or phase speeding for first-order Bragg interactions.

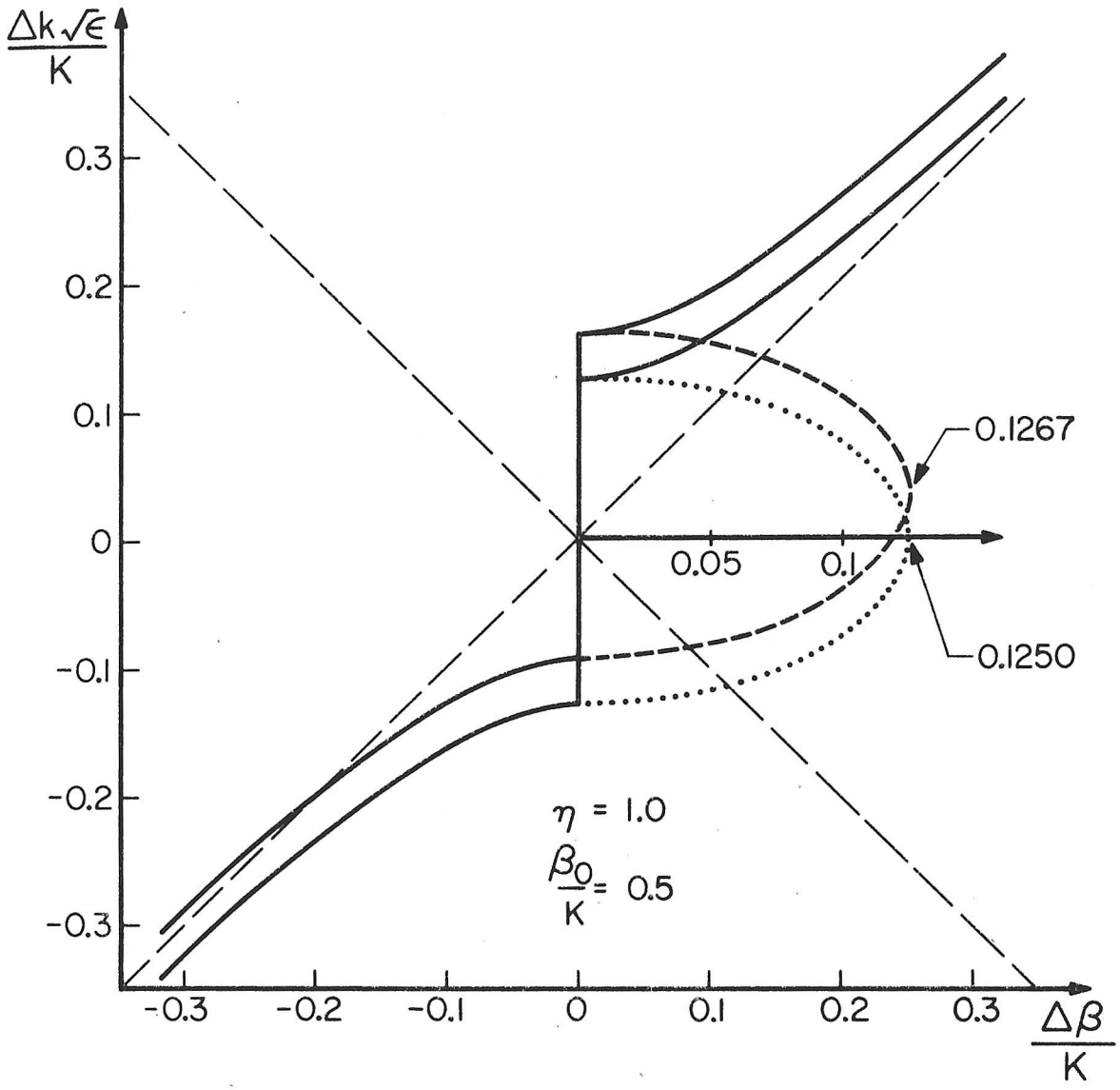

Fig. 2.8 Brillouin diagram of first Bragg interaction with $\eta = 1$. This compares Floquet theory (upper curve) with coupled waves theory (lower curve). Dotted and heavily dashed lines are imaginary parts of $\Delta\beta/K$.

The coupled waves result (lower curve of Figure 2.8) can be used for perturbations other than $\eta = 1$ by multiplying each scale by η.

Figure 2.9 shows similar results for $\eta = 1.0,\ 0.1,\ 0.01$ from the Floquet theory. As η decreases, the coupled waves theory becomes a better approximation to the Floquet theory. The curve for $\eta = 0.01$ is also the coupled waves curve for all three cases since the Floquet theory and the coupled waves theory are graphically indistinguishable.

Results of Figures 2.8-2.9 are summarized in Table 2.1.

	Coupled Waves			Floquet		
	η=1	η=0.1	η=0.01	η=1	η=0.1	η=0.01
Coupling χ/K	0.1250	0.01250	0.001250	0.1267	0.01250	0.001249
Bandgap Shift BGS	0.0	0.0	0.0	0.04	0.0005	<0.0001
Bandgap Width W	0.250	0.0250	0.00250	0.26	0.0255	0.00255

Table 2.1 Summary of coupled waves and Floquet theory at the first Bragg order.

The relative contributions of the different space harmonics are shown in Figure 2.10. The upper and lower curves are the result of matrix truncation at 3x3 and 5x5 elements respectively. Each truncated matrix is centered around the matrix element Δ_{oo} in equation (2.C10). The differences are not large and the 5x5 matrix produces dispersion characteristics that are $\leq 1\%$ different than those of the 19x19 matrices used in Figures 2.7-2.9.

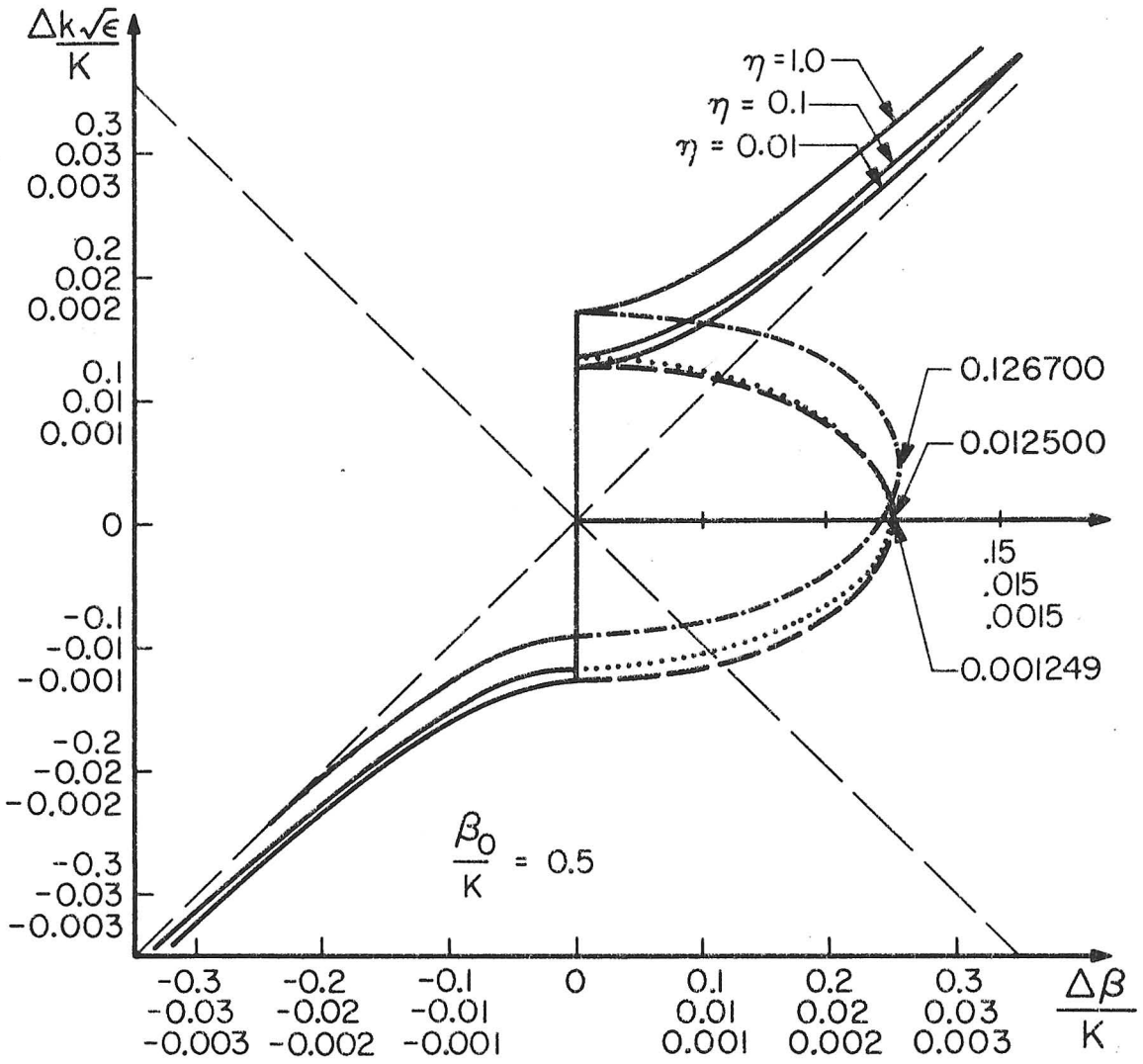

Fig. 2.9 Brillouin diagram at first Bragg order for $\eta = 1.0$ (top curve), $\eta = 0.1$ (middle curve), and $\eta = 0.01$ (bottom curve) using Floquet theory. Bottom curve also represents coupled waves solutions for all three cases. Note difference in scale for each case. Imaginary $\Delta\beta/K$ values are the elliptical curves with separate scale.

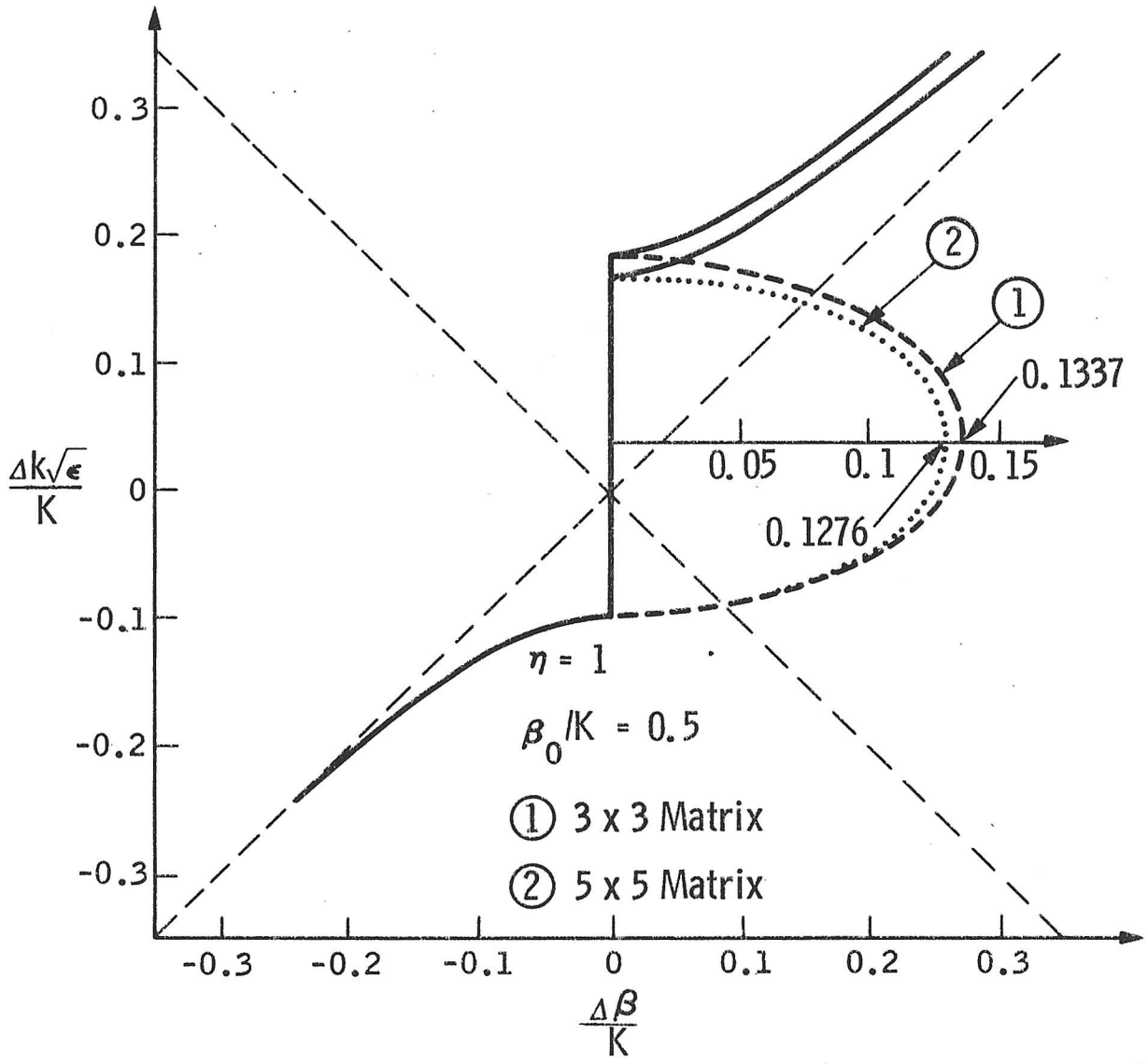

Fig. 2.10 The effect of limiting space harmonics in the Brillouin diagram using Floquet theory at the first Bragg interaction.

F. Modifications and Comments

1. Arbitrary Periodicities

The coupled waves equations were derived for $\epsilon(z) = \epsilon(1+\eta \sum_{p=0}^{\infty} f_p \cos(pKz))$ where only the f_1 term played a role inthe first Bragg order calculations. For generality, consider the expansion of a completely arbitrary (although smooth) $\epsilon(z)$ as

$$\epsilon(z) = \epsilon\left[1+\eta \sum_{p=0}^{\infty} [f_p \cos(pKz)+ g_p \sin(pKz)]\right] \tag{2.F1}$$

where $f_0 \equiv 0 \equiv g_0$

$$\eta f_1 \equiv \eta_1$$

$$\eta g_1 \equiv \eta_2$$

The analysis is similar to the previous calculations which lead to the coupled waves equations (2.B10-13). Following the identical procedure we find

$$F'(z) - i\,\delta\, F(z) = i\,\chi^{+}\, B(z) \tag{2.F2}$$

$$B'(z) - i\,\delta\, B(z) = i\,\chi^{-}\, F(z) \tag{2.F3}$$

where

$$\delta = \frac{k^2\epsilon - \beta_o^2}{2\,\beta_o} \tag{2.F4}$$

$$\chi^{\pm} = \frac{\eta_1 \pm i\eta_2}{4}\ \frac{k^2\epsilon}{\beta_o} \tag{2.F5}$$

The dispersion relation (2.D9) is modified by the substitutions

$$\eta \rightarrow (\eta_1^2 + \eta_2^2)^{\frac{1}{2}} \tag{2.F6}$$

$$\chi^2 \rightarrow \chi^{+}\,\chi^{-} \tag{2.F7}$$

All previous Brillouin diagrams can be used with the above substitutions for the periodicity given by (2. F1). The fact that $\chi^{-} = (\chi^{+})^{*}$, where the asterisk denotes complex conjugate, is a general result which holds for lossless systems.[18]

2. Corrugated Surfaces

The previous results are strictly valid only for volume perturbations. Similar results have been extended to surface perturbations or corrugations.[20, 24] The extension involves the assumption that the surface perturbation can be replaced by an equivalent volume perturbation. However, this assumption, known as the Rayleigh assumption, is valid only for $Kd < 0.448$ (where d = corrugation depth and K = periodicity wavenumber) as shown by Millar.[33] Physically this occurs because deep surface corrugations have proportionately less effect on the surface waves than do shallow corrugations. An exact Floquet analysis which solves the boundary-value problem has been given.[63, 64]

3. Comments

This chapter has set the groundwork for the next calculations. In addition the differences and similarities of the Floquet and coupled waves theory were discussed. In particular the coupled waves theory was seen to be an approximation of the exact theory, where certain space harmonics were retained and combined while others were discarded. A similar process will lead to descriptions at higher-order Bragg resonances in the succeeding chapters.

CHAPTER III

HIGHER-ORDER BRAGG INTERACTIONS

This chapter is an extension of the previous chapter to higher-order Bragg interactions (i.e. $N \geq 2$ in Bragg's Law). Present man-made dielectric periodicities other than superlattices are limited to the order of $\Lambda \sim 1000$ Å. Therefore, some applications in integrated optics require operation at higher-order Bragg interactions. Already higher order DFB lasers have been experimentally demonstrated.[40,70,71] Other optical applications include couplers and filters.

In section A, the coupled waves theory is extended to all Bragg orders for singly periodic media. Explicit expressions are given for all important parameters relating to the bandgap and coupling. Numerical examples are given in section B for the first three Bragg orders. Multiharmonic periodicities and a fourth-order numerical example are given in section C. An example of disappearing bandgaps is also shown. In some of the illustrative numerical examples, we will use large values of the perturbation that may not be physically realizable. However, the objective is to dramatize the effects of the perturbation on the Brillouin diagram. In addition, the extended coupled waves (ECW) examples are easily scaled for other values of η.

A. Extended Coupled Waves (ECW) Theory

1. TEM Waves in Passive Unbounded Media

By extending the assumptions made in Chapter II, we state the following assumptions for N^{th} order Bragg interactions:

1. The most significant space harmonics are $F_1(z) = a_o^+ e^{i\beta z} + a_{-N}^- e^{-i(\beta-NK)z}$ and $B_1(z) = a_o^- e^{-i\beta z} + a_{-N}^+ e^{i(\beta+NK)z}$.
2. To provide cross-coupling between $F_1(z)$ and $B_1(z)$ we account also for the following pairs of space harmonics (a_{-N+1}^-, a_{+1}^+), $(a_{-N+2}^-, a_{+2}^+), \ldots, (a_{-1}^-, a_{N-1}^+)$ which are slowly varying near $k\epsilon^{\frac{1}{2}}/K = N/2$. In this way we account for the intersecting space harmonics between $F_1(z)$ and $B_1(z)$ in the simplest possible manner.
3. Self-coupling which occurs between $F_1(z)$, $B_1(z)$ and their adjacent space harmonics must also be included.
4. Assume $\eta << 1$ although the theory may hold for $\eta \to 1$ as in the first order case.
5. All other space harmonics are ignored.

The derivation is started by including the above mentioned space harmonics of the Floquet theory in the expression for the electric field

$$E(z) = \sum_{n=-(N+1)}^{0} a_n^- e^{-i(\beta+nK)z} + \sum_{n=0}^{N+1} a_n^+ e^{i(\beta+nK)z} \qquad (3.A1)$$

Near the N^{th} order Bragg interaction let

$$\beta \to \beta_o + \Delta\beta = (\pm NK/2 + \Delta\beta) \qquad (3.A2)$$

where the $\pm$ sign is used for space harmonics that intersect each other when $\beta/K \gtrless 0$. The electric field becomes

$$E(z) = \sum_{n=-1}^{N^*/2} \left[a^-_{n-N} e^{-i\Delta\beta z} + a^+_{+n} e^{i\Delta\beta z} \right] \exp[i(1-2n/N)\beta_o z]$$

$$+ \sum_{n=-1}^{N^*/2} \left[a^+_{N-n} e^{i\Delta\beta z} + a^-_{-n} e^{-i\Delta\beta z} \right] \exp - [i(1-2n/N)\beta_o z] \qquad (3.A3)$$

$$+ \binom{1}{0} \left[a^-_{-N/2} e^{-i\Delta\beta z} + a^+_{N/2} e^{i\Delta\beta z} \right]$$

where

$$N^*/2 = \begin{cases} \frac{N-2}{2} & \text{for N even} \\ \frac{N-1}{2} & \text{for N odd} \\ -1 & \text{for N = 1} \end{cases}$$

$$\binom{1}{0} = \begin{cases} 1 & \text{for N even} \\ 0 & \text{for N odd} \end{cases}$$

This can be rewritten as

$$E(z) = \sum_{n=-1}^{N^*/2} \left\{ F_{1-2n/N}(z) \exp[i(1-2n/N)\beta_o z] \right.$$

$$\left. + B_{1-2n/N}(z) \exp[-i(1-2n/N)\beta_o z] \right\} + \binom{1}{0} S(z) \qquad (3.A4)$$

where

$$F_{1-2n/N}(z) = a^-_{n-N} e^{-i\Delta\beta z} + a^+_n e^{i\Delta\beta z}$$

$$B_{1-2n/N}(z) = a^+_{N-n} e^{i\Delta\beta z} + a^-_{-n} e^{-i\Delta\beta z}$$

$$S(z) = a^-_{-N/2} e^{-i\Delta\beta z} + a^+_{N/2} e^{i\Delta\beta z} = F_o(z) = B_o(z)$$

Substitute the assumed form of the solution (3.A4) into the wave equation (2.B5) and use the slowly varying approximation as before.

We drop the arguments in z for simplicity.

$$\left\{ -(1-2n/N)^2 \beta_o^2 F_{1-2/n/N} + 2i(1-2n/N)\beta_o F'_{1-2n/N} \right\} e^{i(1-2n/N)\beta_o z}$$

$$+ \left\{ -(1-2n/N)^2 \beta_o^2 B_{1-2n/N} - 2i(1-2n/N)\beta_o B'_{1-2n/N} \right\} e^{-i(1-2n/N)\beta_o z}$$

$$+ k^2\epsilon \left\{ F_{1-2n/N} e^{i(1-2n/N)\beta_o z} + B_{1-2n/N} e^{-i(1-2n/N)\beta_o z} + S \right\}$$

$$+ \frac{k^2\epsilon\eta}{2} \left\{ F_{1-2n/N} e^{i(1-2n/N)\beta_o z} + B_{1-2n/N} e^{-i(1-2n/N)\beta_o z} \right\}$$

$$\times \left\{ \sum_{p=1}^{\infty} f_p \left[e^{i2p\beta_o z/N} + e^{-i2p\beta_o z/N} \right] \right\} = 0 \qquad (3.A5)$$

$$(n = -1, 0, 1, 2, \ldots.)$$

which is analogous to (2.B9). Next, for simplicity we limit the Fourier coefficients of the periodicity such that $f_p = 0$ for $p \neq 1$ (i.e. singly periodic media). Equate the coefficients of $e^{\pm i(1-2n/N)\beta_o z}$ to zero for each n to get the following N+3 coupled equations.

$$\left.\begin{aligned}
\left[k^2\epsilon - (1+2/N)^2\beta_o^2\right] F_{1+2/N} + 2i(1+2/N)\beta_o F'_{1+2/N} &= \frac{-k^2\epsilon\eta}{2} F_1 \\
(k^2\epsilon - \beta_o^2) F_1 + 2i\beta_o F_1' &= \frac{-k^2\epsilon\eta}{2}(F_{1-2/N} + F_{1+2/N}) \\
\left[k^2\epsilon - (1-2/N)^2\beta_o^2\right] F_{1-2/N} + 2i(1-2/N)\beta_o F'_{1-2/N} &= \frac{-k^2\epsilon\eta}{2}(F_1 + F_{1-4/N}) \\
&\vdots \\
\binom{1}{0} k^2\epsilon S &= -\binom{1}{0}\frac{k^2\epsilon\eta}{2}(F_{2/N} + B_{2/N}) \\
&\vdots \\
\left[k^2\epsilon - (1-2/N)^2\beta_o^2\right] B_{1-2/N} - 2i(1-2/N)\beta_o B'_{1-2/N} &= \frac{-k^2\epsilon\eta}{2}(B_1 + B_{1-4/N}) \\
(k^2\epsilon - \beta_o^2) B_1 + 2i\beta_o B_1' &= \frac{-k^2\epsilon\eta}{2}(B_{1-2/N} + B_{1+2/N}) \\
\left[k^2\epsilon - (1+2/N)^2\beta_o^2\right] B_{1+2/N} - 2i(1+2/N)\beta_o B_{1+2/N} &= \frac{-k^2\epsilon\eta}{2} B_1
\end{aligned}\right\} \qquad (3.A6)$$

We define interaction as meaning the region in the $(k\epsilon^{\frac{1}{2}}, \beta)$ plane near the intersection of two space harmonics. We again note that higher-order interactions refer to interactions with frequency greater than that of the fundamental Bragg frequency defined by $k\epsilon^{\frac{1}{2}}/K = \frac{1}{2}$. Thus each wave, $F(z)_{1-2n/N}$ and $B(z)_{1-2n/N}$, defines an interaction. The coupling diagram, Figure 3.1, and the above set of coupled equations show that $F_1(z)$ and $B_1(z)$ are coupled through N intervening interactions. Since each coupling is proportional to η, the cross-coupling between $F_1(z)$ and $B_1(z)$ should be proportional to η^N. The adjacent interactions to $F_1(z)$ and $B_1(z)$ contribute terms of order η^2 to the phase mismatch and hence both the $F(z)_{1\pm2/N}$ and $B(z)_{1\pm2/N}$ terms need to be retained to obtain correct self-coupling. The $F(z)_{1+2/N}$ and $B(z)_{1+2/N}$ terms will not contribute to the cross-coupling except to order η^{N+2}. This small contribution is ignored.

To show the above statements mathematically, apply the slowly varying assumption and solve the inner N-1 and the outer two equations of (3.A6) to get all waves $F(z)_{1-2n/N}$, $S(z)$, $B(z)_{1-2n/N}$ ($n = -1, +1, 2, 3, \ldots$) in terms of $F_1(z)$ and $B_1(z)$. The outer two equations can be solved trivially for $F(z)_{1+2/N}$ and $B(z)_{1+2/N}$.

We begin by using matrix manipulations on the inner N-1 equations of (3.A6)

$$\left.\begin{aligned} F_{1-2/N} &= \det\|A\|/\det\|C\| \\ B_{1-2/N} &= \det\|G\|/\det\|C\| \end{aligned}\right\} \qquad (3.A7)$$

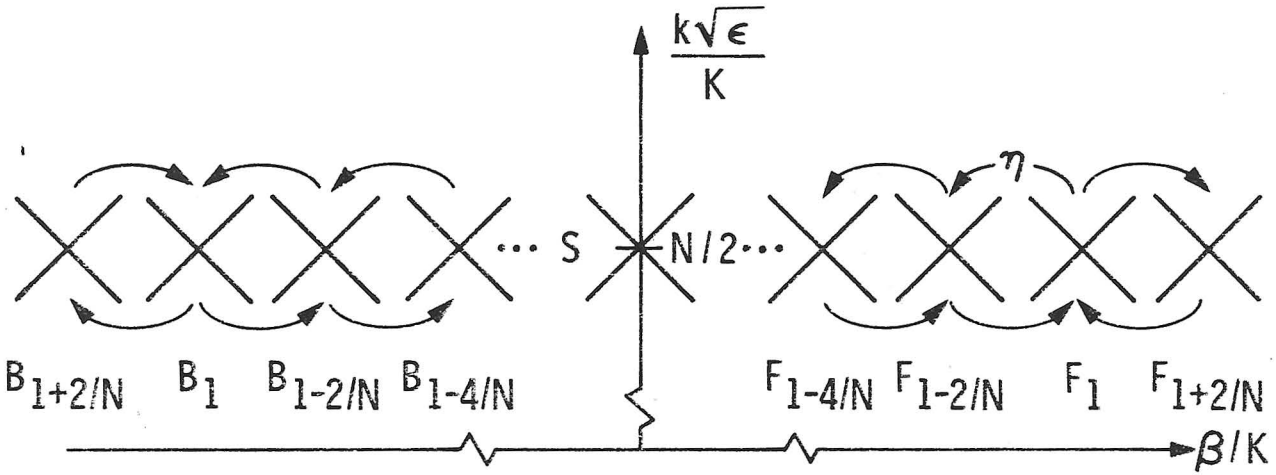

Fig. 3.1 Coupling diagram at N^{th} order Bragg interaction. Dominant cross-coupling between F_1 and B_1 is shown as well as self-coupling for ECW theory.

where

$$\|C\| = \begin{pmatrix} C_1 & C & & & \\ C & C_2 & C & & 0 \\ & \ddots & \ddots & \ddots & \\ & & C & C_2 & C \\ 0 & & & C & C_1 \end{pmatrix} \tag{3.A8}$$

$$\|A\| = \begin{pmatrix} A_1 & C & & & \\ C & C_2 & C & & 0 \\ & \ddots & \ddots & \ddots & \\ & & C & C_2 & C \\ 0 & & & C & C_1 \end{pmatrix} \tag{3.A9}$$

$$\|G\| = \begin{pmatrix} G_1 & C & & & \\ C & C_2 & C & & 0 \\ & \ddots & \ddots & \ddots & \\ & & C & C_2 & C \\ 0 & & & C & C_1 \end{pmatrix} \tag{3.A10}$$

$$C_n = k^2 \epsilon - (1-2n/N)^2 \beta_o^2 \qquad G_2 = A_1 = -k^2 \epsilon \eta F_1^2$$

$$C = \eta k^2 \epsilon / 2 \qquad G_1 = A_2 = -k^2 \epsilon \eta B_1^2$$

Instead of solving (3.A7) exactly, we approximate the determinants for $\eta \ll 1$ when $N \geq 2$. Since $C \ll C_n$, we find

$$\det \|C\| \simeq \prod^{*} f^2(n) \equiv \prod^{*} [k^2 \epsilon - (1-2n/N)^2 \beta_o^2]^2 \tag{3.A11}$$

$$\text{where} \quad \prod\!\!\!\prod^{*} f^2(n) = \begin{cases} \prod_{n=1}^{(N-1)/2} f^2(n) & \text{for N odd} \\ \prod_{n=1}^{N/2} f(n) & \text{for N even} \\ 1 & \text{for N = 1} \end{cases}$$

Approximate $\det\|A\|$ and $\det\|G\|$ in a similar manner.

$$\det\|A\| \simeq \frac{A_1}{C_1} \prod\!\!\!\prod^{*} f^2(n) + (-1)^N A_2 C^{N-2} \tag{3.A12}$$

$$\det\|G\| \simeq \frac{G_1}{C_1} \prod\!\!\!\prod^{*} f^2(n) + (-1)^N G_2 C^{N-2} \tag{3.A13}$$

The solution for $F(z)_{1-2/N}$ becomes

$$F(z)_{1-2/N} = \frac{A_1}{C_1} + \frac{(-1)^N A_2 C^{N-2}}{\prod\!\!\!\prod^{*} f^2(n)} \tag{3.A14}$$

Near the N^{th} Bragg interaction we approximate the free-space wavenumber by

$$k^2\epsilon \rightarrow k_o^2 \epsilon = \beta_o^2 = (NK/2)^2 .$$

The expression for $F(z)_{1-2/N}$ can be approximated by

$$F(z)_{1-2/N} = \frac{-(\eta/2) F_1(z)}{1 - (1-2/N)^2} + \frac{(-k^2\epsilon\,\eta/2^{N-1} B_1(z)}{\prod\!\!\!\prod^{*} f^2(n)} \tag{2.A15}$$

Extend the above formulation to include the N=1 case by introducing the symbol ζ_N.

$$F(z)_{1-2/N} = \frac{-\zeta_N \eta N F_1(z)}{B(1-1/N)} + \frac{(-1)^{N+1}(\eta/2)^{N-1} B_1(z)}{\prod^{*}\{4n(n-N)/N^2\}^2} \qquad (3.A16)$$

where $\zeta_N = \begin{cases} 0 & N = 1 \\ 1 & N \geq 2 \end{cases}$

Similarly for $B(z)_{1-2/N}$ we find the analogous result,

$$B(z)_{1-2/N} = \frac{-\zeta_N \eta N B_1(z)}{8(1-1/N)} + \frac{(-1)^{N+1}(\eta/2)^{N-1} F_1(z)}{\prod^{*}\{4n(n-N)/N^2\}^2} \qquad (3.A17)$$

The expressions for $F(z)_{1+2/N}$ and $B(z)_{1+2/N}$ are trivially found from (3.A6) under the stated approximations as

$$F(z)_{1+2/N} = \frac{-\zeta_N(\eta/2)F_1(z)}{1-(1+2/N)^2} = \frac{\zeta_N \eta N F_1(z)}{8(1+1/N)} \qquad (3.A18)$$

$$B(z)_{1+2/N} = \frac{-\zeta_N(\eta/2)B_1(z)}{1-(1+2/N)^2} = \frac{\zeta_N \eta N B_1(z)}{8(1+1/N)} \qquad (3.A19)$$

Expressions (3.A16-3.A19) are substituted into the following two equations from (3.A6) for $F_1(z)$ and $B_1(z)$

$$(k^2\epsilon - \beta_o^2)F_1(z) + 2i\beta_o F_1'(z) = \frac{-k^2\epsilon\eta}{2}(F(z)_{1-2/N} + F(z)_{1+2/N}) \qquad (3.A20)$$

$$(k^2\epsilon - \beta_o^2)B_1(z) + 2i\beta_o B_1'(z) = \frac{-k^2\epsilon\eta}{2}(B(z)_{1-2/N} + B(z)_{1+2/N}) \qquad (3.A21)$$

Upon rearrangement the following extended coupled wave (ECW) equations are formed.

$$F_1'(z) - i\,\delta_N F_1(z) = i\chi_N B_1(z) \qquad (3.A22)$$

$$-B_1'(z) - i\,\delta_N B_1(z) = i\chi_N F_1(z) \qquad (3.A23)$$

$$\text{where } \delta_N = \frac{k^2 \varepsilon \left\{1 - \zeta_N (\eta/2)^2 \left[\frac{N^2}{2(N^2-1)}\right]\right\} - \beta_o^2}{2\beta_o} \qquad (3.A24)$$

$$= \text{phase mismatch}$$

$$\chi_N = \frac{(-1)^{(N+1)} k^2 \varepsilon \eta^N}{2^{N+1} \beta_o} \frac{1}{\prod^* \{4n(n-N)/N^2\}^2} \qquad (3.A25)$$

$$= \text{coupling coefficient}$$

$$N = \text{Bragg order}$$

$$\beta_o = nK/2$$

The ECW equations agree in form with other work in diffraction or holographic gratings[22, 68, 69] where the periodicity is perpendicular to the propagation direction. However, this is the first time that analytic expressions have been derived for propagation in longitudinally varying media where the coupling, bandgap shift and bandgap width are given explicitly for all Bragg orders.

Table 3.1 presents numerical factors found in the ECW equations for the first five Bragg orders.

N	$\prod^* \{4n(n-N)/N^2\}^2$	$g(N) = (4/N)(1-1/N)$	$1-\zeta_N(\eta/2)^2\{N^2/[2(N^2-1)]\}$
1	1	0	1
2	1	1	$1 - \frac{2}{3}(\eta/2)^2$
3	$(8/9)^2$	8/9	$1 - \frac{9}{16}(\eta/2)^2$
4	$(3/4)^2$	3/4	$1 - \frac{8}{15}(\eta/2)^2$
5	$(16/25)^2$	16/25	$1 - \frac{25}{48}(\eta/2)^2$

Table 3.1 Numerical values for factors in ECW equations.

2. ECW Dispersion Relations

The dispersion relation is derived from the ECW equations as in the first order case.

$$\frac{\Delta\beta_N}{K} = \sqrt{\left(\frac{\delta_N}{K}\right)^2 - \left(\frac{\chi_N}{K}\right)^2} \tag{3.A26}$$

The following approximations may be made in the interaction region when $\Delta\beta_N << K$.

$$\delta_N \simeq \Delta k_N \epsilon^{\frac{1}{2}} - \zeta_N \frac{k^2 \epsilon \eta^2 N^2}{16 \beta_o (N^2-1)} \tag{3.A27}$$

$$\chi_N \simeq \frac{(-1)^{N+1} k_o \epsilon^{\frac{1}{2}} \eta^N}{2^{N+1} \prod^* \{4n(n-N)/N^2\}^2} \tag{3.A28}$$

where

$$\Delta k_N = k - \beta_o/\epsilon^{\frac{1}{2}}$$

$$\Delta\beta_N = \beta - \beta_o$$

$$\beta_o = NK/2$$

The N^{th} order dispersion relation is explicitly

$$\frac{\Delta\beta_N}{K} = \sqrt{\left(\frac{\Delta k_N \epsilon^{\frac{1}{2}}}{K}\right)^2 - \zeta_N \frac{\Delta k_N \epsilon^{\frac{1}{2}}}{K} \frac{\eta^2 N^3}{16(N^2-1)} + \frac{\zeta_N \eta^4 N^6}{1024(N^2-1)^2} - \frac{\eta^{2N}}{4^{N+2}} \left(\frac{N}{\prod^* \{3n(n-N)/N^2\}^2}\right)^2} \tag{3.A29}$$

Note that for real ϵ and η, the maximum imaginary part of $\Delta\beta_N/K$ occurs when $\delta_N/K = 0$. This defines the normalized coupling in terms of the bandgap behavior since,

$$\left| \mathrm{Im}\left\{ \frac{\Delta\beta_N}{K} \right\}_{\max} \right| = \left| \frac{\chi_N}{K} \right| = \left| \frac{\eta^N}{2^{N+2}} \frac{N}{\prod^* \{4n(n-N)/N^2\}^2} \right| \qquad (3.A30)$$

If $\delta_N/K = 0$, then maximum coupling takes place at a wavenumber that is displaced from the exact Bragg condition $k\epsilon^{\frac{1}{2}}/K = N/2$ for $N \geq 2$. This is referred to as bandgap shift (BGS_N) and is defined by

$$BGS_N = \left. \frac{\Delta k_N \epsilon^{\frac{1}{2}}}{K} \right|_{\delta_N = 0} = \frac{\zeta_N \eta^2 N^3}{32(N^2-1)} \qquad (3.A31)$$

We note that this raises the Brillouin diagram and produces phase speeding $O(\eta^2)$ as expected. The bandgap occurs whenever $|\delta_N/K| < |\chi_N/K|$ which causes $\Delta\beta_N/K$ to become imaginary. The bandgap width (W_N) is defined by

$$W_N = 2\left| \frac{\chi_N}{K} \right| = \frac{\eta^N}{2^{N+1}} \frac{N}{\prod^* \{4n(n-N)/N^2\}^2} \qquad (3.A32)$$

Table 3.2 summarizes some of the ECW results for the first five Bragg orders.

N	Coupling χ_N/K	Bandgap shift BGS_N	Bandgap width W_N
1	$\frac{\eta}{8}$	0	$\frac{\eta}{4}$
2	$-\frac{\eta^2}{8}$	$\frac{\eta^2}{12}$	$\frac{\eta^2}{4}$
3	$\frac{243\,\eta^3}{2048}$	$\frac{27\,\eta^2}{256}$	$\frac{243\,\eta^3}{1024}$
4	$-\frac{\eta^4}{9}$	$\frac{2\,\eta^2}{15}$	$\frac{2\,\eta^4}{9}$
5	$\frac{1953125\,\eta^5}{18874368}$	$\frac{125\,\eta^2}{768}$	$\frac{1953125\,\eta^5}{9437184}$

Table 3.2 Summary of the main features of the ECW theory for the first five Bragg orders.

We note the following points about the ECW theory:

1. The ECW derivation is an intuitively based theory that gives explicit values for χ_N/K, δ_N/K, BGS_N and W_N for any Bragg order.
2. The ECW theory predicts coupling coefficients that are proportional to $(\eta/2)^N$ due to cross-coupling. This is expected because of the N interactions between $F_1(z)$ and $B_1(z)$ where each interaction couples with strength $\eta/2$ to adjacent interactions. The sign of the coupling coefficient alternates with Bragg order.
3. The ECW theory predicts that maximum coupling occurs not at exact Bragg resonance but at a shifted frequency instead. This shift is proportional to $N\eta^2$ for $N \geq 2$ and is due to the self-coupling of $F_1(z)$ and $B_1(z)$. This bandgap shift accounts for the phase speeding effect that was first found in the Floquet results.
4. The bandgap width is proportional to $(\eta/2)^N$. Hence for large N, only a small range of frequencies will cause significant coupling between $F_1(z)$ and $B_1(z)$. Also note that for large N, $W_N < 2\ BGS_N$ so that the longitudinal wavenumber β may be real at exact Bragg resonance. Since bandgap width and coupling are proportional, it is impossible to attain large coupling and small bandgaps simultaneously.

5. A simple scaling rule exists such that if η and $\Delta k_N \epsilon^{\frac{1}{2}}/K$ are reduced by the same factor, then $\Delta\beta_N/K$ will be reduced by the identical factor. Thus ECW results for large perturbation can be directly applied to other perturbations.

The extension to sinusoidal perturbations is made in the same manner as in the first order theory. Let $\chi_N(\eta^2) \rightarrow \chi_N(\eta_1^2+\eta_2^2)$ for periodicities of the type $\eta_1 \cos(NKz) + \eta_2 \sin(NKz)$.

The relative magnitude of the waves $F(z)_{1-2n/N}$, $S(z)$, $B(z)_{1-2n/N}$ $(n = 2, 3, \ldots N^*/2)$ can be found from equation (3.A6) in the same manner that $F(z)_{1-2/N}$ and $B(z)_{1-2/N}$ were found. The results are in terms of $F_1(z)$ and $B_1(z)$ which are in turn related by the boundary conditions. We will not need these results now.

B. Numerical Examples

1. Second-Order Interaction

The ECW approach uses the ten space harmonics shown in Fig. 3.2 for N = 2. The explicit dispersion relation is

$$\frac{\Delta\beta_2}{K} = \sqrt{\left(\frac{\Delta k_2\, \epsilon^{\frac{1}{2}}}{K}\right)^2 - \left(\frac{\Delta k_2\, \epsilon^{\frac{1}{2}}}{K}\right)\frac{\eta^2}{6} - \frac{5}{576}\eta^4} \qquad (3.B1)$$

and the phase mismatch and coupling are

$$\delta_2 = \frac{k^2\epsilon\,(1-\eta^2/6) - \beta_o^2}{2\,\beta_o} \qquad (3.B2)$$

$$\chi_2 = -\frac{k^2\,\epsilon\eta^2}{8\,\beta_o} \qquad (3.B3)$$

where $\beta_o = K$

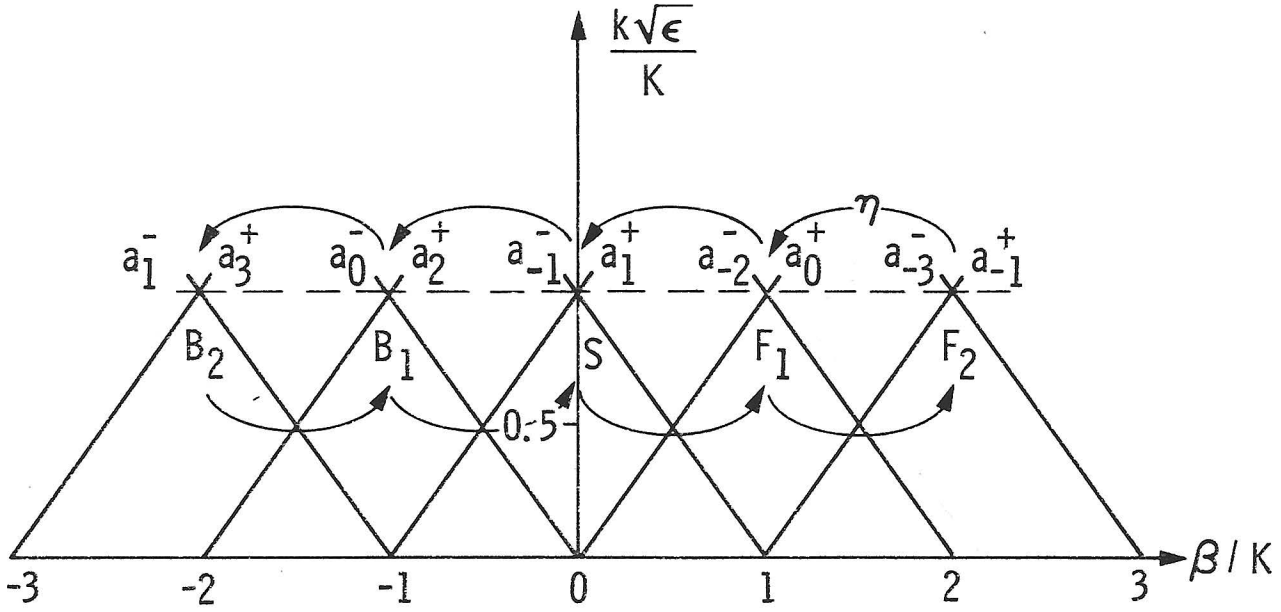

Fig. 3.2 Coupling diagram which shows the ten relevant space harmonics that are used in the ECW theory for second-order interactions.

Note the change in sign of the coupling coefficient from that of the first-order theory. The coupling is provided by S(z) and the bandgap shift is accounted for by $B_2(z)$, S(z) and $F_2(a)$. Phase speeding is the result of the bandgap shift.

Figure 3.3a,b,c shows a comparison of the Floquet and ECW theories at the second Bragg order for $\eta = 1.0$, 0.1 and 0.05 respectively. Although one would not expect the ECW theory to hold as $\eta \to 1$, Figure 3.4 demonstrates the validity of the theory in this case. We note that for $\eta = 1$, the Floquet theory predicts a slightly larger bandgap than does the ECW theory. However, in the practical case of $\eta \leq 0.1$, the two theories become graphically indistinguishable. Table 3.3 summarizes these results for second order Bragg interactions.

	ECW			Floquet		
	$\eta = 1.0$	$\eta = 0.0$	$\eta = 0.05$	$\eta=1$	$\eta=0.1$	$\eta= 0.05$
Coupling χ_2/K	.125	.00125	.0003125	.133	.00125	.000311
Bandgap Shift BGS_2	.0833	.000833	.000208	.10	.00080	.00022
Bandgap Width W_2	.250	.00250	.00625	.26	.0025	.00063

Table 3.3 Summary of ECW and Floquet dispersion relations at the second Bragg order interaction.

Figures 3.4 and 3.5 show the effect of truncating the ECW and Floquet theories. In Figure 3.4, the outermost space harmonics $\left((a_1^-, a_3^+) \text{ and } (a_{-3}^-, a_{-1}^+) \text{ of Figure 3.2}\right)$ are not used for $\eta = 0.1$. In this case the coupling between F_1 and B_1 is given correctly since the

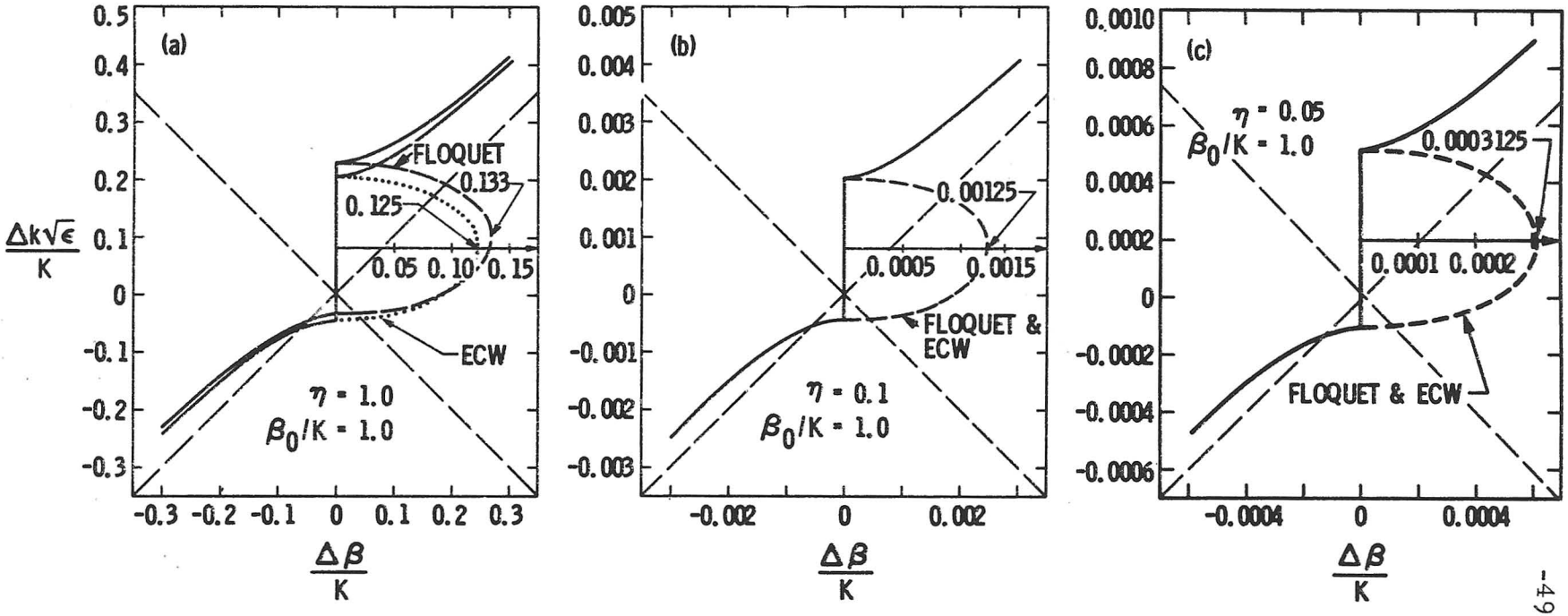

Fig. 3.3 Brillouin diagram at second Bragg order for a) $\eta = 1.0$, b) $\eta = 0.1$, and c) $\eta = 0.05$ showing Floquet and ECW results. Imaginary $\Delta\beta/K$ values are the elliptical curves with separate scale. Note the close agreement of theories for $\eta \leq 0.1$.

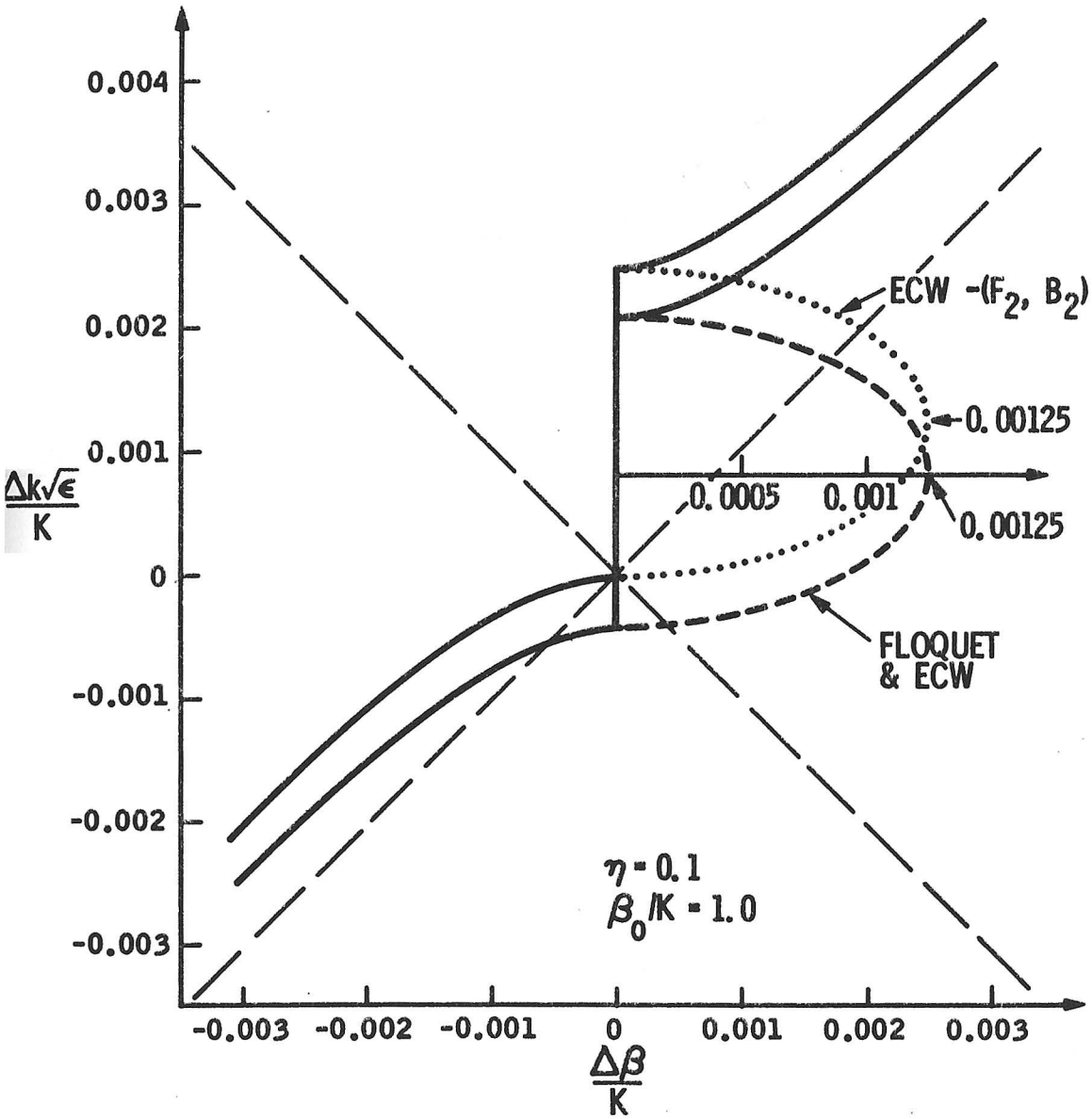

Fig. 3.4 The results of neglecting the effects of F_2 and B_2 in the ECW theory at the second Bragg interaction.

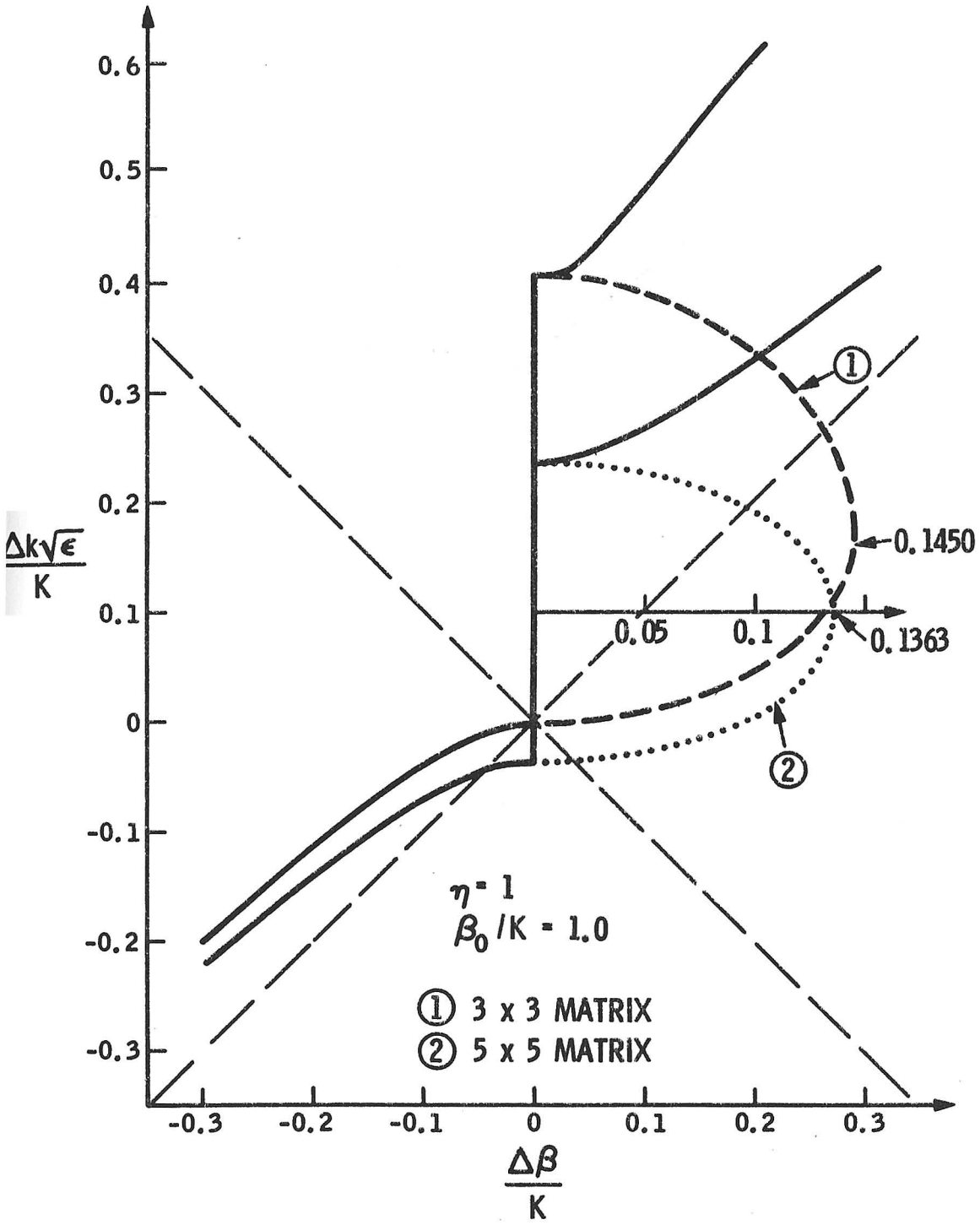

Fig. 3.5 The effect of limiting space harmonics in the Brillouin diagram using Floquet theory at the second Bragg interaction.

cross-coupling is only dependent on S. However, the bandgap shift is not given correctly since S, F_2 and B_2 contribute terms of order η^2 to the self-coupling and bandgap shift. Figure 3.5 shows the effect of limiting the space harmonics in the Floquet theory for $\eta = 1.0$. The upper curve has a greatly enlarged bandgap width for a 3X3 matrix which includes the space harmonics $a_0^{\pm}$, $a_1^{\pm}$ and $a_{-1}^{\pm}$. The lower curve adds the $a_2^{\pm}$ and $a_{-2}^{\pm}$ space harmonics. The resulting 5X5 matrix produces results that are graphically indistinguishable from the 19X19 matrix used for all other Floquet results.

2. Third-Order Interaction

The ECW approach has twelve space harmonics $\left((a_{-4}^{-}, a_{-2}^{+}), (a_{-3}^{-}, a_{-1}^{+}), (a_{-2}^{-}, a_0^{+}), (a_1^{-}, a_1^{+}), (a_0^{-}, a_2^{+}), (a_1^{-}, a_3^{+}), (a_2^{-}, a_4^{+})\right)$ for N = 3. The results are similar to the N=2 case. The explicit dispersion relation is

$$\frac{\Delta\beta_3}{K} = \sqrt{\left(\frac{\Delta k_3\, \epsilon^{\frac{1}{2}}}{K}\right)^2 - \frac{27}{128}\left(\frac{\Delta k_3\, \epsilon^{\frac{1}{2}}}{K}\right)\eta^3 - \frac{14499\,\eta^6}{1048576}} \qquad (3.B4)$$

and the phase mismatch and coupling are

$$\delta_3 = \frac{k^2\epsilon\,(1 - 9\eta^3/64) - \beta_o^2}{2\,\beta_o} \qquad (3.B5)$$

$$\chi_3 = \frac{81k^2\,\epsilon\,\eta^3}{1024\,\beta_o} \qquad (3.B6)$$

where $\beta_o = 3K/2$

Figure 3.6a, b displays the results of ECW and Floquet calculations for $\eta = 1.0,\ 0.5$ at the third Bragg interaction. Note that for the first time the half width ($=W_N/2$) is less than the bandgap shift

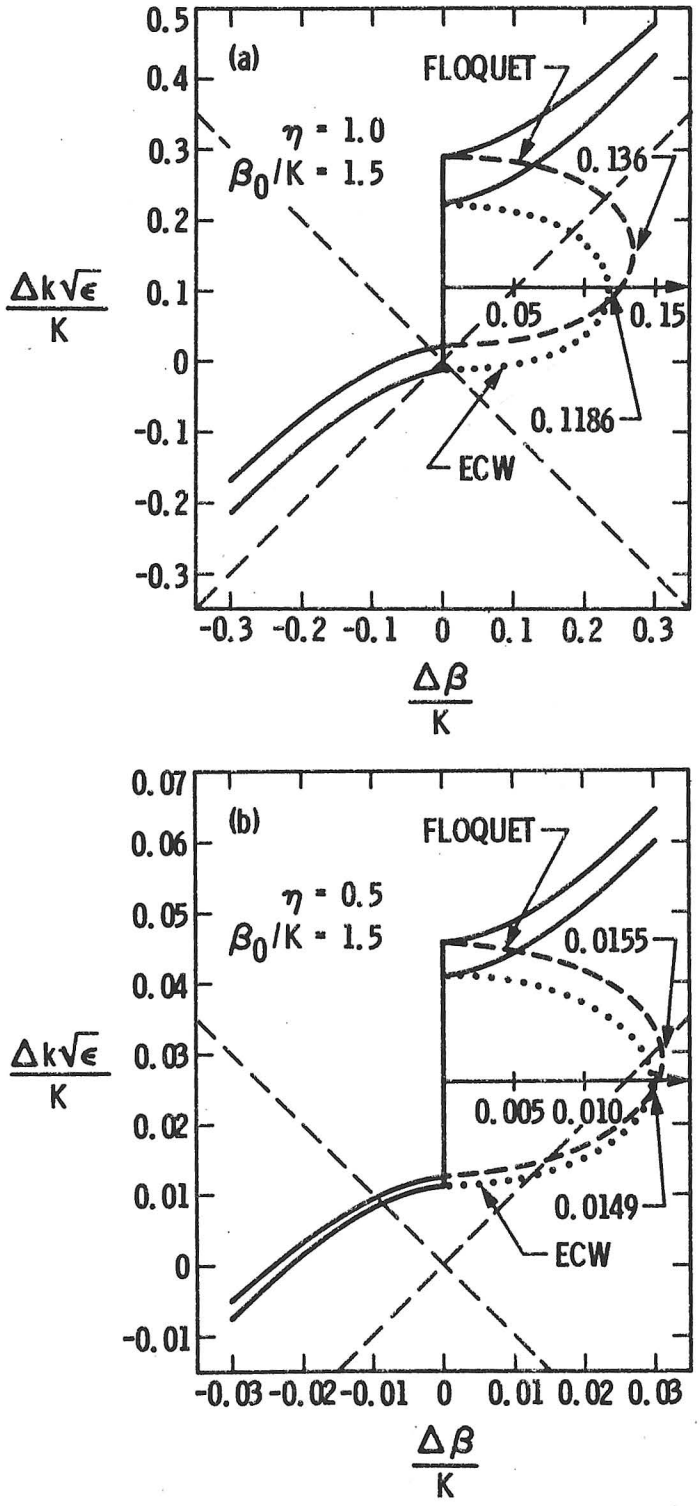

Fig. 5.6 Brillouin diagram at third Bragg order for a) $\eta = 1.0$ and b) $\eta = 0.5$ showing Floquet and ECW results. Imaginary $\Delta\beta/K$ values are the elliptical curves with separate scale.

(= BSG_N) which causes the entire bandgap to be above the exact Bragg wavenumber. This effect becomes more pronounced with increasing order and decreasing perturbation since $W_N \propto (\eta/2)^N$ whereas $BSG_N \propto (\eta/2)^2$. Although the ECW theory does not approximate the Floquet theory for N = 3 as well as it does for N = 2 (compare Figures 3.3a and 3.6a), the ECW approximation improves as η decreases. This is an expected result since in the ECW theory all waves except F_1 and B_1 are assumed to be slowly varying. However, as N increases, more of the waves contribute to the coupling between F_1 and B_1. Table 3.4 summarizes the results of Figure 3.6.

	ECW		Floquet	
	$\eta = 1$	$\eta = 0.5$	$\eta = 1$	$\eta = 0.5$
Coupling χ_3/K	.1186	.0149	.136	.0155
Bandgap Shift BGS_3	.105	.0264	.16	.030
Bandgap Width W_3	.211	.0297	.27	.033

Table 3.4 Summary of ECW and Floquet dispersion relations at the third Bragg order interaction.

Figure 3.7 shows the effect of increasing the matrix order that is used in the Hill's determinant for the Floquet dispersion relation (2.E1). It is apparent that space harmonics of order $n > 2N+1$ must be used to insure accuracy of the Floquet result. Graphs are shown for 7X7, 9X9 and 17X17 size matrices. As before, 19X19 size matrices have been used in the Floquet theory for other figures in this section.

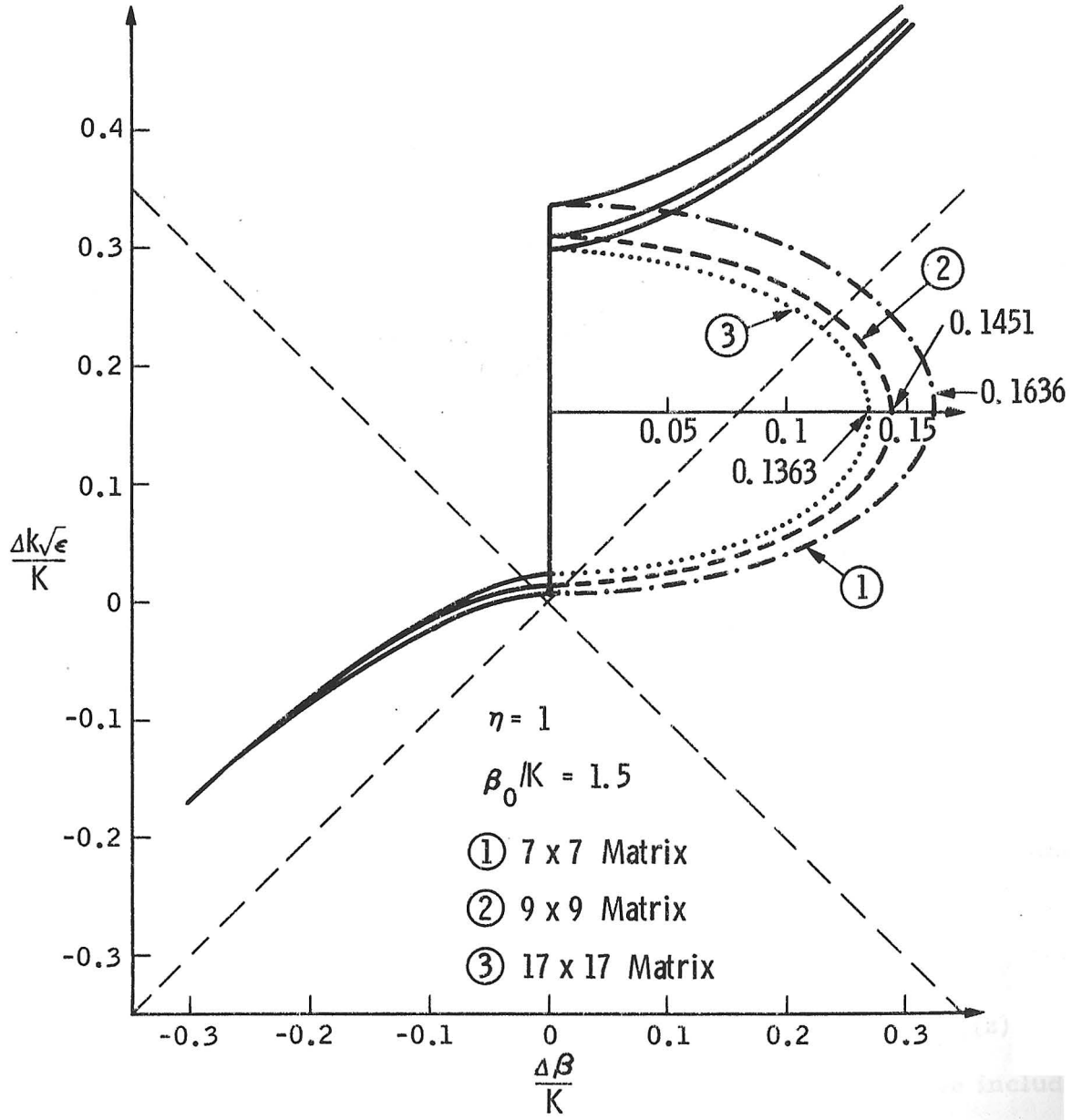

Fig. 3.7 The effect of limiting space harmonics in the Brillouin diagram using Floquet theory at the third Bragg interaction.

C. Multiharmonic Perturbations in ECW Theory

Higher-order Bragg interactions are interactions in the region of $k \epsilon^{\frac{1}{2}}/K \simeq \beta/K \simeq N/2$ where $N \geq 2$. However, there can be competing processes between different Fourier components, $f_p \cos(pKz)$, of multiharmonic (i.e. $p = 1, 2, 3, \ldots$) periodicities for $N \geq 2$. In particular we may find passbands where bandgaps existed in the singly periodic case. This latter fact has been of interest in solid-state theory where the Saxon-Hunter theorem[65] states that a forbidden level in an infinite lattice of pure type-A potentials and in a lattice of pure type-B potentials is also forbidden in any alloy containing both type A and type B potentials. As applied to our problem, this theorem implies that bandgaps formed by two dielectric periodicities $\tilde{f}(Kz)$ and $\tilde{\tilde{f}}(Kz)$ are just the bandgaps caused by $\tilde{f}(Kz)$ and $\tilde{\tilde{f}}(Kz)$ separately. A number of counter-examples[65,66] have been given to the Saxon-Hunter theorem. The ECW approach will show explicitly the effect of multiharmonic periodicities upon the bandgap.

The extension of the ECW theory is straightforward. However, the results for arbitrary multiharmonic periodicities become cumbersome. Several special cases will illustrate the general theory.

From the previous sections we know that the waves between $F_1(z)$ and $B_1(z)$ are needed to couple energy from $F_1(z)$ to $B_1(z)$. We also know that the waves $F(z)_{1+2/N}$ and $B(z)_{1+2/N}$ have to be included to properly account for the bandgap shift. In addition, other waves that can couple significant energy between $F_1(z)$ and $B_1(z)$ or that couple $F_1(z)$ and $B_1(z)$ to themselves have to be included.

Since the Fourier component $[\eta f_p \cos pK^2]$ couples energy between intersections, p intersections apart with strength approximately proportional to ηf_p, then coupling diagrams will again help to show the waves that should be included in the ECW theory. Figure 3.8 demonstrates some of the possible couplings for N = 2.

We list the possible couplings and strengths shown in Figure 3.8:

1. two first-order couplings $\propto (\eta f_1)^2$;
2. one second-order coupling $\propto \eta f_2$;
3. one third- and one first-order coupling $\propto (\eta f_1)(\eta f_3)$;
4. one third-, one second- and one first-order coupling $\propto (\eta f_1)(\eta f_2)(\eta f_3)$;
5. one fourth- and one second-order coupling $\propto (\eta f_4)(\eta f_2)$;
6. one fourth- and two first-order couplings $\propto (\eta f_4)(\eta f_1)^2$.

The mathematical solution consists of writing a set of equations analogous to (3.A6) where the right hand terms are augmented by all of the possible couplings by each Fourier component of the periodicity, f_p.

1. <u>N^{th} Order Bragg Interaction with f_1 and f_N</u>

Consider the periodicity made up of Fourier components $[\eta f_1 \cos Kz + \eta f_N \cos NKz]$ at the N^{th} Bragg order. We assume the non-trivial case where $O[(\eta f_1)^N] \sim O(\eta f_N)$ so that contributions to the cross-coupling from the two Fourier components are of the same order. The major bandgap shift is given by terms $O[(\eta f_1)^2]$. Figure 3.9 is the coupling diagram which shows the important space harmonics and couplings that are used in this case.

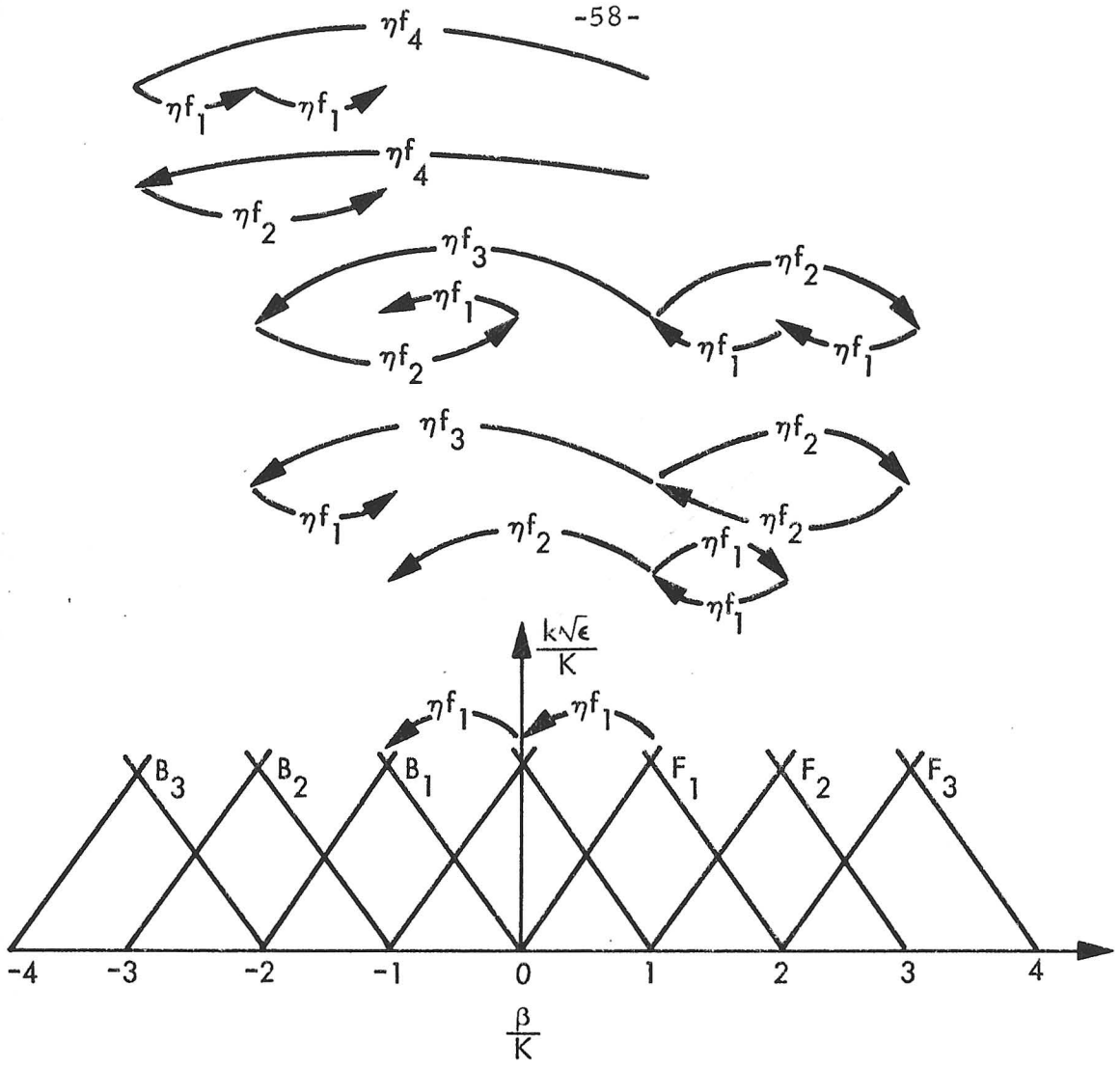

Fig. 3.8 Coupling diagram that shows several of the possible cross-couplings from F_1 to B_1 and self-couplings for F_1 when N = 2. The approximate magnitude of the coupling strangths are shown.

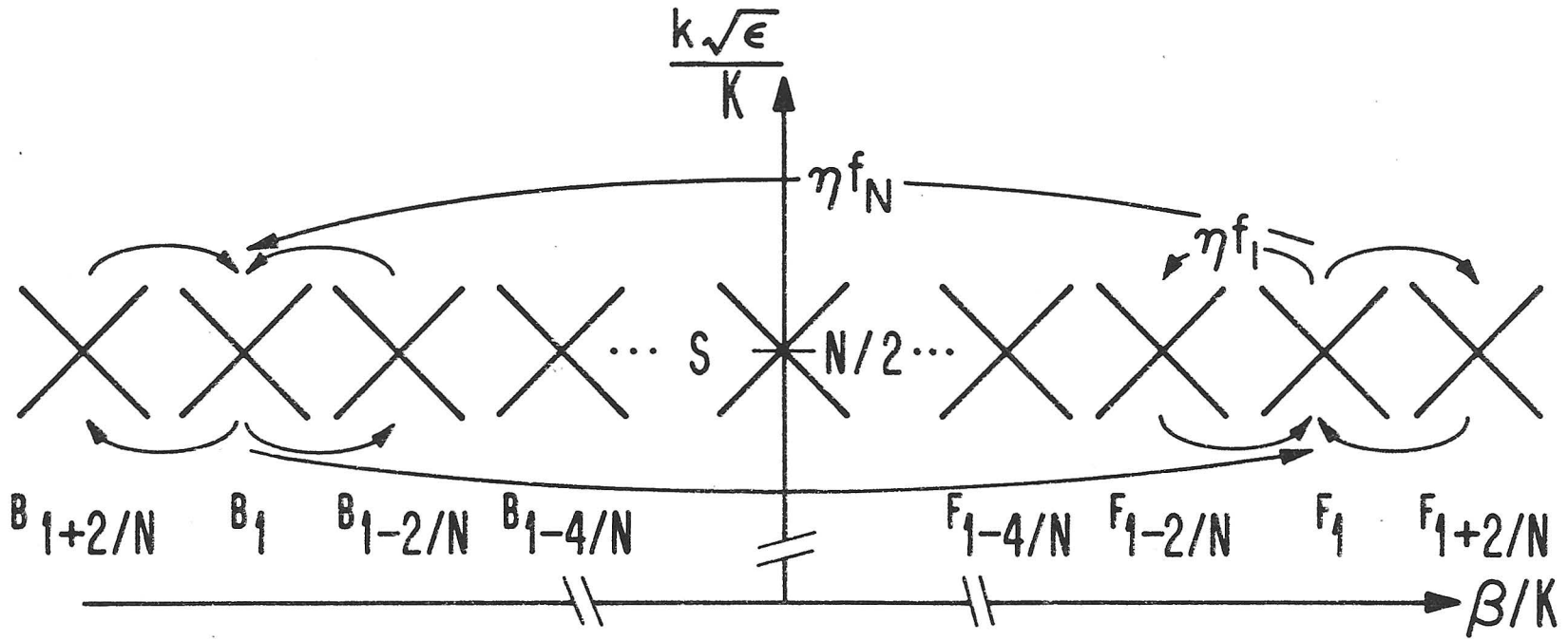

Fig. 3.9 Coupling diagram at the N^{th} Bragg order when $O[(\eta f_1)^N] \sim O(\eta f_N)$.

Since the coupling ηf_N only affects the equations for $F_1(z)$ and $B_1(z)$ and the coupling ηf_1 is used to couple $F_1(z)$ to $B_1(z)$ as well as the coupling $F_1(z) \rightarrow F(z)_{1-2/N} \rightarrow F_1(z)$ and $F_1(z) \rightarrow F(z)_{1+2/N} \rightarrow F_1(z)$, we can write by inspection from Figure 3.9 and equation (3.A6),

$$\left.\begin{aligned}
(k^2\epsilon-(1+2/N)^2\beta_o^2)F_{1+2/N}+2i(1+2/N)\beta_o F'_{1+2/N} &= \frac{-k^2\epsilon}{2}\eta f_1 F_1 \\
(k^2\epsilon-\beta_o^2)\ F_1 + 2i\,\beta_o\,F_1' &= \frac{-k^2\epsilon}{2}\left[(\eta f_1(F_{1-2/N}+F_{1+2/N})+\eta f_N B_1\right] \\
&\vdots \\
\binom{1}{0}k^2\epsilon S &= -\binom{1}{0}\frac{k^2\epsilon}{2}\eta f_1(F_{2/N}+B_{2/N}) \\
&\vdots \\
(k^2\epsilon-\beta_o^2)B_1 - 2i\beta_o B_1' &= \frac{-k^2\epsilon}{2}\left[(\eta f_1(B_{1-2/N}+B_{1+2/N})+\eta f_N F_1\right] \\
(k^2\epsilon-(1+2/N)^2\beta_o^2)B_{1+2/N}-2i(1+2/N)\beta_o B'_{1+2/N} &= \frac{-k^2\epsilon}{2}\eta f_1 B_1
\end{aligned}\right\} \quad (3.C1)$$

The only difference from the previous coupled equations (3.A6) is the change of notation $\eta \rightarrow \eta f_1$ and the addition of the $\eta f_N B_1$ and $\eta f_N F_1$ terms. It is apparent from the N+3 coupled equations (3.C1) that the bandgap shift will be due to ηf_1 as before but that the coupling coefficient will be the algebraic sum of terms involving ηf_1 and ηf_N. Solve the coupled equations as before to find

$$F_1'(z) - i\,\delta_N F_1(z) = i\,\chi_N B_1(z) \quad (3.C2)$$

$$-B_1'(z) - i\,\delta_N B_1(z) = i\chi_N F_1(z) \quad (3.C3)$$

$$\delta_N = \frac{k^2\epsilon\left\{1-\zeta_N(\eta f_1/2)^2[\,,N^2/2(N^2-1)\,]\right\}-\beta_o^2}{2\beta_o} \quad (3.C4)$$

$$\chi_N = \frac{k^2\epsilon}{2\beta_o}\left[\frac{\eta f_N}{2} + \frac{(-1)^{N+1}(\eta f_1)^N}{2^N}\frac{1}{\prod^{*}\{4n(n-N)/N^2\}^2}\right] \quad (3.C5)$$

$$\frac{\Delta\beta_N}{K} = \sqrt{\left(\frac{\delta_N}{K}\right)^2 - \left(\frac{\chi_N}{K}\right)^2} \quad (3.C6)$$

Table 3.2 may be used to find the appropriate bandgap shift. The effective coupling coefficient is found by adding the values for χ_1 and χ_N. Hence the results in equations (3.C2-3.C6) could be written down by inspection.

An interesting case arises when $\chi_N = 0$. For example at the second Bragg order, $\chi_2 = 0$ implies

$$\left.\frac{\Delta\beta_2}{K}\right|_{\chi_2=0} = \frac{\delta_2}{K} = \frac{\Delta k_2\,\epsilon^{\frac{1}{2}}}{K} - \frac{(\eta f_1)^2}{12} \quad (3.C7)$$

which occurs when $\eta f_2 = (\eta f_1)^2/2$. Here the bandgap disappears but the phase speeding effect is still given by the $(\eta f_1)^2/12$ term in (3.C7). It is interesting to note that a periodic medium does not necessarily have bandgaps but it will still have the phase speeding property. In practical cases, if the effects of ηf_1 and ηf_N cancel each other, other periodicities in the media may still cause bandgaps.

Figure 3.10a,b shows the ECW and Floquet results for $\pm\eta f_2 = (\eta f_1)^2/2 = 1/4$ at the second Bragg order. In the first case the effects of ηf_1 and ηf_2 cancel, and the ECW theory predicts no bandgap. The Floquet theory shows a greatly diminished bandgap with a coupling coefficient $\chi_2/K = 0.00568$. The Floquet theory bandgap can be reduced by an order of magnitude, and perhaps more by slightly adjusting the ratio $f_2/\eta f_1^2$ away from $f_2/\eta f_1^2 = 0.5$. For

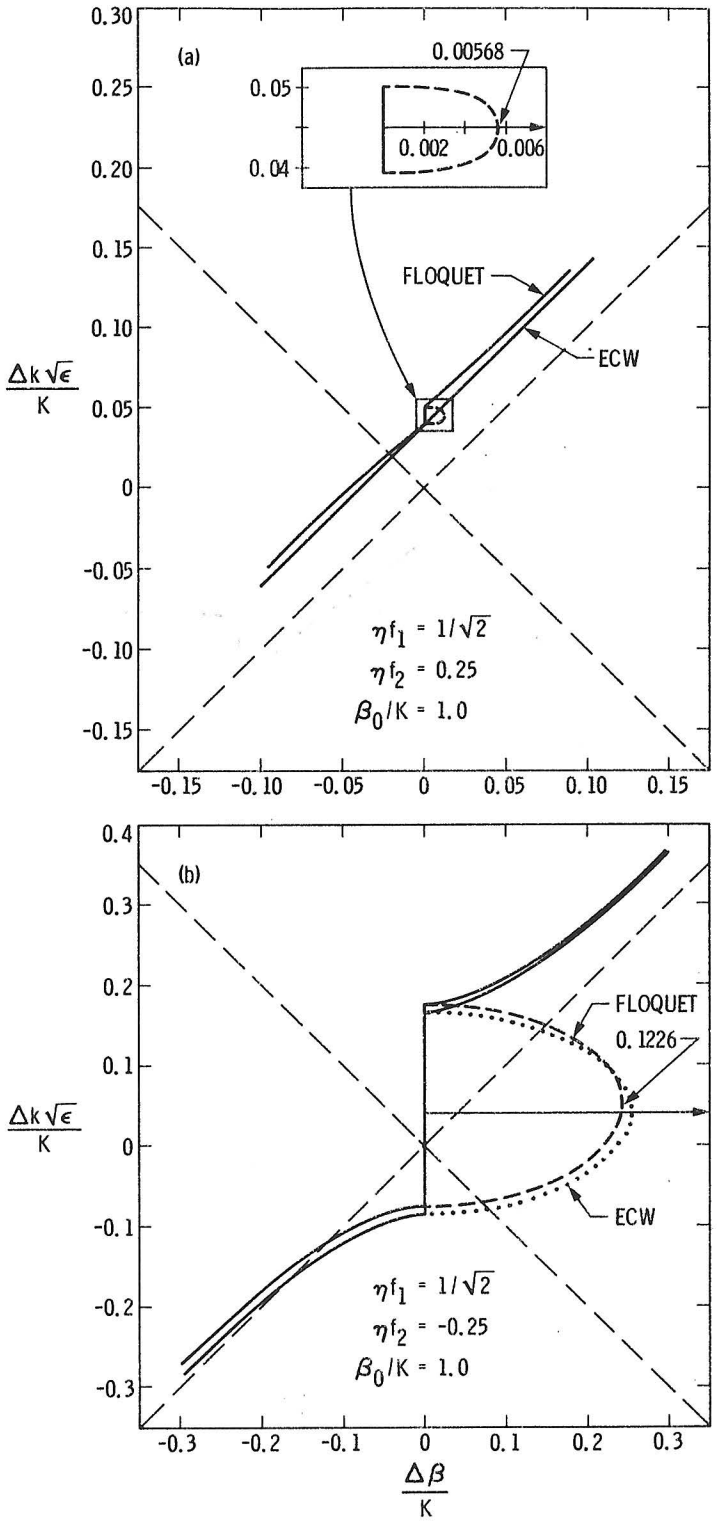

Fig. 3.10 Brillouin diagram at second Bragg order for a) $\eta f_1 = \sqrt{0.5}$, $\eta f_2 = 0.25$ and b) $\eta f_1 = \sqrt{0.5}$, $\eta f_2 = -0.25$ showing ECW and Floquet results for multiharmonic periodicities. Imaginary $\Delta\beta/K$ values are the elliptical curves with separate scale. Note the dependence of the bandgap upon the sign of ηf_2.

$f_2/\eta f_1^2 = 0.55$, $\chi_2/K < 0.0002$. The second case shows the large bandgap that occurs when the effect of ηf_1 and ηf_2 is additive.

The vanishing of the bandgap is due to the relative phasing of f_1 and f_N and is therefore dependent upon the symmetry of the periodicity. Analogous effects have been noted in the electronic stopbands of crystals[65, 86] and in stability diagrams of transverse magnetic (TM) wave propagation in periodic dielectrics.[57]

2. Fourth-Order Bragg Interaction with f_1, f_2 and f_4

In the preceding case, the resulting coupling coefficient was a direct sum of the coupling coefficients of the two Fourier components. This is not always the case. To illustrate, consider a fourth-order Bragg interaction where $O(\eta f_1)^4 \sim O(\eta f_2)^2 \sim O(\eta f_4)$. That is, the Fourier components ηf_1, ηf_2 and ηf_4 contribute values of the same order of magnitude (i.e. $O(\eta f_4)$) to the cross-coupling. The details of possible couplings and the relevant space harmonics are shown in the coupling diagram of Figure 3.11. Weaker couplings such as those proportional to $(\eta f_1)^4 \eta f_2$ have been neglected.

From Figure 3.11 and equation (3.A6) we write by inspection the following coupled equations.

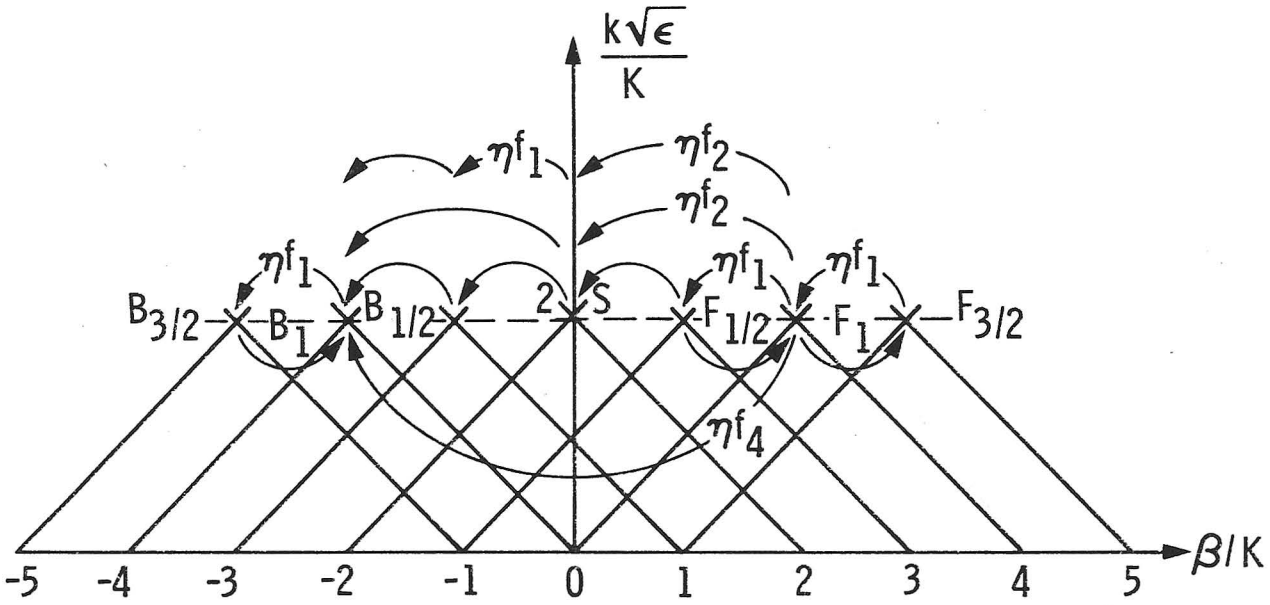

Fig. 3.11 Coupling diagram at fourth-order Bragg interaction for ECW theory. Dominant couplings are shown when $(\eta f_1)^4$, $(\eta f_2)^2$ and ηf_4 are of the same order of magnitude.

$$
\left.
\begin{aligned}
(k^2\epsilon - 9/4\,\beta_o^2)F_{\frac{3}{2}} + 3i\beta_o F_{\frac{3}{2}}' &= \frac{-k^2\epsilon\eta}{2}(f_1F_1) \\
(k^2\epsilon - \beta_o^2)F_1 + 2i\beta_o F_1' &= \frac{-k^2\epsilon\eta}{2}[f_1(F_{\frac{1}{2}}+F_{\frac{3}{2}})+f_2 S+f_4 B_1] \\
(k^2\epsilon - \tfrac{1}{4}\beta_o^2)F_{\frac{1}{2}}+i\beta_o F_{\frac{1}{2}}' &= \frac{-k^2\epsilon\eta}{2}[f_1(F_1+S)+f_2 B_{\frac{1}{2}}] \\
k^2\epsilon S &= \frac{-k^2\epsilon\eta}{2}[f_1(F_{\frac{1}{2}}+B_{\frac{1}{2}})+f_2(F_1+B_1)] \\
(k^2\epsilon - \tfrac{1}{4}\beta_o^2)B_{\frac{1}{2}}-i\beta_o B_{\frac{1}{2}}' &= \frac{-k^2\epsilon\eta}{2}[f_1(B_1+S)+f_2 F_{\frac{1}{2}}] \\
(k^2\epsilon - \beta_o^2)B_1 - 2i\beta_o B_1' &= \frac{-k^2\epsilon\eta}{2}[f_1(B_{\frac{1}{2}}+B_{\frac{3}{2}})+f_2 S+f_4 F_1] \\
(k^2\epsilon - 9/4\,\beta_o^2)B_{\frac{3}{2}}-3i\beta_o B_{\frac{3}{2}}' &= \frac{-k^2\epsilon\eta}{2}(f_1B_1)
\end{aligned}
\right\} \quad (3.C8)
$$

where the arguments with respect to z have been dropped. Solve the coupled equations as before to find

$$F_{\frac{3}{2}} = \frac{2}{5}\eta f_1 F_1 \qquad (3.C9)$$

$$B_{\frac{3}{2}} = \frac{2}{5}\eta f_2 B_2 \qquad (3.C10)$$

$$F_{\frac{1}{2}} = \frac{16}{9}F_1\left[\frac{3\eta^2}{16}f_1f_2 - \frac{3\eta}{8}f_1 - \frac{\eta^3}{8}f_1f_2^2 + \frac{\eta^3}{8}f_1^3\right] + \frac{16}{9}B_1\left[\frac{7\eta^2}{16}f_1f_2 - \frac{\eta^3}{8}f_1f_2^2 - \frac{\eta^3}{8}f_1^3\right] \qquad (3.C11)$$

$$B_{\frac{1}{2}} = \frac{16}{9}F_1\left[\frac{7\eta^2}{16}f_1f_2 - \frac{\eta^3}{8}f_1f_2^2 - \frac{\eta^3}{8}f_1^3\right] + \frac{16}{9}B_1\left[\frac{3\eta^2}{16}f_1f_2 + \frac{\eta^3}{8}f_1^3 - \frac{\eta^3}{8}f_1f_2^2 - \frac{3\eta}{8}f_1\right] \qquad (3.C12)$$

$$S = \frac{16}{9}(F_1+B_1)\left[\frac{\eta^3}{8}f_2^3 + \frac{3\eta^2}{16}f_1^2 - \frac{9\eta}{32}f_2 - \frac{\eta^3}{8}f_1^2f_2\right] \qquad (3.C13)$$

These values are substituted into the equations for $F_1(z)$ and $B_1(z)$ in (3. C8) to find the coupled equations for $F_1(z)$ and $B_1(z)$. The resulting values for δ_4 and χ_4 are

$$\delta_4 = \frac{k^2\epsilon \left[1 - \frac{2\eta^2}{15} f_1^2\right] - \beta_o^2}{2\beta_o} \qquad (3.C14)$$

$$\chi_4 = \frac{k^2\epsilon\eta}{4\beta_o}\left[-\frac{2}{9}\eta^3 f_1^4 - \frac{\eta}{2} f_2^2 + \frac{10\eta^2 f_1^2 f_2}{9} + f_4\right] \qquad (3.C15)$$

where $\beta_o = 2K$ and where smaller order terms are neglected.

As expected, the above expressions reduce to the first-order case if $f_1 = f_2 = 0$, to the second-order case if $f_1 = f_4 = 0$, and the fourth-order case if $f_2 = f_4 = 0$. However, the presence of the mixed term $f_1^2 f_2$ means that the above results cannot be obtained from simple superposition of the terms from each component. As in the previous case, a proper choice of f_1, f_2, and f_4 would allow us to eliminate the bandgap.

The different terms in the expression of χ_4 can be easily explained as shown in Fig. 3.11. There are four possible ways to achieve a fourth-order coupling with the three Fourier components f_1, f_2, and f_4. These are:

1. four couplings through f_1;
2. any combination of one coupling through f_2 and two couplings through f_1;
3. one coupling through f_4.

The $f_1^2 f_2$ term in equation (3. C14) has a large numerical coefficient because this coupling can occur in three different ways.

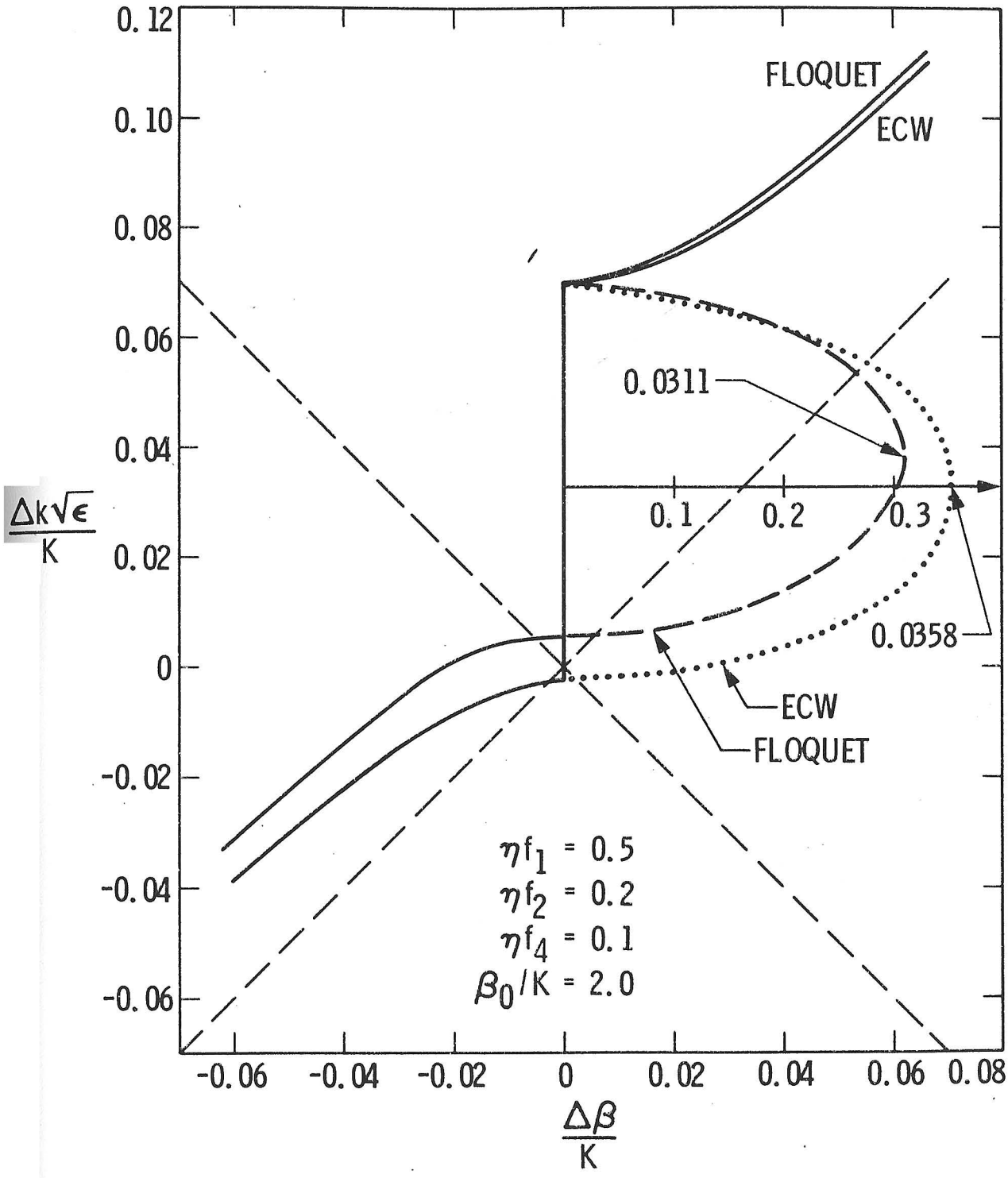

Fig. 3.12 Brillouin diagram at fourth Bragg order when $\eta f_1 = 0.5$, $\eta f_2 = 0.2$, and $\eta f_4 = 0.1$ showing ECW and Floquet results. Imaginary $\Delta\beta/K$ values are the elliptical curves with separate scale.

Fig. 3.12 compares the ECW and the Floquet solution for the values $\eta f_1 = 0.5$, $\eta f_2 = 0.2$ and $\eta f_4 = 0.05$. Note the close approximation of the ECW theory to the Floquet solution at the fourth Bragg order with several harmonic periodicities even when the perturbation is relatively large.

D. Comments on ECW Theory

The predictive abilities of the ECW theory have been summarized at the end of Section A. The numerical examples demonstrate the accuracy of the ECW theory at higher Bragg orders and for multiharmonic periodicities. The ECW theory is particularly attractive for small perturbations where the Floquet theory is cumbersome and time consuming. This is relevant to present optical applications where often $\eta \leqslant 10^{-3}$.

The extension to higher Bragg orders opens up the possibility of using the many first-order results of the literature at higher Bragg orders by the use of the proper δ_N and χ_N. Several extensions of this nature will be made in a later chapter.

Two interesting results have been explained in this chapter. First, the phase speeding effect was observed to be a result of self-coupling and occurs regardless of the value of the higher frequency Fourier components f_p. Second, the disappearing bandgaps were explained through simple interference effects of different periodicity frequencies. This opens up the possibility of controlling feedback through the relative phases of two harmonics since feedback or coupling strength is directly proportional to bandgap width.

It is anticipated that a similar analysis could be applied to bounded media, space-time periodic media and active media. The latter case will be covered in detail in the next two chapters.

Parts of this chapter have been summarized elsewhere[53] and the results have been confirmed through calculations that use the method of multiple scales.[95]

CHAPTER IV

COMPLEX PERIODIC MEDIA

Although the study of wave propagation in periodic structures has been a popular subject since late last century, most of the analytical studies have dealt with simple (passive and lossless) periodic media. The recent development of DFB lasers[23,30,58] has extended the applicability of periodic structures to the case of complex ($\epsilon = \epsilon_r + i\epsilon_i$, $\eta = \eta_r + i\eta_i$) periodic media. In their analysis of DFB lasers Kogelnik and Shank[23] briefly discuss the Brillouin diagram near the first-order Bragg interaction when the gain coefficient is modulated. Using Floquet theory, Wang[25,58] presents a more detailed analysis of the first-order Brillouin diagram for active periodic media. Higher-order[71] and multiply-resonant[70] DFB lasers have been mentioned very recently in the literature.

In this chapter we investigate in detail both the ECW and the Floquet theory for complex media at the first few Bragg orders. Analogous results will hold for higher even and odd orders. In section A we use the exact Floquet solution to plot the Brillouin diagram for several values of the perturbation and average dielectric constant. In section B we use the approximate but simple ECW solution to study in detail the changes in the Brillouin diagram for the first three Bragg orders in singly periodic media. A short discussion of multiharmonic periodicities is given in section C, and section D summarizes the results of the chapter.

As in the previous chapter, some of the parameters in the numerical examples will be larger than those that might be

experimentally obtained. However, this exaggeration is again used to dramatize the periodicity effects. The ECW examples are easily scaled for other values of gain/loss and perturbation.

A. Floquet Solution

We consider the case of a TEM wave propagating along the z axis in an unbounded medium with a periodically modulated dielectric constant:

$$\epsilon(z) = \epsilon_r + i\epsilon_i + \epsilon_r \sum_p (\eta_r + i\eta_i)_p f_p \cos pKz \qquad (4.A1)$$

where

$$\epsilon_r = \mathrm{Re}\{\epsilon\} \qquad \epsilon_i = \mathrm{Im}\{\epsilon\}$$

$$\eta_r = \mathrm{Re}\{\eta\} \qquad \eta_i = \mathrm{Im}\{\eta\}$$

and $f_0 \equiv 0$, $f_1 \equiv 1$, and $|\eta_{r_p} f_p| \leq 1$, $|\eta_{i_p} f_p| \leq 1$ for $p = 1, 2, 3, \ldots$. Index coupling will refer to the case where $\eta_i = 0$ and gain/loss coupling will refer to the case where $\eta_r = 0$. Note that gain (loss) media implies $\epsilon_i < 0$ ($\epsilon_i > 0$) for $e^{-i\omega t}$ excitation. The Hill's determinant equation

$$\sin^2(\pi\beta/K) = \Delta(0) \sin^2(\pi k \epsilon^{\frac{1}{2}}/K) \qquad (4.A2)$$

of chapter II still holds with minor changes in the matrix elements Δ_{pn}:

$$\Delta_{pn} = \begin{cases} 1 & p = n \\ \dfrac{-k^2\epsilon}{p^2K^2 - k^2\epsilon} \dfrac{\eta f_{|n-p|}\, \epsilon_r}{2\epsilon} & p \neq n \end{cases} \qquad (4.A3)$$

These elements make up the Hill's determinant $\Delta(0) = \det \|\Delta\|$.

Several examples of the Floquet solution for singly periodic media are given in the Brillouin diagram Figure 4.1 for real frequencies. The example for simple periodic media (real ϵ and η) was found in chapter III and is given in curve 1 of Figure 4.1a. There are two main characteristics. First, note the presence of bandgaps in frequency where β becomes complex. These are known as non-inverting bandgaps. Second, note the phase speeding that is a result of upward bandgap shift.

The Brillouin diagram changes drastically for gain or loss coupling where the perturbation is imaginary. In curve 2 of Figure 4.1a we plotted the case for real frequency where $\epsilon = \epsilon_r$ and $\eta = i\eta_i$. This corresponds to media with successive amplifying and lossy layers while the average gain (or loss) is zero. Note the inverting bandgaps (i.e. bandgaps in longitudinal wavenumber) at odd Bragg orders. The pattern of non-inverting and inverting bandgaps alternate with Bragg order. However, bandgaps of both types are shifted toward lower frequency. This latter effect can be understood from the average velocity which was given by

$$\langle v \rangle = \frac{c}{\epsilon^{\frac{1}{2}}} \left[1 + \frac{3\pi}{16} \eta^2 + O(\eta^4)\right] \qquad (4.A4)$$

for $|\eta| < 1$. It is apparent that phase speeding (positive bandgap shift) occurs for $\eta = \eta_r$ and phase slowing (negative bandgap shift) occurs for $\eta = i\eta_i$. This also follows naturally from the definition of BGS_N that was given in the previous chapter (3.A31).

Let us now consider the case of complex media where only the real part of the dielectric constant is sinusoidally perturbed

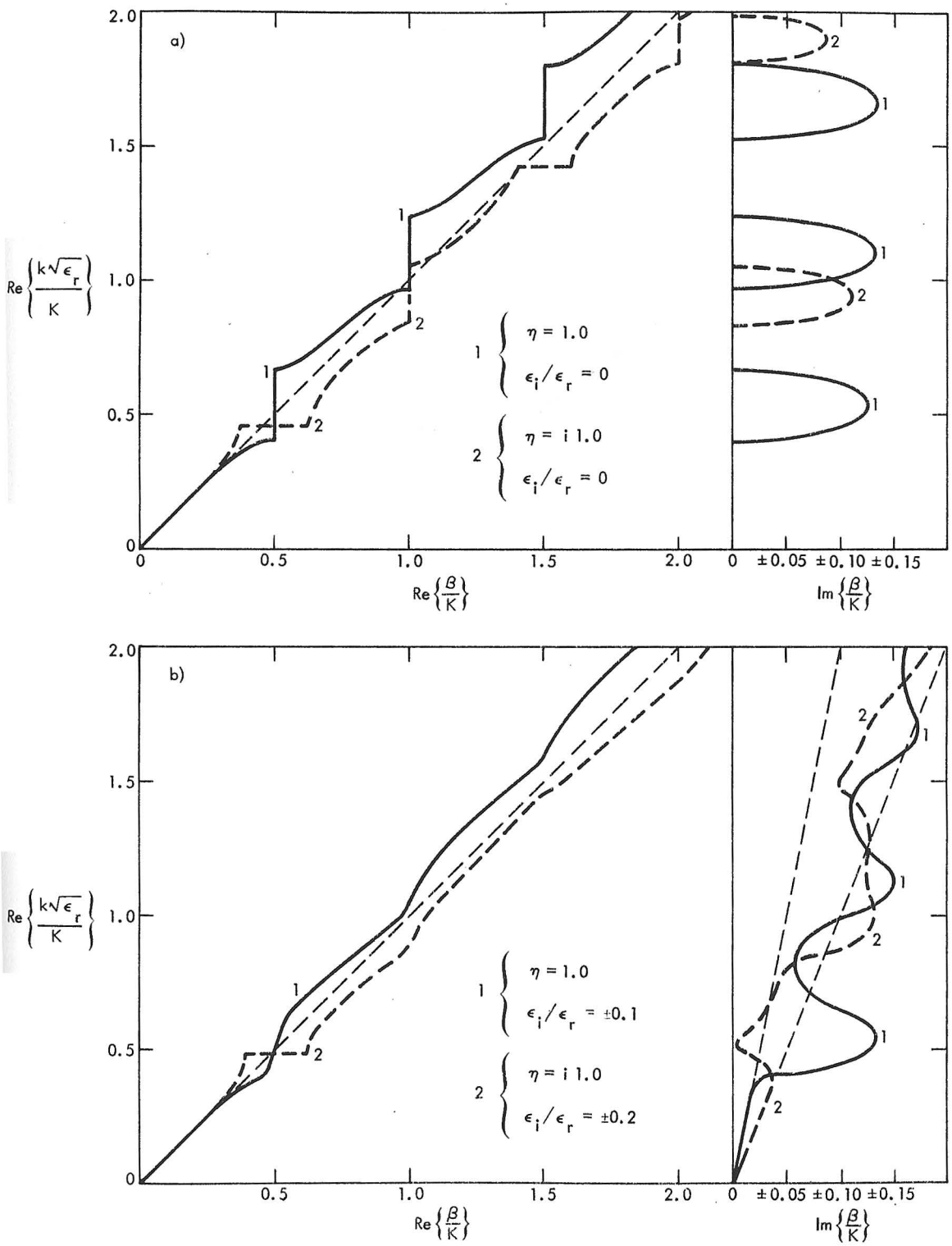

Fig. 4.1 Brillouin diagram for first three Bragg orders using Floquet theory and real frequency using: a) index coupling (curve 1) and gain/loss coupling (curve 2) when $\epsilon_i/\epsilon_r = 0$; b) similar results for finite ϵ_i/ϵ_r. The light dashed lines are the unperturbed values (η=0).

but average gain or loss is present (i.e. $\epsilon = \epsilon_r + i\epsilon_i$, $\eta = \eta_r$). The corresponding Brillouin diagram for real frequency is shown in curve 1 of Figure 4.1b. For $\epsilon_i \neq 0$, we observe that $\mathrm{Re}\{\beta/K\}$ is no longer a constant across the Bragg region and the effective spatial gain or loss increases appreciably near the Bragg frequencies.[25, 76] The unperturbed value (η=0) is shown by the light dashed lines.

When the gain or loss is sinusoidally perturbed, the spatial gain or loss diminishes near the odd-order Bragg resonances and is enhanced near the even-order resonances. This case is illustrated in curve 2 of Fig. 4.1b where there is an average imaginary dielectric constant and imaginary perturbation. Again the light dashed lines represent the unperturbed values.

We see that the spatial gain can be either enhanced or diminished near Bragg resonances. This behavior depends upon Bragg order and perturbation or coupling type.

The sign of $\mathrm{Im}\{\beta/K\}$ and $\mathrm{Im}\{k\,\epsilon_r^{\frac{1}{2}}/K\}$ (not shown) have not been specified because the correct root of the dispersion relation is dependent upon the stability of the wave. For passive media, $\epsilon_i > 0$ and the correct signs are chosen to indicate spatially and temporally decaying waves since no sources are present. Hence, the media does not support instabilities. However, instabilities may arise in active periodic media where $\epsilon_i < 0$ for some (or all) z. In this case an analysis of wavepackets in the periodic medium must be made.[73] This case is taken up in the following chapter. For the present we will only examine monochromatic waves and will not specify the correct sign of the dispersion relation roots.

B. ECW Theory for Complex Media

1. Analytic Expressions

Since we again assume a solution to the wave equation of the form

$$E(z) = \sum_{n=-1}^{N^*/2} \left[F(z)_{1-2n/N} \exp\left[i(1-2n/N)\beta_o z\right] + B(z)_{1-2n/N} \exp\left[-i(1-2n/N)\beta_o z\right] + \binom{1}{0} S(z) \right] \quad (4.B1)$$

where the symbols have the same meaning as in chapter III. This implies that the gain/loss and the perturbation of the media are small. Hence for a singly periodic effective dielectric constant

$$\epsilon(z) = \epsilon_r + i\epsilon_i + \epsilon_r(\eta_r + i\eta_i)\cos Kz \quad (4.B2)$$

we assume

$$|\eta_r|,\ |\eta_i|,\ |\epsilon_i/\epsilon_r| \ll 1$$

However, as in the case of simple media, we might expect the ECW dispersion relations to be a good approximation to the Floquet results even as

$$|\eta_r|,\ |\eta_i|,\ |\epsilon_i/\epsilon_r| \to 1 .$$

Following the identical analysis that led to the ECW expressions (3.A20-3.A25) we find immediately that for the N^{th} Bragg order

$$\delta_N = \frac{k^2\epsilon_r(1+i\epsilon_i/\epsilon_r)\left\{1-\zeta_N\left[(\eta_r+i\eta_i)/2\right]^2\left[\frac{N^2}{2(N^2-1)}\right]\right\}-\beta_o^2}{2\beta_o} \quad (4.B3)$$

$$\chi_N = \frac{(-1)^{N+1} k^2 \epsilon_r (\eta_r + i\eta_i)^N}{2^{N+1} \beta_o} \frac{1}{\prod^* \{4n(n-N)/N^2\}^2} \qquad (4.B4)$$

where $\beta_o = NK/2$. Note that the coupling coefficient χ_N is not affected by ϵ_i. The dispersion relation as before is

$$\left(\frac{\Delta\beta_N}{K}\right)^2 = \left(\frac{\delta_N}{K}\right)^2 - \left(\frac{\chi_N}{K}\right)^2 \qquad (4.B5)$$

2. First-Order Interactions

At the first order Bragg interaction we have the approximate expressions

$$\frac{\delta_1}{K} \simeq \frac{\Delta k_1 \epsilon_r^{\frac{1}{2}}}{K} + \frac{i\epsilon_i}{4\epsilon_r} \qquad (4.B6)$$

$$\frac{\chi_1}{K} \simeq \frac{\eta_r + i\eta_i}{8} \qquad (4.B7)$$

which give

$$\left(\frac{\Delta\beta_1}{K}\right)^2 = \frac{\Delta k_i \epsilon_r^{\frac{1}{2}}}{K} - \left(\frac{\epsilon_i}{4\epsilon_r}\right)^2 + i\left(\frac{\Delta k_1 \epsilon_r^{\frac{1}{2}}}{K}\right)\frac{\epsilon_i}{2\epsilon_r} - \frac{\eta_r^2 - \eta_i^2}{64} - \frac{i\eta_r\eta_i}{32} \qquad (4.B8)$$

where

$$\Delta k_1 = k - \beta_o/\epsilon_r^{\frac{1}{2}}$$

$$\Delta\beta_1 = \beta - \beta_o$$

Note that at the first Bragg order, ϵ_i only affects the phase mismatch δ_1, and η_i only affects the coupling χ_1. For index coupling, the maximum value of $\mathrm{Im}\{\Delta\beta_1/K\}$ occurs exactly at Bragg resonance

$\Delta k_1 \epsilon_r^{\frac{1}{2}}/K = 0$. The value is

$$\left| \mathrm{Im}\left\{ \frac{\Delta\beta_1}{K} \right\}_{\max} \right| = \left| \left[\frac{\epsilon_i^2}{16\epsilon_r^2} + \frac{\eta_r^2}{64} \right]^{\frac{1}{2}} \right|$$

Hence, near Bragg resonance, the effect of spatial gain or loss and the perturbation add as the sum of their squares for index coupling. This enhancement of spatial gain or loss has been observed in the Floquet solution of Figure 4.1b and is shown in Figure 4.2a for the ECW solution for several values of ϵ_i/ϵ_r when $\eta = 0.1$. Far from the Bragg resonance $\mathrm{Im}\{\Delta\beta_1/K\} = \pm \delta_1/K$, the unperturbed value. The temporal gain or loss, $\mathrm{Im}\{\Delta k_1 \epsilon_r^{\frac{1}{2}}/K\}$, remains constant across the bandgap with value $\epsilon_i/4\epsilon_r$.

For gain or loss coupling, χ_1^2 changes sign and therefore $\Delta\beta_1/K$ is real if $\epsilon_i = 0$. This produces an inverted bandgap as shown in the previous Floquet results. The ECW results are shown in Figure 4.2b for several values of ϵ_i/ϵ_r when $\eta = i\,0.1$. Two classes of behavior appear that depend upon the sign of

$$A = [|\epsilon_i/\epsilon_r| - |\eta_i/2|] .$$

For $A < 0$, a bandgap of width $2[\eta_i^2/64 - \epsilon_i^2/(4\epsilon_r)]^{\frac{1}{2}}$ appears in $\mathrm{Re}\{\Delta\beta_1/K\}$, and $\mathrm{Im}\{\Delta\beta_1/K\} = 0$ at Bragg resonance. The two roots of $\mathrm{Im}\{\Delta k_1 \epsilon_r^{\frac{1}{2}}/K\}$ are of opposite sign. For $A > 0$, there is no bandgap and the gain or loss coupling diminishes the average spatial gain or loss near Bragg resonance. This is due to the fact that the coefficients of η_i^2 and ϵ_i^2 have opposite sign in (4.B8). In this case, the two roots of $\mathrm{Im}\{\Delta k_1 \epsilon_r^{\frac{1}{2}}/K\}$ are of the same sign.

Thus, the effect of finite ϵ_i can either enhance ($\eta = \eta_r$) or reduce ($\eta = i\eta_i$) the effective spatial gain or loss near the first Bragg

Fig. 4.2 Brillouin diagram at first Bragg order using: a) index coupling; b) gain/loss coupling; and c), d) both couplings in the ECW theory.

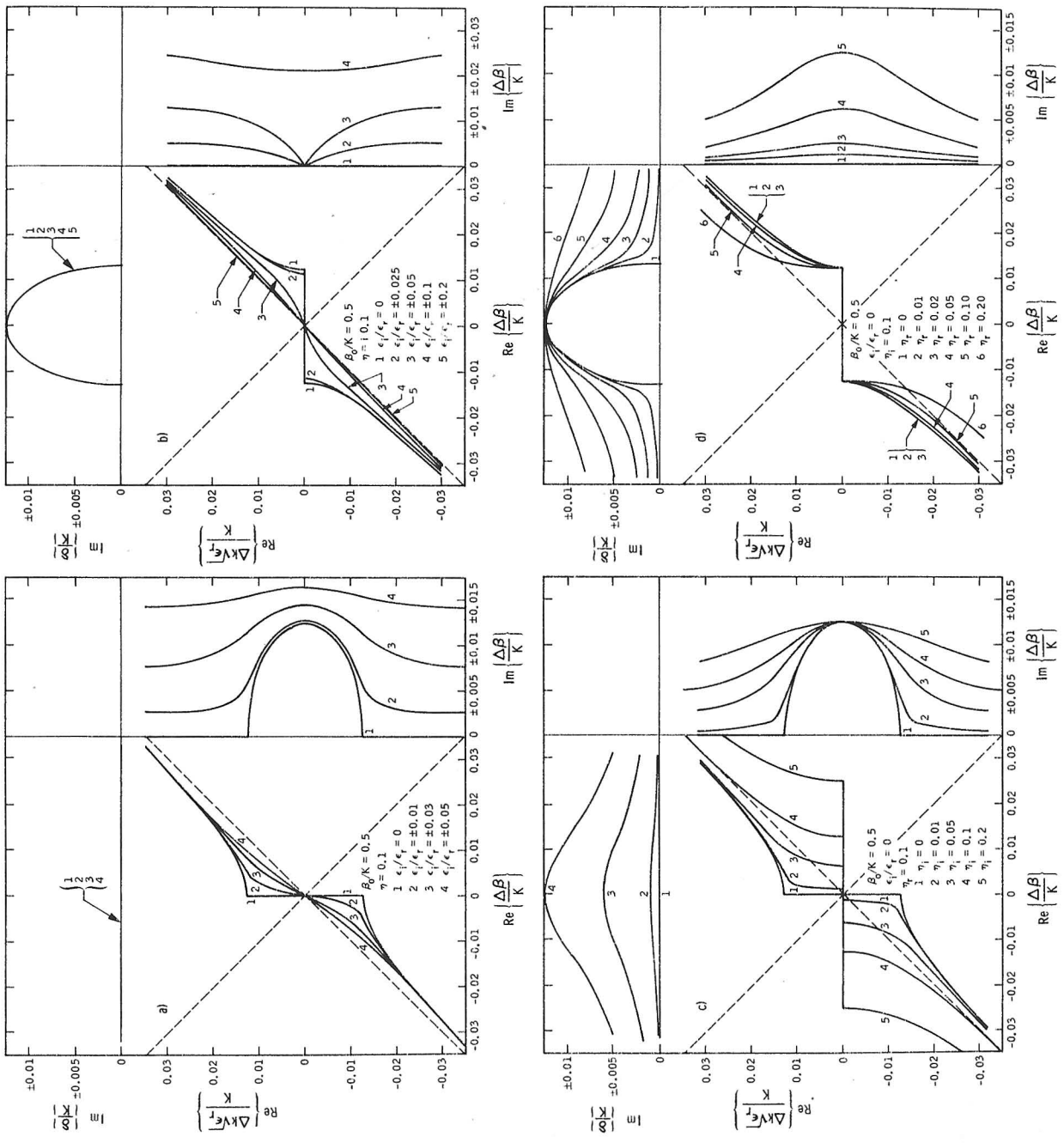
a)
b)
c)
d)
$\beta_0/K = 0.5$
$\eta_r = 0.1$
$\eta_i = 0.1$
$\epsilon_i/\epsilon_r = 0$
$\epsilon_i/\epsilon_r = \pm 0.01$
$\epsilon_i/\epsilon_r = \pm 0.03$
$\epsilon_i/\epsilon_r = \pm 0.05$
$\epsilon_i/\epsilon_r = \pm 0.025$
$\epsilon_i/\epsilon_r = \pm 0.1$
$\epsilon_i/\epsilon_r = \pm 0.2$
$\eta_i = 0$
$\eta_i = 0.01$
$\eta_i = 0.05$
$\eta_i = 0.1$
$\eta_i = 0.2$
$\eta_r = 0$
$\eta_r = 0.01$
$\eta_r = 0.02$
$\eta_r = 0.05$
$\eta_r = 0.10$
$\eta_r = 0.20$
$\mathrm{Re}\left\{\frac{\Delta}{K}\right\}$
$\mathrm{Im}\left\{\frac{\Delta}{K}\right\}$
$\mathrm{Re}\left\{\frac{\Delta K V \epsilon_r}{K}\right\}$
$\mathrm{Im}\left\{\frac{\delta}{K}\right\}$

Fig. 4.2

resonance. For both cases of coupling, increased ϵ_i/ϵ_r tends to mask the effect of the coupling or perturbation.

Figures 4.2c, d show the effect of having complex coupling ($\eta = \eta_r + i\eta_i$) in a media with no average gain or loss. As the ratio η_i/η_r is increased, the bandgap region changes from the shape typical of index coupling to the shape typical of gain or loss coupling for $\mathrm{Re}\{\Delta\beta_1/K\}$ and $\mathrm{Re}\{\Delta k_1 \epsilon_r^{\frac{1}{2}}/K\}$. The values of $\mathrm{Im}\{\Delta\beta_1/K\}$ and $\mathrm{Im}\{\Delta k_1 \epsilon_r^{\frac{1}{2}}/K\}$ tend to peak in the Bragg interaction region.

3. Second-Order Interaction

The second-order Bragg interaction and all even-order interactions produce very different dispersion relations from those of the first-order for gain or loss coupling. This was seen in the Floquet results of Figure 4.1. The change is due to the term $(i\eta_i)^{2N}$ in the dispersion relation which takes on different signs depending upon the oddness or evenness of N. In the second-order Bragg region, the approximate relations are

$$\frac{\delta_2}{K} \simeq \frac{\Delta k_2 \epsilon_r^{\frac{1}{2}}}{K} - \frac{(\eta_r + i\eta_i)^2}{12} + \frac{i\epsilon_i}{2\epsilon_r}\left[1 - \frac{(\eta_r + i\eta_i)^2}{6}\right] \qquad (4.B9)$$

$$\frac{\chi_2}{K} \simeq -\frac{(\eta_r + i\eta_i)^2}{8} \qquad (4.B10)$$

where $\Delta k_2 = k - \beta_o/\epsilon_r^{\frac{1}{2}}$; $\beta_o = K$.

Note that the perturbation affects not only the coupling χ_2, but also the phase mismatch δ_2. In fact, η now acts to modify the gain or loss from $\epsilon_i/(2\epsilon_r)$ to the effective value $\epsilon_i(1-\eta^2/6)/(2\epsilon_r)$.

The Brillouin diagram for the case of index coupling is shown in Figure 4.3a for various values of ϵ_i/ϵ_r with $\eta = 0.1$. The result

is similar to the first-order case with the exception of the bandgap shift. Again, at the center of the bandgap, the effective gain or loss and the perturbation add as the sum of their squares. The spatial gain or loss is greatly enhanced near Bragg resonance when $|\epsilon_i/\epsilon_r| \ll |\eta|^2$ whereas the temporal gain or loss remains constant.

In the case of gain or loss coupling, a difference occurs since χ^2 is proportional to η^4 in (4.B10) and the bandgap shift changes sign which causes the Brillouin diagram to be a mirror image of the index coupling case about the axis $\delta_2/K = 0$. That is, at the second Bragg order, the difference between index and gain or loss coupling is a matter only of positive or negative bandgap shift. This is demonstrated in Figure 4.3b for $\eta = i\,0.1$ and several values of ϵ_i/ϵ_r. This dependence of the phase mismatch upon η^2 accounts for the phase speeding and slowing effects shown by previous Floquet results. The temporal gain or loss is constant as in the index coupling case.

Figures 4.3c,d are similar mirror images about $\mathrm{Re}\{\Delta k_2 \epsilon_r^{\frac{1}{2}}/K\} = 0$ for $\epsilon_i/\epsilon_r = 0$ and various ratios η_i/η_r. The symmetry is expected since η always enters as an even power in the dispersion relation. From (4.B9-10) it is evident that $\mathrm{Im}\{\Delta\beta_2/K\} = 0$ at $\Delta k_2\, \epsilon_r^{\frac{1}{2}}/K = 0$ only when $|\eta_i| = |\eta_r|$. This corresponds to curve 5 and is similar in shape to the gain or loss coupling Brillouin diagram at the first Bragg order. For $\mathrm{Im}\{\Delta k_2\, \epsilon_r^{\frac{1}{2}}/K\} = \pm\, \eta_r \eta_i/12$, $\mathrm{Im}\{\Delta\beta_2/K\} = 0$ for $\eta_r \lesseqgtr \eta_i$. Thus for complex coupling, the perturbation will mask the spatial gain or loss for some frequency near Bragg resonance, while a large spatial gain or loss will occur for nearby frequencies. In

Fig. 4.3 Brillouin diagram at second Bragg order using: a) index coupling; b) gain/loss coupling; and c), d) both couplings in the ECW theory.

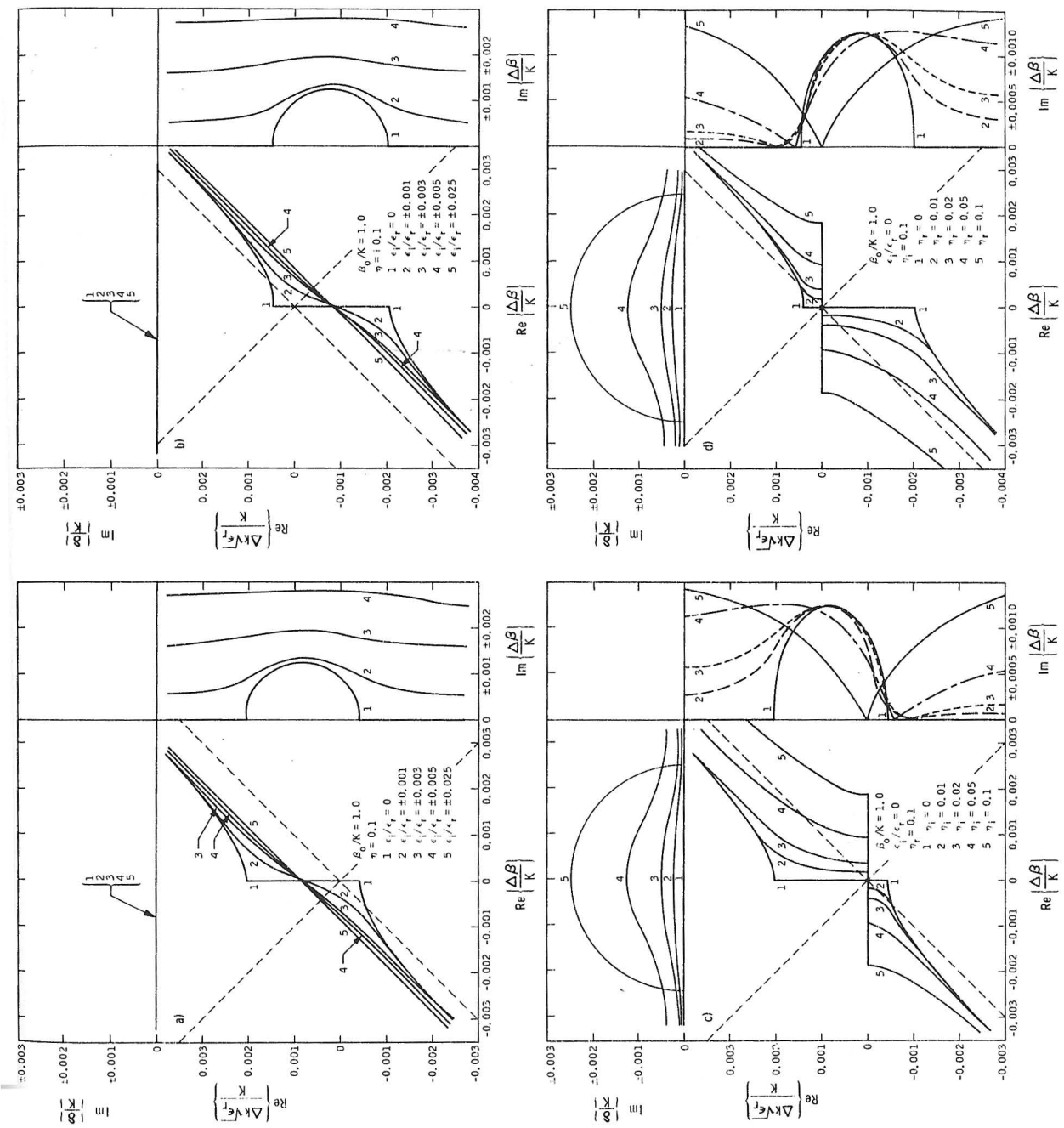
a)
b)
c)
d)
$\beta_0/K = 1.0$
$\eta = i\ 0.1$
1 $\epsilon_i/\epsilon_r = 0$
2 $\epsilon_i/\epsilon_r = \pm 0.001$
3 $\epsilon_i/\epsilon_r = \pm 0.003$
4 $\epsilon_i/\epsilon_r = \pm 0.005$
5 $\epsilon_i/\epsilon_r = \pm 0.025$
$\beta_0/K = 1.0$
$\epsilon_i/\epsilon_r = 0$
$\eta_i = 0.1$
1 $\eta_r = 0$
2 $\eta_r = 0.01$
3 $\eta_r = 0.02$
4 $\eta_r = 0.05$
5 $\eta_r = 0.1$
$\beta_0/K = 1.0$
$\epsilon_i/\epsilon_r = 0$
$\eta_r = 0.1$
1 $\eta_i = 0$
2 $\eta_i = 0.01$
3 $\eta_i = 0.02$
4 $\eta_i = 0.05$
5 $\eta_i = 0.1$
$\mathrm{Re}\left\{\frac{\Delta k \sqrt{\epsilon_r}}{K}\right\}$
$\mathrm{Im}\left\{\frac{\Delta\beta}{K}\right\}$
$\mathrm{Im}\left\{\frac{\beta}{K}\right\}$

Fig. 4.3

all cases of both index and gain or loss coupling, the temporal gain or loss is peaked in the vicinity of Bragg resonance.

4. Third-Order Interaction

From the structure of the dispersion relation it is apparent that odd Bragg order interactions will exhibit similar Brillouin diagrams for index and gain or loss coupling. To exemplify this, consider the third Bragg order approximate parameters,

$$\frac{\delta_3}{K} \simeq \frac{\Delta k_3 \eta_r^{\frac{1}{2}}}{K} - \frac{27}{256}\left(1+\frac{\epsilon_i}{\epsilon_r}\right)\left(\eta_r + i\eta_i\right)^2 - \frac{i\,3\epsilon_i}{4\epsilon_r} \qquad (4.B11)$$

$$\frac{\chi_3}{K} \simeq \frac{243}{2048}\left(\eta_r + i\eta_i\right)^3 \qquad (4.B12)$$

where $\Delta k_3 = k - \beta_o/\epsilon_r^{\frac{1}{2}}$

$\beta_o = 3K/2$

Figure 4.4a, b demonstrates the dispersion characteristics for index and gain or loss coupling respectively. Except for the bandgap shift, the results are nearly identical to the first-order case. That is, the perturbation and gain or loss add at the center of the bandgap to enhance the spatial gain or loss for index coupling. In the case of gain or loss coupling the Brillouin diagram exhibits two distinct behaviors which depend upon strength of the gain or loss relative to the perturbation. For small average loss or gain, the effective spatial loss or gain is zero at the bandgap center.

The case of both index and gain or loss coupling is shown in Figure 4.4c, d. In all third-order cases, the temporal gain or loss is peaked in the Bragg region just as for the first-order case.

Fig. 4.4 Brillouin diagram at third Bragg order using: a) index coupling, b) gain/loss coupling and c/, d) both couplings in the ECW theory.

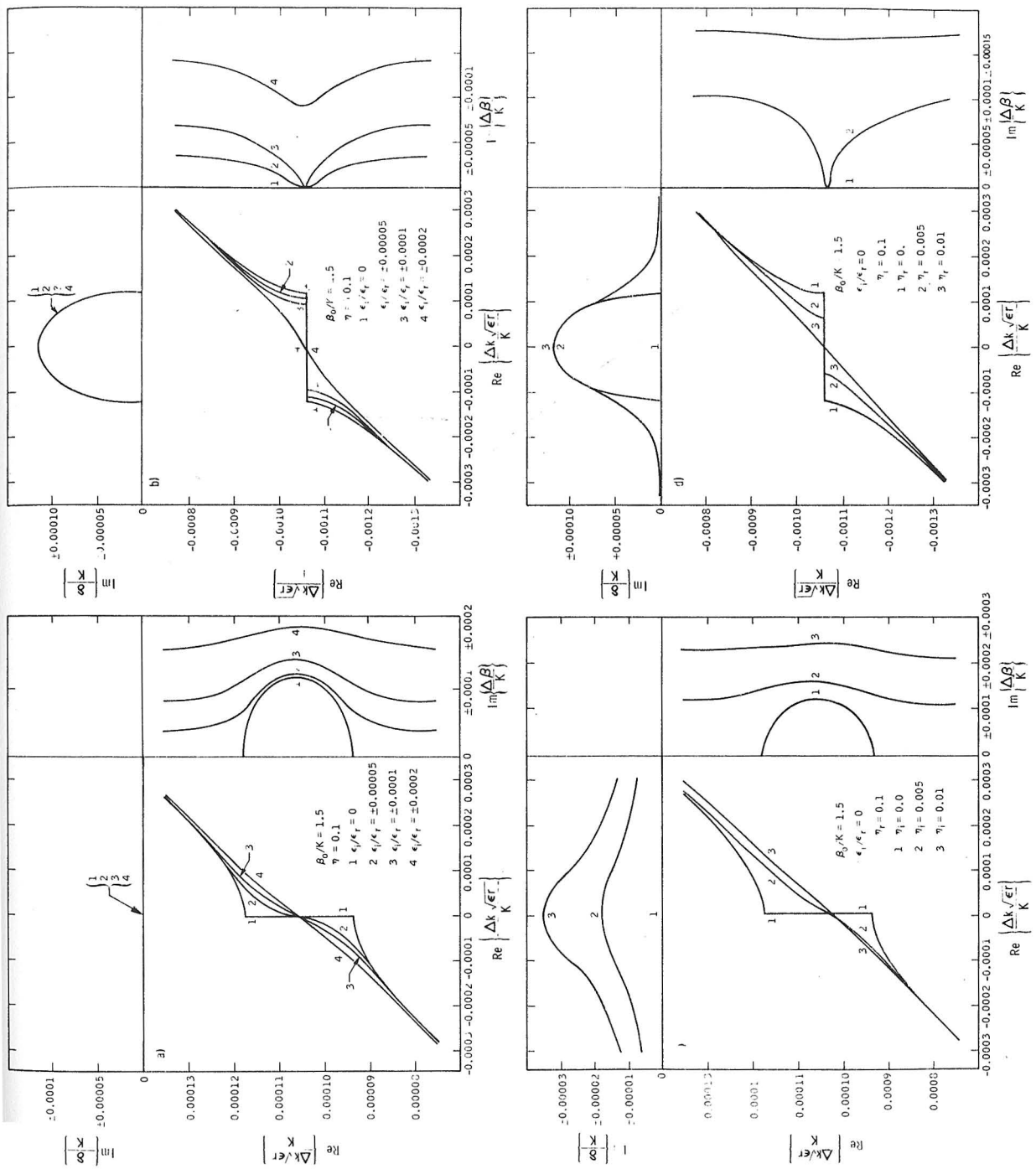
a)
b)
d)
Re $\left\{\frac{\Delta k\sqrt{\epsilon_r}}{K}\right\}$
Im $\left\{\frac{\delta}{K}\right\}$
Im $\left\{\frac{\Delta\beta}{K}\right\}$
$\beta_0/K = 1.5$
$\eta = 0.1$
1 $\epsilon_i/\epsilon_r = 0$
2 $\epsilon_i/\epsilon_r = \pm 0.00005$
3 $\epsilon_i/\epsilon_r = \pm 0.0001$
4 $\epsilon_i/\epsilon_r = \pm 0.0002$
β_0/K 1.5
$\epsilon_i/\epsilon_r = 0$
1 $\eta_i = 0.0$
2 $\eta_i = 0.005$
3 $\eta_i = 0.01$

Fig. 4.4

C. Multiharmonic Periodicities

Recent experimental work in higher-order DFB lasers[41, 71] and in multiply-periodic DFB lasers[70] make the results of multiharmonic ECW theory timely. As in the passive-lossless case, ECW theory cannot give explicit dispersion relations for arbitrary Bragg order N, since the number of significant Fourier components (f_p) have to be specified. However, the extension is straightforward, although laborious, for any specific case.

Consider the case where f_1 and f_N are the significant Fourier components of the periodicity and

$$\epsilon(z) = \epsilon_r + i\epsilon_i + \epsilon_r[\eta_1 f_1 \cos Kz + \eta_N f_N \cos(Nkz + \theta)] \tag{4.C1}$$

where $\eta_P = (\eta_r + i\,\eta_i)_P$, $P = (1, N)$ and $O(\eta_1 f_1)^N \sim O(\eta_N f_N)$.

Following the derivation of the previous chapter we find the slightly modified ECW equations:

$$\begin{aligned} F_1'(z) - i\,\delta_N F_1(z) &= i\,\chi_N^{+} B_1(z) \\ -B_1'(z) - i\,\delta_N B_1(z) &= i\,\chi_N^{-} F_1(z) \end{aligned} \tag{4.C2}$$

where

$$\delta_N = \frac{k^2\epsilon\left\{1 - \zeta_N(\eta_1 f_1/2)^2\left[\frac{N^2}{2(N^2-1)}\right]\right\} - \beta_o^2}{2\beta_o} \tag{4.C3}$$

$$\chi_N^{\pm} = \frac{k^2\epsilon}{2\beta_o}\left\{\frac{\eta_N f_N[\cos\theta \pm i\sin\theta]}{2} + \frac{(-1)^{N+1}(\eta_1 f_1)^N}{2^N}\ \frac{1}{\prod^{*}\{4n(n-N)/N^2\}^2}\right\} \tag{4.C4}$$

The resulting dispersion relation is

$$\left(\frac{\Delta\beta_N}{K}\right)^2 = \left(\frac{\delta_N}{K}\right)^2 - \frac{\chi_N^+ \chi_N^-}{K^2} \qquad (4.C5)$$

By varying the phase between the Fourier components, χ_N can be varied while δ_N remains constant. This allows control of the coupling and bandgap width $[= \frac{1}{2}(\chi_N^+ \chi_N^-)^{\frac{1}{2}}]$ without change in the bandgap shift.

For N = 2, the explicit dispersion relation is

$$\left(\frac{\Delta\beta_2}{K}\right)^2 = \left[\frac{\Delta k_2 \epsilon_r^{\frac{1}{2}}}{K} - \frac{(\eta_1 f_1)^2}{12}\right]^2 - \frac{1}{16}\left[(\eta_2 f_2)^2 + \frac{(\eta_1 f_1)^4}{4} - (\eta_1 f_1)^2 \eta_2 f_2 \cos\theta\right] \qquad (4.C6)$$

Figure 4.5 shows two examples of multiharmonic Brillouin diagrams at the second Bragg order. In Figure 4.5a, the index coupling case is shown when $(\eta_1 f_1)^2/2 = \eta_2 f_2 = 0.1$ and $\epsilon_i = 0$. The bandgap width and $\mathrm{Im}\{\Delta\beta_2/K\}_{max}$ both vary as $\sin(\theta/2)$. Figure 4.5b represents the case of index coupling with spatial wavenumber K and gain/loss coupling with wavenumber 2K. The result shows not only the $\mathrm{Re}\{\Delta\beta_2/K\}$ typical of gain/loss coupling, but also the effective gain/loss typical of index coupling. In both cases shown, $\mathrm{Im}\{\Delta k_2 \epsilon_r^{\frac{1}{2}}/K\} = 0$ for $\mathrm{Re}\{\Delta\beta_2/K\}$. The results for lossy media are similar if $(\epsilon_i/\epsilon_r)^2 \ll \chi_2^+ \chi_2^-/K^2$.

D. Comments on Complex Periodic Media

The extension of chapter III results to complex media has been mathematically straightforward for both the Floquet and the ECW results. However, interesting new features appeared in this

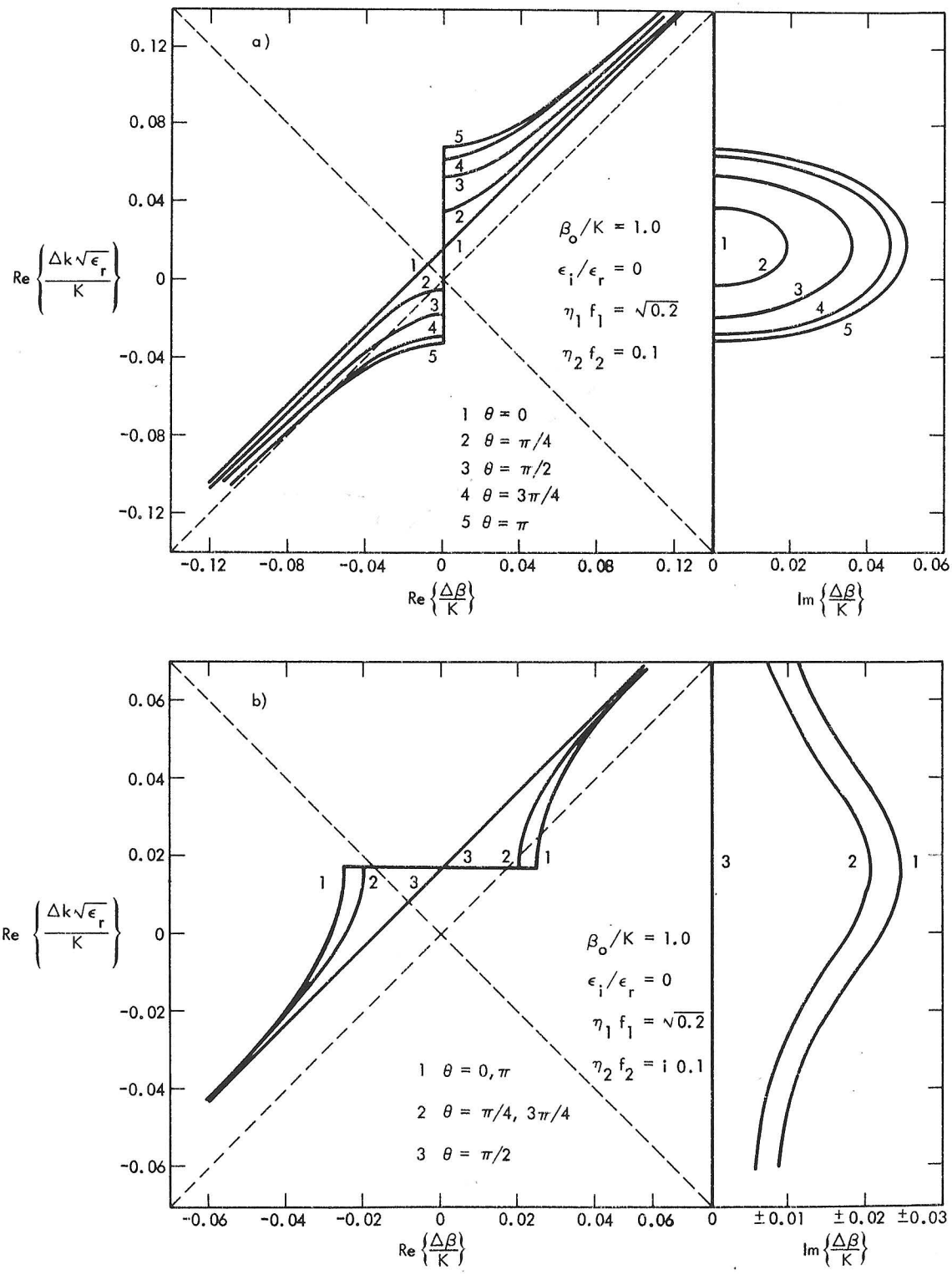

Fig. 4.5 Brillouin diagram at second Bragg order using multiharmonic periodicities in the ECW theory: a) index coupling with relative phase θ between two periodicities; b) index and gain/loss coupling. Note $\mathrm{Im}\{\Delta k \epsilon_r^{\frac{1}{2}}/K\} = 0$ for $\mathrm{Re}\{\Delta\beta/K\}$.

chapter:

1. Even and odd Bragg orders produce non-inverting and inverting bandgaps, respectively, for gain/loss coupling. Index coupling always produces the usual non-inverting bandgaps.
2. Phase speeding and positive bandgap shifts are produced by index coupling while gain/loss coupling produces phase slowing and negative bandgap shifts.
3. The average effective spatial gain or loss (i.e. $\mathrm{Im}\{\Delta\beta_N/K\}$) is significantly enhanced or diminished near Bragg resonance whenever $|\epsilon_i/\epsilon_r| < |\eta|^N$. Enhancement or reduction depends upon coupling type and Bragg order.
4. Temporal gain/loss (i.e. $\mathrm{Im}\{\Delta k_N \epsilon_r^{\frac{1}{2}}/K\}$) is either constant or is peaked at the bandgap center.
5. Multiharmonic periodicities offer great flexibility in changing the bandgap shape through phase and coupling variations. If the Fourier components f_p are dynamically generated, this opens the possibility of quickly controlling the feedback strength in DFB lasers or filters. Possible applications are in the areas of microwave and optical filters, switches and modulators.

In this chapter, Floquet and ECW results were not directly compared because little or no graphical differences appear whenever

$$|\eta_i|,\ |\eta_r|,\ |\epsilon_i/\epsilon_r| \leq 0.1$$

for the first few Bragg orders. The accuracy of the ECW results is similar to that of the passive-lossless case. The only notable difference occurred in the first order gain/loss coupling case where the ECW results predict $\mathrm{Im}\{\Delta\beta_1/K\} = 0$ at exact Bragg resonance. The Floquet result gives a small but finite value here for $\mathrm{Im}\{\Delta\beta_i/K\}$.

Portions of this chapter have been summarized elsewhere.[96]

CHAPTER V

STABILITY OF BRAGG INTERACTIONS IN ACTIVE PERIODIC MEDIA

The problem of wave stability was briefly mentioned in the previous chapter with regard to choosing the correct root of the dispersion relation for the frequency and longitudinal wavenumber. It is evident that the preceding monochromatic plane wave analysis is inadequate to predict the correct spatial and temporal behavior of waves in periodic media in all but the simplest (passive and lossless) cases. Our purpose is to formulate the stability problem in such a way that the preceding ECW equations can unambiguously define wave characteristics.

The problem of wave stability was greatly clarified through the original work of Sturrock[72] which provided a method for distinguishing between growing waves (unstable media) and decaying waves (stable media) through the dispersion relation. Sturrock further divided unstable media into convectively unstable and absolutely unstable media. The former referred to waves which grew and then decayed at a given point in space like waves in traveling-wave amplifiers. The latter referred to waves which grow everywhere in space as those waves found in backward wave oscillators. This work was extended by Briggs[73] and was formulated as a mathematical prescription which unambiguously classified waves according to their stability. A large number of electron-stream interactions demonstrated the usefulness of Briggs' method in plasma physics. The

stability criterion was again extended to include time-varying media by Cassedy[56] who examined the stability of parametric interactions due to space-time periodicities.

In this chapter, the stability of time-independent active periodic media is studied at the first- and higher-order Bragg resonances. The stability classification depends only upon the dispersion relation or the Brillouin diagram and hence the ECW theory of the previous two chapters will be used. We will follow the procedure suggested by Briggs. This requires the formulation of the field response as a function of a source, localized in space and time.

In section A the ECW equations are developed with sources present and the stability criterion is stated. The application of the criterion to the first two Bragg resonances is carried out in detail in section B. These resonances are the archetypes for all odd- and even-order Bragg interactions. Explicit values for instability threshold, frequency and growth rate are given. Section C contains a brief explanation of the effects of complex coupling (i.e. $\eta = \eta_r + i\eta_i$) and multiharmonic periodicities upon instability parameters. A short discussion of the results is given in section D.

A. ECW Equations with Sources

We carry out the usual manipulations with the Maxwell equations that include a current density source $J(z)$. The resulting inhomogeneous wave equation[67] for a TEM wave in longitudinally periodic media is

$$\left[\frac{\partial^2}{\partial z^2} + k^2\epsilon(z)\right]E(z,\omega) = -i\omega\mu_o J(z,\omega) \qquad (5.A1)$$

$$\text{where } \begin{Bmatrix} E(z,\omega) \\ J(z.\omega) \end{Bmatrix} = \int_{-\infty}^{\infty} \begin{Bmatrix} E(z,t) \\ J(z,t) \end{Bmatrix} e^{i\omega t}\, dt$$

$$\epsilon(z) = \epsilon_r + i\epsilon_i + \epsilon_r \sum_p (\eta_r + i\eta_i)_p f_p \cos pKz$$

Assume that E(z) is made up of the N+3 waves $F(z)_{1+2n/N}$, $F_1(z), \ldots,$ $B_1(z)$, $B(z)_{1+2n/N}$ that are used in the ECW formulation. We then find the following N+3 ECW equations for singly periodic media at the N^{th} Bragg order.

$$\left.\begin{aligned}
&[k^2\epsilon - (1+2/N)^2\beta_o^2]F_{1+2N} + 2i(1+2/N)\beta_o F'_{1+2/N} = \frac{-k^2\epsilon\eta}{2}F_1 - i\omega\mu_o J^+_{1+2/N} e^{-i(1+2/N)\beta_o z} \\
&[k^2\epsilon - \beta_o^2]F_1 + 2i\beta_o F'_1 = \frac{-k^2\epsilon\eta}{2}(F_{1-2/N} + F_{1+2/N}) - i\omega\mu_o J^+_1 e^{-i\beta_o z} \\
&\qquad\vdots \\
&[k^2\epsilon - \beta_o^2]B_1 - 2i\beta_o B'_1 = \frac{-k^2\epsilon\eta}{2}(B_{1-2/N} + B_{1+2/N}) - i\omega\mu_o J^-_1 e^{i\beta_o z} \\
&[k^2\epsilon - (1+2/N)^2]B_{1+2/N} - 2i(1+2/N)\beta_o B'_{1+2/N} = \frac{-k^2\epsilon\eta}{2}B_1 - i\omega\mu_o J^-_{1+2/N} e^{i(1+2/N)\beta_o z}
\end{aligned}\right\} \qquad (5.A2)$$

where the arguments with respect to z and t have been dropped and the primes denote differentiation with respect to z. The current densities $J^{\pm}(z)_{1-2n/N}$ are the portions of J(z) which are in phase synchronism with the rest of the equation. We accomplish this by truncation in wavenumber space such that

$$J^{\pm}_{1-2n/N}(\beta_{\mp}(1-2n/N)\beta_o) = J(\beta_{\mp}(1-2n/N)\beta_o)\,\text{rect}\{[\beta_{\mp}(1-2n/N)\beta_o]/\Delta\hat{\beta}\} \qquad (5.A3)$$

$$(n = -1, 0, 1, 2, \ldots)$$

where

$$J(\beta) = \int_{-\infty}^{\infty} J(z)e^{-i\beta z}\, dz$$

$$\text{rect}(\beta) = \begin{cases} 1 & |\beta| < \frac{1}{2} \\ 0 & |\beta| > \frac{1}{2} \end{cases}$$

$$\Delta\hat{\beta} \ll \beta_o$$

As we shall see, the exact truncation details are unimportant since the current will only contribute to the field at wavenumber $\beta = \beta_o$. Since we are particularly interested in the waves $F_1(z)$ and $B_1(z)$, assume that the current is slowly varying in wavenumber over the N+3 significant waves. Thus, we consider only the current contributions $J_1^+(z)$ and $J_1^-(z)$ and ignore current contributions $O(\eta)$. Using the above approximation and the other usual ECW approximations we find the coupled equations,

$$\left.\begin{aligned} F_1'(z,\omega) - i\delta_N F_1(z,\omega) &= i\chi_N B_1(z,\omega) - \frac{\omega\mu_o}{2\beta_o} J_1^+(z,\omega)e^{-i\beta_o z} \\ -B_1'(z,\omega) - i\delta_N B_1(z,\omega) &= i\chi_N F_1(z,\omega) - \frac{\omega\mu_o}{2\beta_o} J_1^-(z,\omega)e^{i\beta_o z} \end{aligned}\right\} \quad (5.A4)$$

These equations can be solved by taking Fourier transforms with respect to z and solving for $F_1(\Delta\beta, \omega)$ and $B_1(\Delta\beta, \omega)$. The inverse transforms produce the time and space variation,

$$F_1(z,t) = \frac{i\mu_o}{NK^2} \int\int_{-\infty}^{\infty} \frac{\omega\{(\Delta\beta+\delta)J_1^+(\Delta\beta+\beta_o,\omega) - \chi J_1^-(\Delta\beta-\beta_o,\omega)\}e^{i(\Delta\beta z - \omega t)}}{D(\Delta\beta,\omega)} \frac{d\Delta\beta\, d\omega}{(2\pi)^2} \quad (5.A5)$$

$$B_1(z,t)=\frac{i\mu_o}{NK^2}\int\int_{-\infty}^{\infty}\frac{\omega\{(\Delta\beta+\delta)J_1^-(\Delta\beta-\beta_o,\omega)-\chi J_1^+(\Delta\beta+\beta_o,\omega)\}e^{i(\Delta\beta z-\omega t)}}{D(\Delta\beta,\omega)}\frac{d\Delta\beta d\omega}{(2\pi)^2} \tag{5.A6}$$

where

$$D(\Delta\beta,\omega) = \left(\frac{\Delta\beta}{K}\right)^2 - \left(\frac{\delta}{K}\right)^2 + \left(\frac{\chi}{K}\right)^2 = 0 \tag{5.A7}$$

is the dispersion relation and the radian frequency ω is related to the wavenumber by $\omega = c(k_o+\Delta k)/\epsilon_r^{\frac{1}{2}}$ and $\beta-\beta_o = \Delta\beta$ as before. All subscripts N have been dropped for simplicity. Assume that the current is turned on at t = 0, hence J(z, t) = 0 for t < 0.

It is apparent that the integrand of (5.A5-6), excluding the currents, is the Green's function for a periodic medium in the ECW approximation. It is of similar form to an exact expression which accounts for all space harmonics and current components.[75]

As pointed out by both Sturrock and Briggs, it is necessary to investigate wave packets in space and time due to localized sources. Therefore, the previous ECW equations (5.A4) with a source turned on at t = 0 are a useful start. The remaining problem is to find how $F_1(z,t)$ and $B_1(z,t)$ behave asymptotically by choosing the contours of integration correctly and unambiguously. Note that the poles of the integrand, or the roots of $D(\Delta\beta,\omega)$, determine the field response.

For causality, it is necessary to carry out the frequency integration <u>above</u> all singularities. The integration contour is shown in Figure 5.1a. Note that no roots appear in the region enclosed by the contour for t < 0. This contour is the rotated Bromwich contour that is used for Laplace transforms. The contour in the wavenumber plane is ambiguous since the roots of $D(\Delta\beta,\omega)$ may cross the real $\Delta\beta$

axis for different values of $\omega(= \omega_r + i\omega_i)$. This difficulty has been remedied by Briggs[73] by use of the following physical criterion: for a source with sufficiently large temporal growth rate (i.e. large $\omega_i = s > 0$), the waves away from the source must spatially decay. Therefore, if the contour is chosen in the ω plane to satisfy causality for $\omega_i = s$, the roots of $D(\Delta\beta, \omega)$ will determine the response for $F(z, t)$ and $B(z, t)$ and must represent spatially decaying waves. Figure 5.1b shows this condition. Since it is convenient to integrate along the axis $\omega_i = 0$, we depress the contour around singularities down to the real ω axis (Figure 5.1c). As $\omega_i \to 0$ for fixed ω_i, the roots of $D(\Delta\beta, \omega)$ will: 1) stay in the same half plane of $\Delta\beta$; 2) cross the real $\Delta\beta$ axis; or 3) merge from opposite sides of the real $\Delta\beta$ axis in pairs for some $\omega_i = \sigma > 0$. As shown by Briggs, the above cases lead respectively to: 1) decaying waves (stable media); 2) amplifying waves (convectively unstable media); or 3) time growing waves (absolutely unstable media). In the first case, the contour in the $\Delta\beta$ plane along real $\Delta\beta$ axis is not deformed (i.e. decaying roots) while in the second case the contour is deformed (i.e. amplifying roots) by root crossings (Figure 5.1d). In the third case, as $\omega_i \to \sigma$ for some $\omega_r = \omega_o$ (Figure 5.1e), the merging root behavior in the $\Delta\beta$ plane (Figure 5.1f) prevents the distortion of the contour since the integration must be carried out between the merging roots. The details of the integration are carried out in Appendix A for absolute instabilities with the proper contours shown in Figure A.1. It can be shown (equation (A.7)) that the field varies as

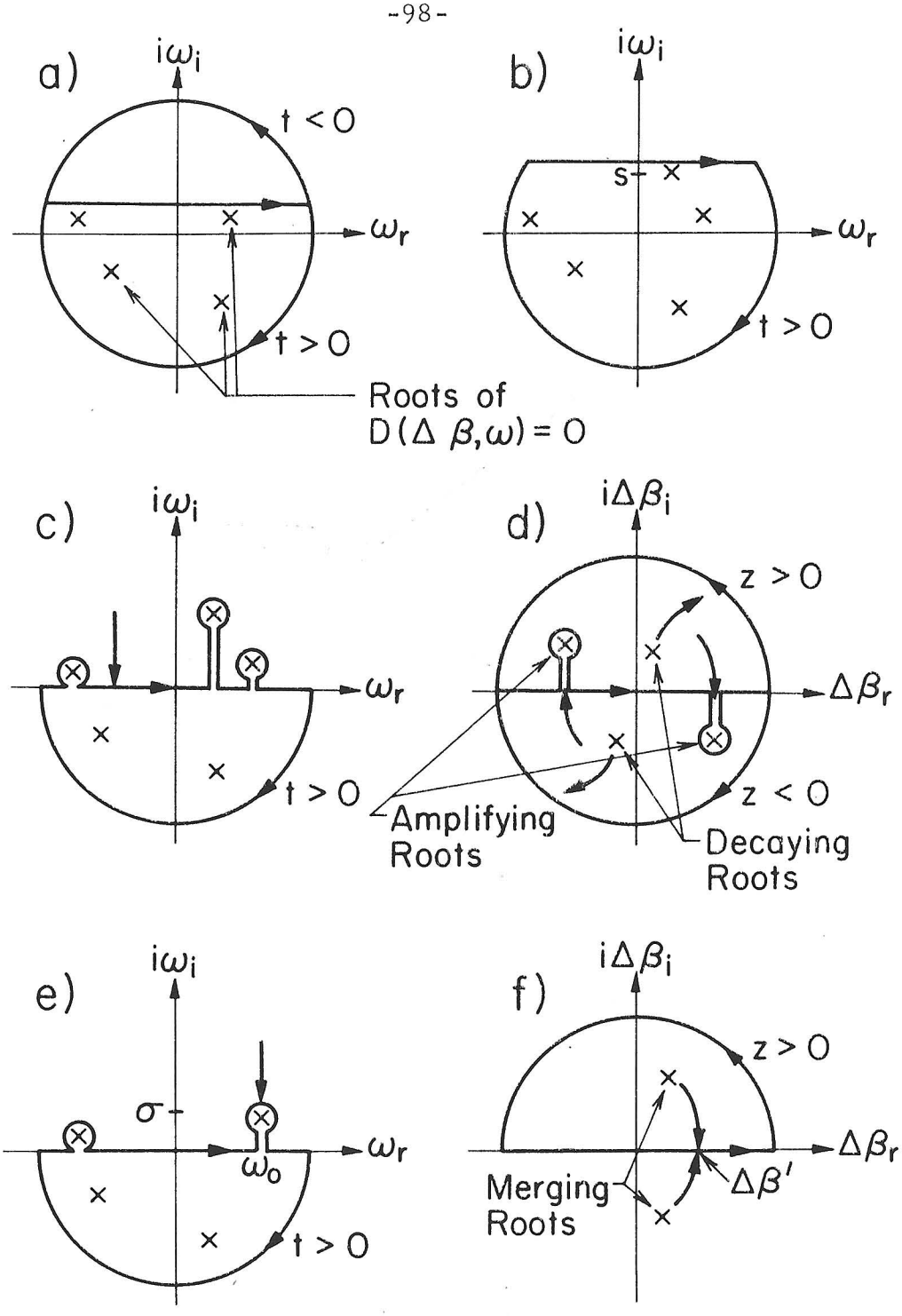

Fig. 5.1 Integration contours in a) ω plane for causality, b) ω plane for $t > 0$ and time growing source, c) ω plane with deformation to ω_r axis, d) $\Delta\beta$ plane which corresponds to c) with changing roots, e) ω plane for absolute instability at $\omega_i = \sigma$, f) $\Delta\beta$ plane corresponding to e).

$$F(z,t) \propto \frac{e^{i[\Delta\beta' z - \omega_o t]} e^{\sigma t}}{t^{\frac{1}{2}}} \qquad (5.A8)$$

Note that the frequency and wavenumber of the instability are just that of the merging roots (i.e. $\Delta\beta = \Delta\beta'$, $\omega = \omega' = \omega_o + i\sigma$). Therefore, the waves grow in time as $e^{\sigma t}$. The absolute instability parameters are determined from the mapping of the dispersion equation roots in the $\Delta\beta$ plane for variable ω_i and different constant values of ω_r.

B. Application of Stability Criteria to Bragg Resonances

The Brillouin diagrams take on different characteristics for even and odd Bragg orders in the case of index ($\eta = \eta_r$) and gain ($\eta = i\,\eta_i$) coupling. Thus, we will examine in detail the first and second Bragg resonances for singly periodic media since they are the archetypes of all even and odd Bragg order n interactions.

The first-order Brillouin diagrams are repeated in Figure 5.2a, b for the case of index and gain coupling respectively with various values of average gain or loss. Figures 5.3 and 5.4 show a mapping of the roots of $D(\Delta\beta, \omega)$ in the $\Delta\beta$ plane as ω_i varies from large positive values to zero for several values of ω_r. Normalized frequency $\Delta k\, \epsilon_r^{\frac{1}{2}}/K$ is used instead of ω. Figure 5.3a shows the case of no average gain or loss ($\epsilon_i = 0$) and index coupling which corresponds to curve 1 of Figure 5.2a. The merging root behavior is noticed for $\mathrm{Re}\{\Delta k\, \epsilon_r^{\frac{1}{2}}/K\} = \eta_r/8$ when $\mathrm{Im}\{\Delta k\, \epsilon_r^{\frac{1}{2}}/K\} = 0$. Thus, the instability has no temporal growth and the medium is actually stable. This is also noted from the fact that $\mathrm{Im}\{\Delta k\, \epsilon_r^{\frac{1}{2}}/K\} = 0$ for all $\mathrm{Re}\{\Delta\beta/K\}$ and hence no instability is possible. Therefore, the physical notion

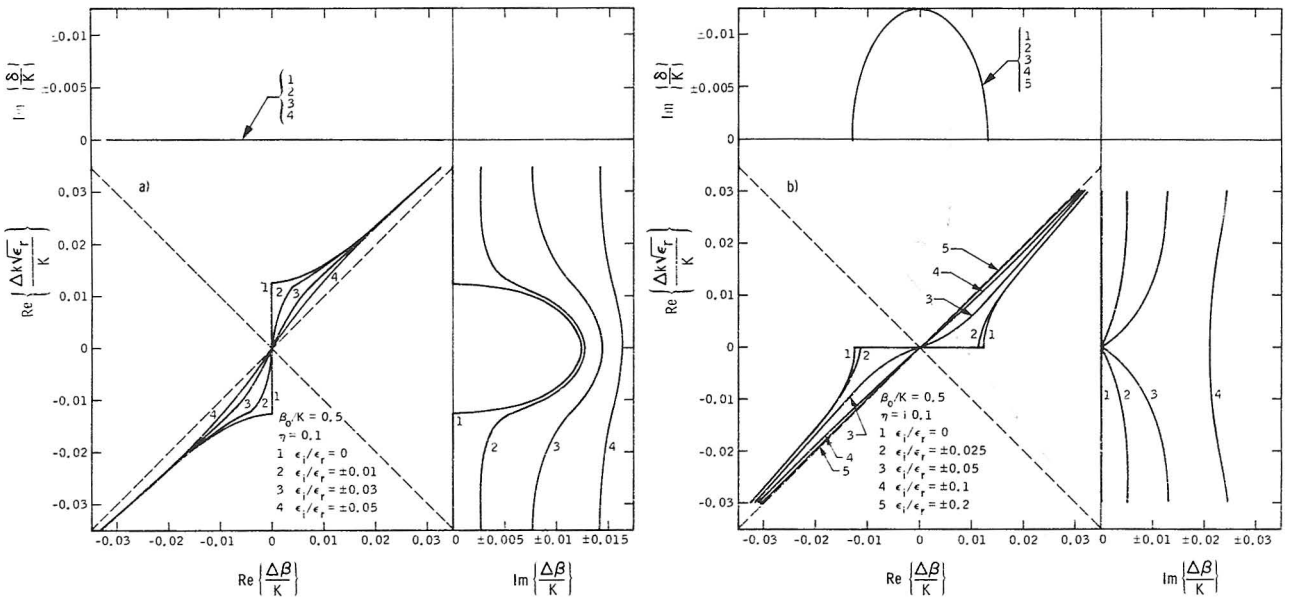

Fig. 5.2 Brillouin diagram at the first Bragg order for the ECW theory showing a) index and b) gain/loss coupling.

of the stability of passive periodic media is confirmed. Since there are no root crossings, the proper choice of the sign of $\mathrm{Im}\{\Delta\beta/K\}$ is that which indicates spatially decaying waves. Figure 5.3b shows the case of index coupling with average loss ($\epsilon_i > 0$) which corresponds to curve 3 of Figure 5.2a. There are no root crossings or mergings and hence the media is stable. The proper signs for $\mathrm{Im}\{\Delta k\, \epsilon_r^{\frac{1}{2}}/K\}$ and $\mathrm{Im}\{\Delta\beta/K\}$ indicate temporally and spatially decaying outgoing waves. The case of index coupling with average gain ($\epsilon_i < 0$) which corresponds to curve 3 of Figure 5.2a is shown in Figure 5.3c. In all cases, similar curves exist for $\mathrm{Re}\{\Delta k\, \epsilon_r^{\frac{1}{2}}/K\} < 0$ which are mirror images about the imaginary $\Delta\beta/K$ axis. Note that the root crossing occurs for $\Delta k\, \epsilon_r^{\frac{1}{2}}/K = i\,\epsilon_i/4\epsilon_r \pm \eta_r/8$. Thus, absolute instabilities occur for index coupling with (the threshold condition) positive average gain at the bandgap edges corresponding to $\mathrm{Re}\{\Delta k\, \epsilon_r^{\frac{1}{2}}/K\} = \pm \eta_r/8$. The normalized temporal growth rate is $\mathrm{Im}\{\Delta k\, \epsilon_r^{\frac{1}{2}}/K] = -\epsilon_i/4\epsilon_r$ and the longitudinal wavenumber $\beta = \beta_o$ is real. (Bandgap edges will refer to the lossless case for this chapter.)

Figure 5.4 shows similar mappings of the dispersion equation roots for gain coupling. In Figure 5.4a, b, c the merging root behavior occurs at the value $\Delta k\, \epsilon_r^{\frac{1}{2}}/K = -i\,\epsilon_i/4\epsilon_r + i|\eta_i|/8$. Thus, for gain modulation, absolute instability occurs at the center of the bandgap for average gain ($\epsilon_i < 0$) and average loss ($\epsilon_i > 0$) whenever the threshold $\epsilon_i/\epsilon_r < |\eta_i|/2$ is satisfied. The result for zero average gain is not surprising since the inverted bandgaps are similar to those of parametric instabilities and backward wave oscillators. However, note that gain-coupled media may also have instabilities

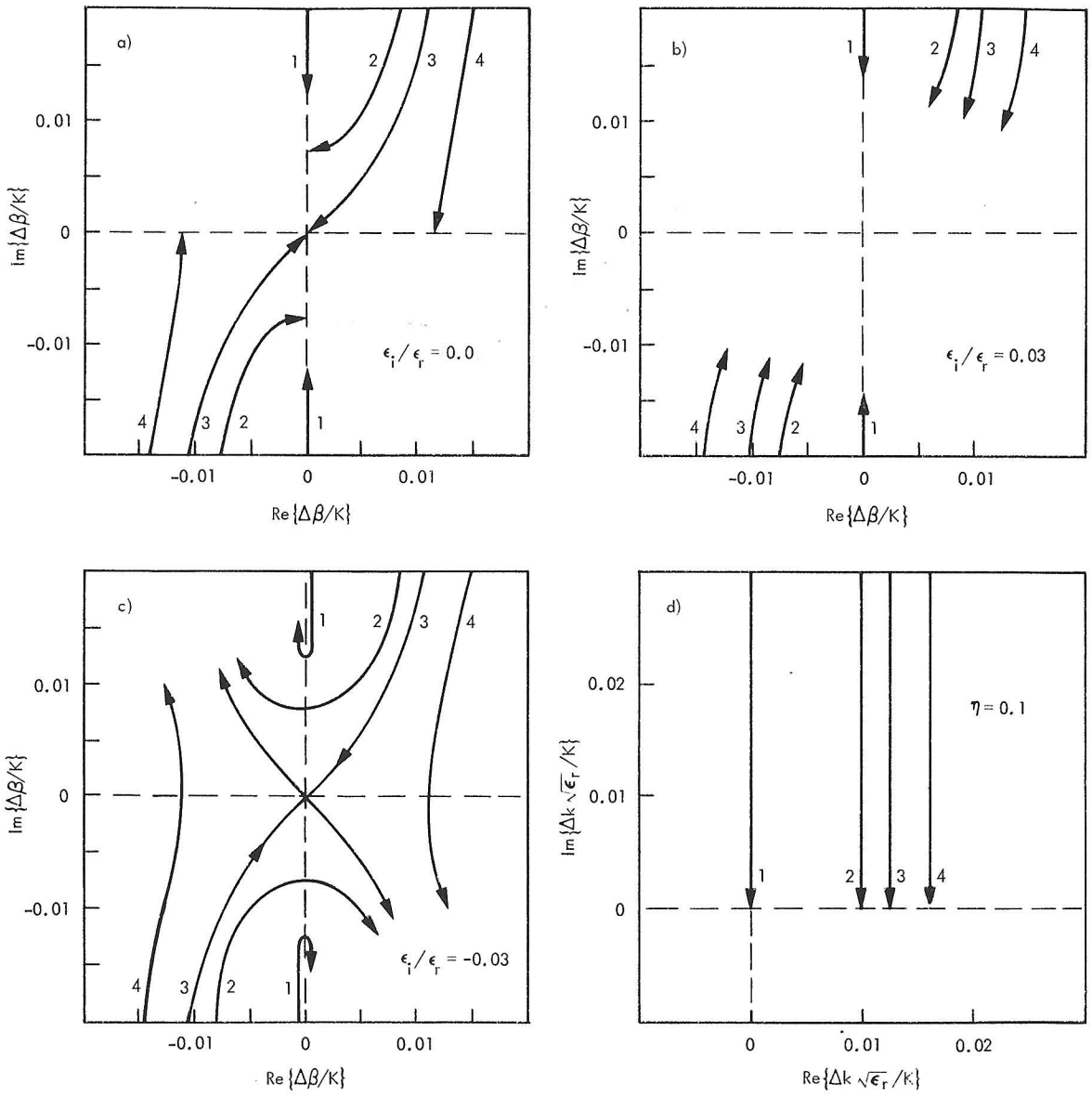

Fig. 5.3 Locus of the roots of the dispersion relation in the $\Delta\beta/K$ plane at the first Bragg order for index coupling with average gain a) $\epsilon_i/\epsilon_r = 0.0$, b) $\epsilon_i/\epsilon_r = 0.03$ and c) $\epsilon_i/\epsilon_r = -0.03$. Locus of $\Delta k\, \epsilon_r^{\frac{1}{2}}/K$ for the above is given in d). Similar loci in the $\Delta\beta/K$ plane are produced for $\mathrm{Re}\{\Delta k \epsilon^{\frac{1}{2}}/K\} < 0$.

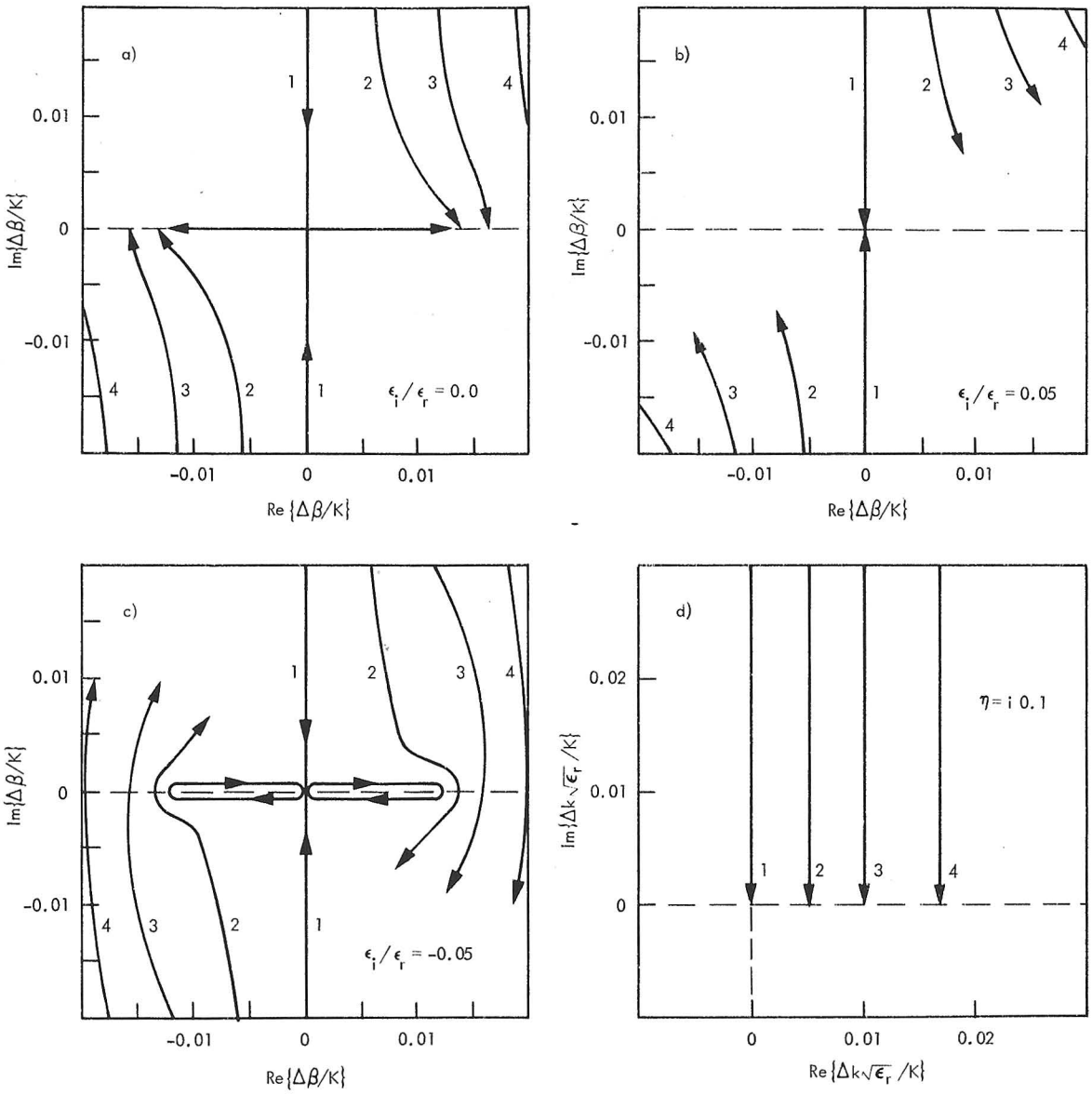

Fig. 5.4 Locus of the roots of the dispersion relation in the $\Delta\beta/K$ plane at the first Bragg order for gain coupling with average gain a) $\epsilon_i/\epsilon_r = 0.0$, b) $\epsilon_i/\epsilon_r = 0.05$ and c) $\epsilon_i/\epsilon_r = -0.05$. Locus of $\Delta k\, \epsilon_r^{\frac{1}{2}}/K$ for the above is given in d).

when the average gain is negative as long as the gain periodically takes on positive values (i.e. the average loss is less than some fraction of the variation).

As evidenced by the structure of the dispersion relations of chapters III and IV and the repeated Brillouin diagram of Figure 5.5, index and gain coupling at the second Bragg resonance display similar characteristics, to the first-order index coupling diagrams (i.e. no inverted bandgaps appear). Thus, the stability of both index and gain coupling at the second Bragg resonance should be similar to that of the first order index coupling case since the stability criteria is dependent only upon the dispersion relation. The only difference should be in the sign of the bandgap shift, and hence the relative instability frequency, which is positive or negative for index or gain coupling respectively. Indeed this is true. The mapping of the complex roots (not shown) of $D(\Delta\beta, \omega)$ as $\omega_i \to 0$ resembles Figure 5.3. The absolute instability occurs at the bandgap edges for index or gain coupling with temporal growth rate given by $\mathrm{Im}\{\Delta k\, \epsilon_r^{\frac{1}{2}}/K\}$ at the bandgap. The threshold condition requires positive gain ($\epsilon_i < 0$) for absolute instabilities at the second Bragg resonance for both coupling types.

The results of odd and even Bragg resonances show different stability characteristics as exemplified by the specific cases of N= 1, 2 discussed above. The mathematical conditions for absolute instability parameters can be found from the above considerations and the ECW dispersion relation. For any Bragg order N, oscillation takes place at

$$\mathrm{Re}\{\delta_N/K\} = \pm\, \mathrm{Re}\{\chi_N/K\} \qquad (5.B1)$$

with temporal growth rate

$$\mathrm{Im}\{\delta_N/K\} = +\, \mathrm{Im}\{\chi_N/K\} \qquad (5.B2)$$

at or above the threshold

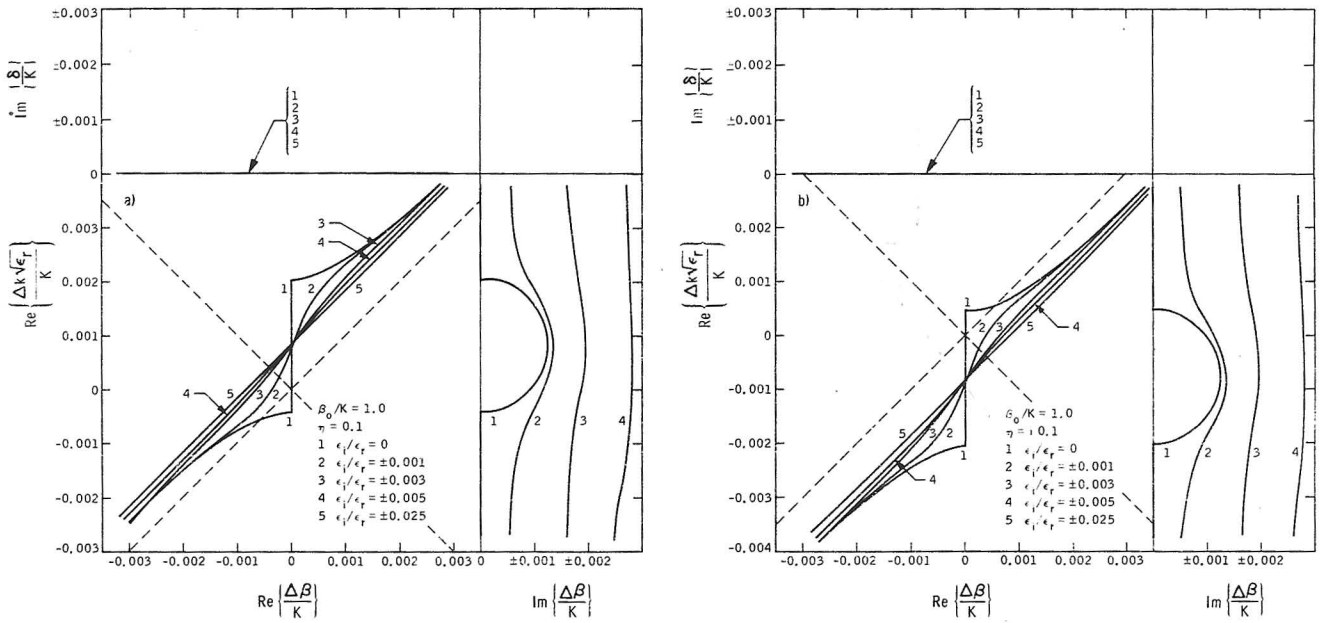

Fig. 5.5 Brillouin diagram of the second Bragg order for the ECW theory, showing a) index and b) gain/loss coupling.

$$\mathrm{Im}\{\Delta k_N \varepsilon_r^{\frac{1}{2}}/K\} = 0 \ . \qquad (5.B3)$$

The results for the first few Bragg resonances are summarized in Table 5.1. It is noted that with increasing Bragg order, the threshold approaches zero for all couplings since η is usually small. Also the instability frequencies tend to cluster above (index coupling) or below (gain coupling) the exact Bragg resonance for higher Bragg orders. This is due to the bandgap shift.

The first two Bragg resonances have been shown to be archetypical of all Bragg resonances. In particular we found that for index coupling, absolute instabilities occur for positive average gain at both bandgap edges with temporal growth rates given by $\omega_i = \sigma$ at the bandgap. For gain coupling, the behavior is identical to the index coupling case for N even, with the exception of the instability frequency which is shifted due to the bandgap shift. For gain coupling with odd N, absolute instabilities occur only at the center of the bandgap with temporal growth rates equal to the value of ω_i at the bandgap.

The correct choice for the sign of $\mathrm{Im}\{\Delta\beta/K\}$ depends upon the position of the roots of the dispersion relation as $\omega_i \to 0$ or at the merging root point $\omega_i = \sigma$. If the roots have crossed the real $\Delta\beta/K$ axis the outgoing waves are amplifying and if they do not cross, the outgoing waves are decaying. Thus, for the case of absolute instabilities, there will be both amplifying and decaying waves at frequencies adjacent to the instability (see Figure 5.3-4). However, this behavior is overshadowed by the absolute instability and is not important for infinite media. The proper sign of $\mathrm{Im}\{\delta/K\}$ is chosen by the fact that

Coupling	Order	Threshold	Frequency	Growth Rate
$\eta = \eta_r$	N=1	$\frac{\epsilon_i}{\epsilon_r} = 0$	$\pm\frac{\eta_r}{8}$	$-\frac{\epsilon_i}{4\epsilon_r}$
$\eta = i\eta_i$	N=1	$\frac{\epsilon_i}{\epsilon_r} = \frac{\lvert\eta_i\rvert}{2}$	0	$-\frac{\epsilon_i}{4\epsilon_r} + \frac{\lvert\eta_i\rvert}{8}$
$\eta = \eta_r$	N=2	$\frac{\epsilon_i}{\epsilon_r} = 0$	$\frac{\eta_r^2}{12} \pm \frac{\eta_r^2}{8}$	$-\frac{\epsilon_i}{2\epsilon_r}\left(1 - \frac{\eta_r^2}{6}\right)$
$\eta = i\eta_i$	N=2	$\frac{\epsilon_i}{\epsilon_r} = 0$	$-\frac{\eta_i^2}{12} \pm \frac{\eta_i^2}{8}$	$-\frac{\epsilon_i}{2\epsilon_r}\left(1 + \frac{\eta_i^2}{6}\right)$
$\eta = \eta_r$	N=3	$\frac{\epsilon_i}{\epsilon_r} = 0$	$\frac{27\eta_r^2}{256} \pm \frac{243\eta_r^3}{2048}$	$-\frac{3\epsilon_i}{4\epsilon_r}\left(1 - \frac{9\eta_r^2}{64}\right)$
$\eta = i\eta_i$	N=3	$\frac{\epsilon_i}{\epsilon_r} = \frac{81\lvert\eta_i\rvert^3}{512} \Big/ \left[1 + \frac{9\eta_i^2}{64}\right]$	$-\frac{27\eta_i^2}{256}$	$-\frac{3\epsilon_i}{4\epsilon_r}\left(1 + \frac{9\eta_i^2}{64}\right) + \frac{243\lvert\eta_i\rvert^3}{2048}$
$\eta = \eta_r$	N=4	$\frac{\epsilon_i}{\epsilon_r} = 0$	$\frac{2\eta_r^2}{15} \pm \frac{\eta_r^4}{9}$	$-\frac{\epsilon_i}{\epsilon_r}\left(1 - \frac{2\eta_r^2}{15}\right)$
$\eta = i\eta_i$	N=4	$\frac{\epsilon_i}{\epsilon_r} = 0$	$-\frac{2\eta_i^2}{15} \pm \frac{\eta_i^4}{9}$	$-\frac{\epsilon_i}{\epsilon_r}\left(1 + \frac{2\eta_i^2}{15}\right)$

Table 5.1 Threshold, instability frequency and temporal growth rate for index and gain coupling at the first four Bragg orders. All frequency and growth rate values are in units of $\Delta k \epsilon_r^{\frac{1}{2}}/K$.

the dominant time behavior is controlled by the highest root in the ω plane. This is equal to the value $\omega_i = \sigma$ that occurs when the roots of $\Delta\beta/K$ merge.

In all cases where the gain is not large enough to support absolute instabilities, the medium is stable and the outgoing waves decay spatially due to coupling and losses. Thus, because there are no axis crossings of the roots of $D(\Delta\beta, \omega)$ in the $\Delta\beta/K$ plane, the sign of $\mathrm{Im}\{\Delta\beta/K\} > 0$ is specified for outgoing waves. The sign of $\mathrm{Im}\{\delta/K\}$ is chosen to correspond to the least lossy wave (i.e. $\mathrm{Im}\{\delta/K\} > 0$) since this root produces the dominant field contribution. Thus, for stable media the periodicity will enhance the spatial decay and not affect the temporal decay for index and even-order gain coupling. For odd-order gain coupling the spatial and temporal decay are both diminished.

C. Complex Coupling and Multiharmonic Periodicities

In practical cases, both index and gain periodicity will occur together ($\eta = \eta_r + i\,\eta_i$). This case, referred to as complex coupling, will usually cause absolute instabilities to occur at two frequencies due to finite η_r. The explicit conditions are involved for arbitrary Bragg order but reduce to the following form at first order: absolute instabilities will occur in pairs at the bandgap edges ($\mathrm{Re}\{\Delta k_1\, \epsilon_r^{\frac{1}{2}}/K\} = \pm\, \eta_r/8$) with a growth rate $\mathrm{Im}\{\Delta k_1\, \epsilon_r^{\frac{1}{2}}/K\} = -\epsilon_i/4\epsilon_r + |\eta_i|/8$; the threshold is $\epsilon_i/\epsilon_r = |\eta_i|/2$ and thus cannot be reduced below the gain coupling value.

At even Bragg resonances, where the threshold was previously zero, a reduction in threshold can take place for the case of complex couplings. As an example consider the second Bragg

resonance. Figure 5.6 repeats the Brillouin diagram for complex coupling and $\epsilon_i/\epsilon_r = 0$. For equal amounts of index and gain coupling (i.e. $\eta_r = \eta_i$) the curves give inverted bandgaps. Thus, one expects absolute instabilities at exact Bragg resonance. It can be shown that the instability threshold is reduced to $\epsilon_i/\epsilon_r = 5|\eta_i \eta_r|/6$ (average loss). Two absolute instabilities occur for $\eta_r \neq \eta_i$ and $\epsilon_i/\epsilon_r = 0$ at the frequencies where $\mathrm{Im}\{\Delta\beta_2/K\}$ is zero and where it is maximum. Thus, as the ratio η_i/η_r approaches zero or infinity, the instability frequencies merge to the center of the bandgap and as $\eta_i/\eta_r \rightarrow 1$ the instability frequencies tend to merge in pairs toward exact Bragg resonance. The growth rates are found from the value of $\mathrm{Im}\{\Delta k_2\, \epsilon_r^{\frac{1}{2}}/K\}$ at the bandgap center.

The application of the stability criteria to multiharmonic periodicities is similar to the previous analysis (chapters III, IV) with the proper phase mismatch δ_N and coupling χ_N substituted into the dispersion relation. Although there is little or no effect at the first Bragg order for changes from sinusoidal periodicities to other typical periodicities, the effects at higher Bragg orders ($N \geq 2$) may be significant due to Fourier components f_N. It can be shown (Appendix B) that the coupling is increased from values $O(\eta^2)$ for sinusoidal periodicities to values $O(\eta)$ for sawtooth periodicities at the second Bragg resonance.

At the third Bragg order, the coupling can be increased from values $O(\eta^3)$ to values $O(\eta)$ for square-, triangular- or sawtooth-wave periodicities. This implies that instability

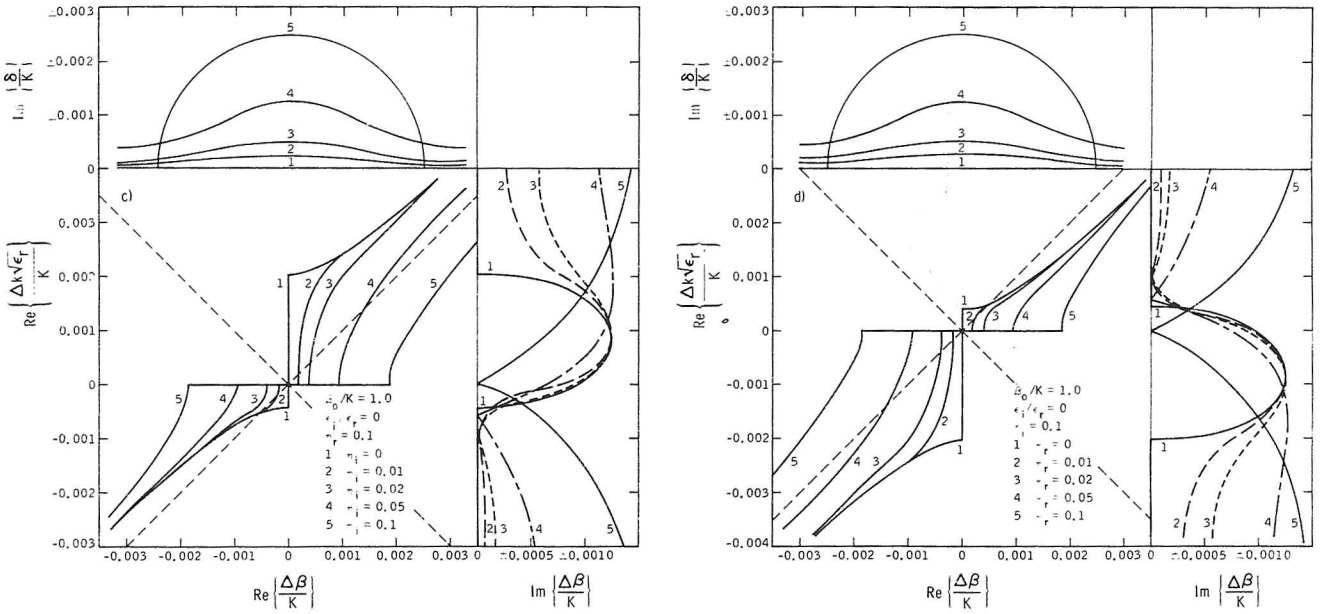

Fig. 5.6 Brillouin diagram at second Bragg order for ECW theory when both index and gain/loss coupling are present.

thresholds can be changed at higher Bragg orders by the use of non-sinusoidal periodicities. Typically, $|\eta| \sim O(10^{-2}\text{-}10^{-5})$ in integrated optics applications.

D. Comments on Stability

In this chapter we have found the stability criteria for time-independent periodic media. This media may support either decaying (stable) or temporally growing (absolutely unstable) waves in basically dispersionless dielectrics. The ECW equations provided explicit values of threshold, instability frequency and temporal growth rates for absolute instabilities. Average positive gain was required for oscillation at the bandgap edges for index coupling and even-order gain coupling. For odd-order gain coupling, the average gain could be negative if the gain periodically took on positive values and the oscillation took place at the bandgap center. In some cases both types of coupling or multiharmonic periodicities could reduce thresholds.

There has been some question as to the effect of boundaries upon DFB oscillation. It is apparent from the preceding sections that instability takes place when certain modes of the active periodic media achieve threshold. No boundaries are needed since feedback action is produced by the periodicity.

It appears that for frequencies other than the instability frequencies, waves may either decay or be convectively amplified if the structure is short enough such that the absolute instabilities do not occur. In this case, the active periodic structure might be

used as a filter-amplifier. However, each individual system must be considered along with the boundary conditions to determine stability.[35, 73, 74]

The results of this chapter have been summarized.[97]

CHAPTER VI

APPLICATIONS OF ECW THEORY

The results of previous chapters have depended only upon the dispersion diagram of unbounded periodic media. In this chapter several cases of bounded media will be discussed. The use of the ECW equations allows behavior at all Bragg orders to be approximated easily. The purpose of this chapter is not an exhaustive coverage of periodic structures but rather an indication of a wide range of problems which may be solved by the use of the previous theory.

In section A, longitudinally bounded passive media (i.e. DFB filters) will be covered along with examples of transients in a periodic slab. In section B the characteristics of higher-order DFB lasers will be given. Section C will cover the case of holographic grating diffraction and the last section will characterize the propagation of Gaussian beams in periodic media.

A. DFB Filters

1. Effect of Longitudinal Boundaries

We consider waves in a periodic slab of length ℓ. The ECW equations account for Bragg coupling or scattering from the periodicities but not for the coupling or scattering due to the boundaries. The equations can be easily modified. The relative dielectric constant is now

$$\epsilon(z) = \epsilon_r + i\epsilon_i + \mathrm{rect}(z/\ell)\, \epsilon_r \sum_p (\eta_r + i\eta_i)_p f_p \cos pKz$$

where

$$\text{rect}(z/\ell) = \begin{cases} 1 & |z| < \ell/2 \\ 0 & |z| > \ell/2 \end{cases}$$

For simplicity, consider singly periodic media with no average loss or gain (i.e. $f_p = 0$ for $p \neq 1$, $\epsilon_i = 0$). The additional Fourier components available for coupling or scattering arise from rect(z/ℓ) and have not been accounted for previously. These components are proportional to the Fourier transform,

$$\eta \int_{-\infty}^{\infty} \text{rect}(z/\ell) \cos Kz \, e^{i\beta z} \, dz = \frac{\eta\ell}{2} \left\{ \frac{\sin(\beta+K)\ell/2}{(\beta+K)\ell/2} + \frac{\sin(\beta-K)\ell/2}{(\beta-K)\ell/2} \right\} \tag{6.A1}$$

Thus, the additional available perturbation per unit length is proportional to the right-hand side of (6.A1) divided by the length ℓ. As in the case of multiharmonic periodicities, only the strongest effect (i.e. first order in η) of the boundary perturbation of (6.A1) upon F_1 and B_1 are considered. For higher-order Bragg interactions, the coupling diagram of Figure 6.1 is helpful. Not only is there the usual cross-coupling through terms $O(\eta^N)$ and self-coupling through terms $O(\eta^2)$, but there is cross- and self-coupling proportional to $\eta\Phi$ and $\eta\Theta$, respectively, where

$$\left.\begin{aligned} \Phi &= \zeta_N \frac{\sin(\beta+K/2)\ell}{(\beta+K/2)\ell} + \frac{\sin(\beta-K/2)\ell}{(\beta-K/2)\ell} \\ \Theta &= \zeta_N \left\{ \frac{\sin(\beta+K)\ell/2}{(\beta+K)\ell/2} + \frac{\sin(\beta-K)\ell/2}{(\beta-K)\ell/2} \right\} \end{aligned}\right\} \tag{6.A2}$$

are the boundary effects. This is due to the terms $[-k^2\epsilon_r\eta(\Theta F_1 + \Phi B_1)/2]$ and $[-k^2\epsilon_r\eta(\Theta B_1 + \Phi F_1)/2]$ which are added respectively to the F_1 and B_1 equations of the ECW equations (3.A6). Consequently, the

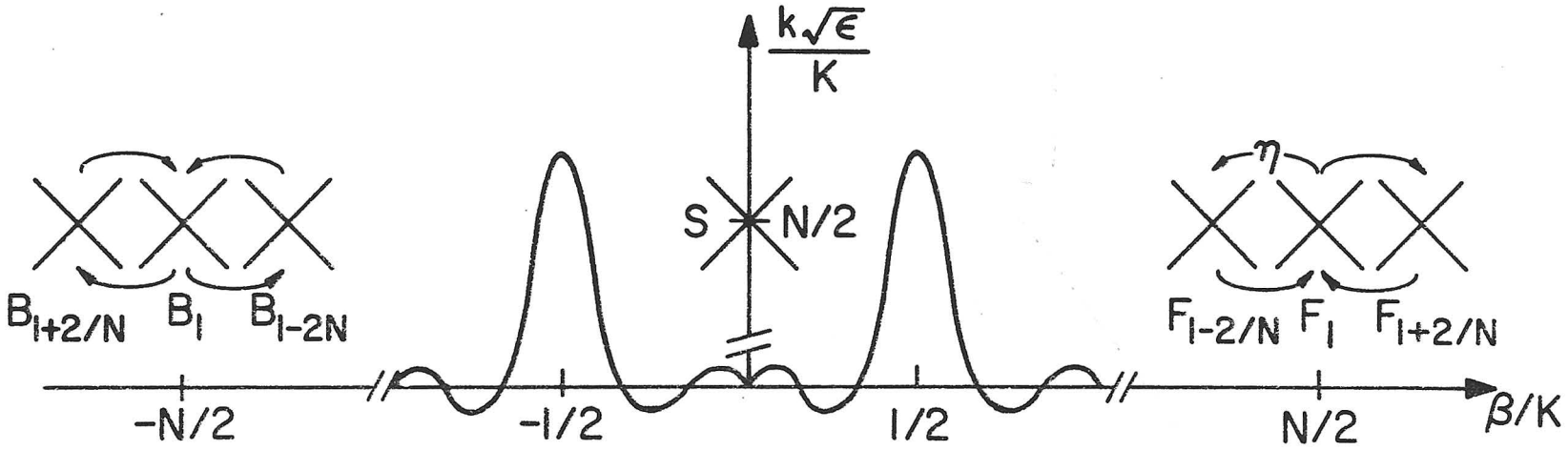

Fig. 6.1 Coupling diagram with Φ superimposed for a given $K\ell$. Cross coupling occurs due to both the periodicity perturbation and the boundary perturbation. The self-coupling due to the boundary effect Θ is small and is not shown.

modified ECW equations become identical to the former ECW equations with the changes $\delta_N \rightarrow \tilde{\delta}_N$ and $\chi_N \rightarrow \tilde{\chi}_N$ where

$$\left.\begin{aligned} \frac{\tilde{\delta}_N}{K} &= \frac{\delta_N}{K} - \frac{N\eta}{8} \quad \textcircled{H} \\ \frac{\tilde{\chi}_N}{K} &= \frac{\chi_N}{K} + \frac{N\eta}{8} \quad \Phi \end{aligned}\right\} \tag{6.A3}$$

In each case the first term of the above equation expresses the effect of the periodicity while the second term expresses the effect of the boundary. For higher-order interactions, the latter effect predominates in coupling when $K\ell << (\eta/2)^{1-N}$ while the opposite is true for $K\ell >> (\eta/2)^{1-N}$. This is expected since for thick slabs the extra Fourier components introduced by the truncated periodic media are tightly clustered around the components introduced by the periodicity of the infinite media and no new effects are observed. However, for thin slabs, the truncation produces Fourier components at many multiples of the Bragg wavenumber which are capable of directly coupling F_1 to B_1. In this case the boundary coupling ($\propto \eta\Phi$) predominates. Note that the above inequalities denote the region where the results of the infinite media can be directly applied to the longitudinally bounded case. Also note that the boundary effects can be reduced if the perturbation is gradually truncated at the slab ends. A similar effect has been noted in quantum mechanical scattering.[79] The boundary effect seldom affects the phase mismatch since it is negligible when $K\ell >> \eta^{-1}$.

2. ECW Reflection and Transmission Coefficients

In this subsection we consider the general case of transversely and longitudinally bounded structures where each coupled wave represents a different mode. Hence, the longitudinal wavenumbers may be different for each mode.[31] For simplicity the numerical examples will correspond to the special case of coupling between waves of identical modes in thick slabs although the analytic results are given for the general case using the ECW approximations.

Figure 6.2 schematically shows the configuration. Consider a positive phase velocity wave $F_1(z)\, U_p(x) e^{i\beta_p z}$ which couples to a negative phase velocity wave $B_1(z)\, U_q(x)\, e^{i\beta_q z}$. The subscripts p, q refer to the mode number of the transverse distribution U(x). The phase match condition for significant coupling at the N^{th} Bragg order is

$$\beta_p + \beta_q \simeq NK \tag{6.A4}$$

where $K = 2\pi/\Lambda$ and Λ is the fundamental spatial period. The boundary conditions are found from Figure 6.3 by use of the ECW equations which correspond to continuity of the electric field at $z = \pm \ell/2$.

$$\begin{aligned} e^{-i\beta\ell/2} + R_N e^{i\beta\ell/2} = \sum_{n=-1}^{N^*/2} & F_{1-2n/N}(z=-\ell/2)\, e^{-i(1-2n/N)\ell/2} \\ & + B_{1-2n/N}(z=-\ell/2)\, e^{i(1-2n/N)\ell/2} \\ & + \begin{pmatrix} 1 \\ 0 \end{pmatrix} S(z=-\ell/2) \end{aligned} \tag{6.A5}$$

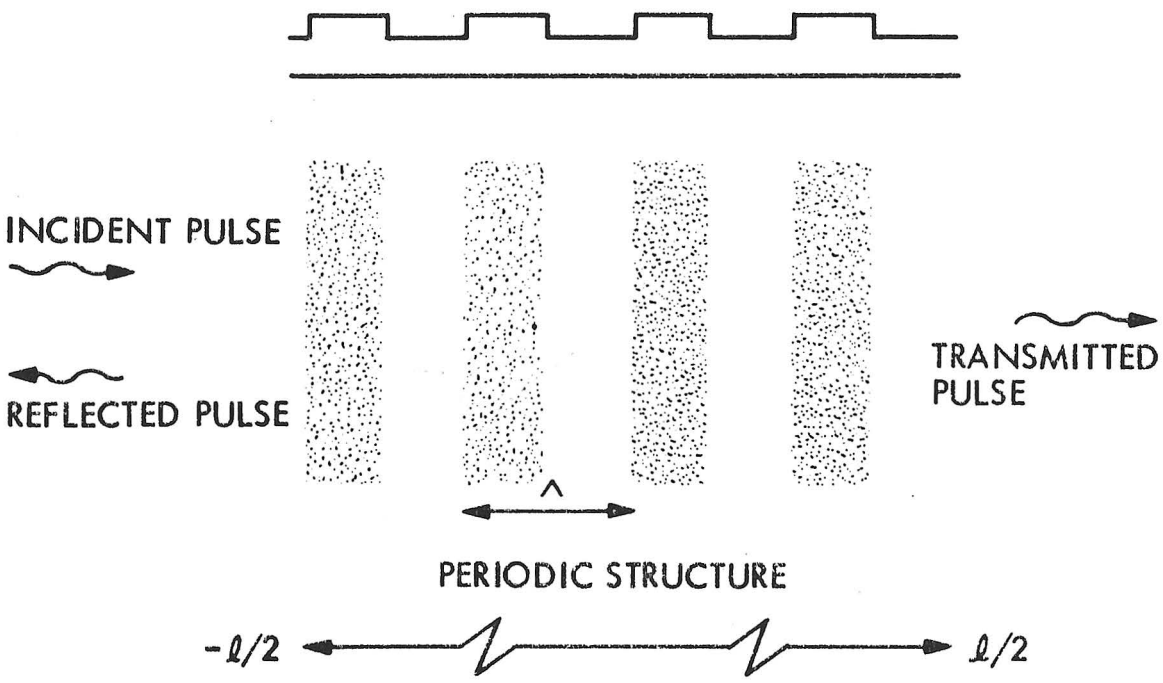

Fig. 6.2 Configuration of pulses and periodic slab.

$$T_N e^{i\beta \ell/2} = \sum_{n=-1}^{N^*/2} F(z=\ell/2) e^{i(1-2n/N)\ell/2} + B(z=\ell/2) e^{-i(1-2n/N)\ell/2} + \binom{1}{0} S(z=\ell/2) \qquad (6.A6)$$

where

$$N^*/2 = \begin{cases} \frac{N-2}{2} & \text{for N even} \\ \frac{N-1}{2} & \text{for N odd} \\ 1 & \text{for N = 1} \end{cases}$$

$$\binom{1}{0} = \begin{cases} 1 & \text{for N even} \\ 0 & \text{for N odd} \end{cases}$$

and R_N and T_N are the reflection and transmission coefficients. Similar equations result from matching the derivatives (or the magnetic field) at $z = \pm \ell/2$. The only additional equations needed are the ECW equations modified for transversely bounded media.

$$\left.\begin{aligned} F_1(z) - i\tilde{\delta}_p F_1(z) &= i\tilde{\chi}_{pq} B_1(z) \\ -B_1(z) - i\tilde{\delta}_q B_1(z) &= i\tilde{\chi}_{qp} F_1(z) \end{aligned}\right\} \qquad (6.A7)$$

where the coupling and phase mismatch are assumed to be known. Instead of solving the above equations exactly, a perturbation scheme is introduced which significantly simplifies the calculation and eliminates the boundary coupling which has been accounted for previously. Introduce the ordering parameter λ which will eventually be set to unity.[77] Consider a power series solution of the form

$$\left.\begin{aligned} F_1 &= F_1^{(0)} + \lambda F_1^{(1)} + \lambda^2 F_1^{(2)} + \ldots \\ B_1 &= B_1^{(0)} + \lambda B_1^{(1)} + \lambda^2 B_1^{(2)} + \ldots \end{aligned}\right\} \qquad (6.A8)$$

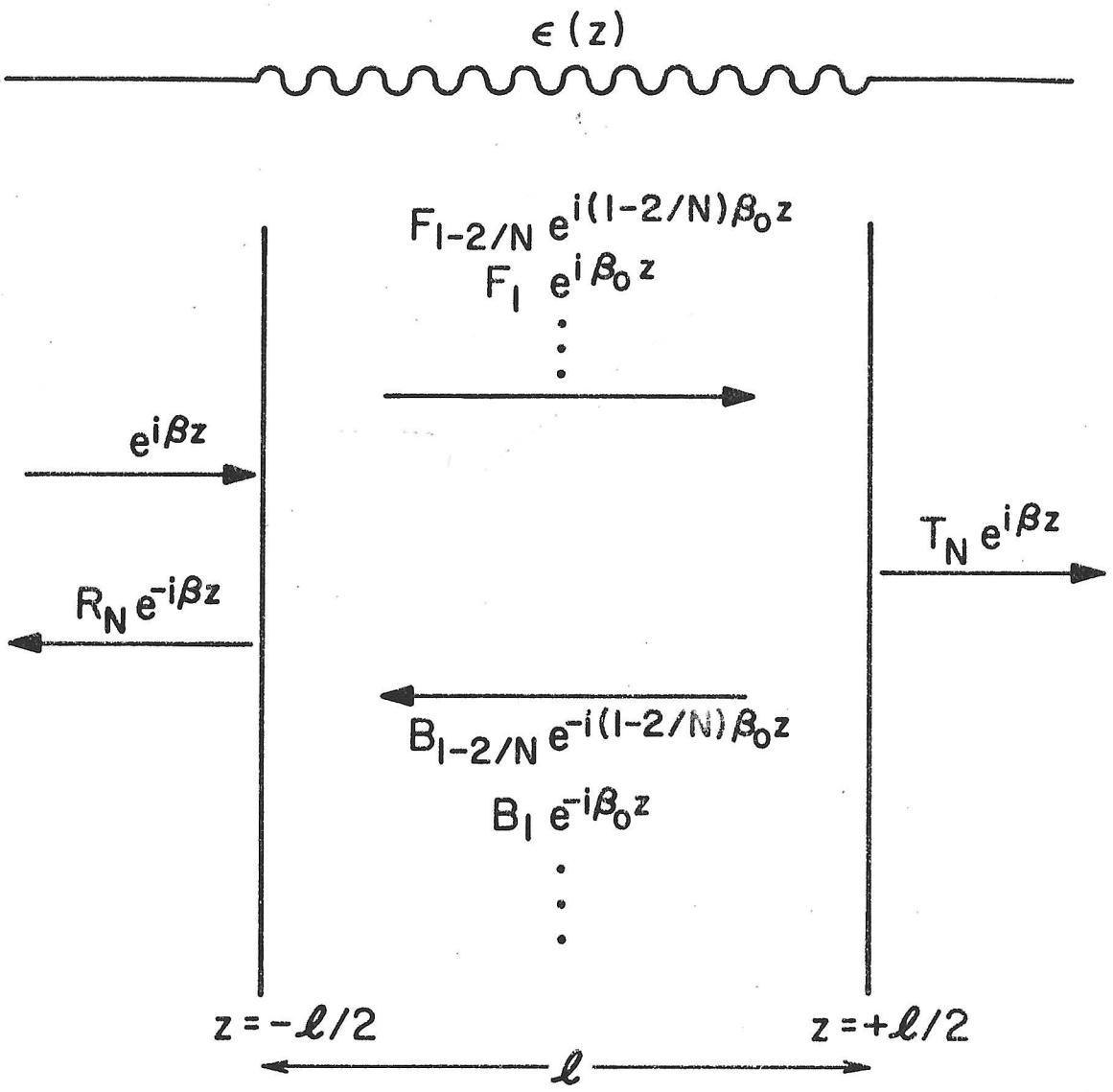

Fig. 6.3 ECW waves in periodic slab for coupling between identical modes (i.e. $\beta_p = \beta_q = \beta$).

for the waves and let the smallness be specified by $\lambda\eta$. If all the waves are solved in terms of F_1 and B_1 (see equation (3.A6)), then the electric field continuity equation becomes,

$$e^{-i\beta \ell/2} + R_N e^{i\beta \ell/2} = \left[F_1^{(0)} + \lambda F_1^{(1)} + \lambda^2 F_1^{(2)} + \ldots\right]\Big|_{z=-\ell/2} e^{-i\beta_o \ell/2}[1+O(\lambda\eta)] + \left[B_1^{(0)} + \lambda B_1^{(1)} + \lambda^2 B_1^{(2)} + \ldots\right]\Big|_{z=-\ell/2} e^{i\beta_o \ell/2}[1+O(\lambda\eta)] \tag{6.A10}$$

$$T_N e^{i\beta \ell/2} = \left[F_1^{(0)} + \lambda F_1^{(1)} + \lambda^2 F_1^{(2)} + \ldots\right]\Big|_{z=\ell/2} e^{i\beta_o \ell/2}[1+O(\lambda\eta)] + \left[B_1^{(0)} + \lambda B_1^{(1)} + \lambda^2 B_1^{(2)} + \ldots\right]\Big|_{z=\ell/2} e^{-i\beta_o \ell/2}[1+O(\lambda\eta)] \tag{6.A11}$$

where $\beta = \beta_o + \Delta\beta_N$

$\beta_o = NK/2$

near the N^{th} Bragg resonance. By equating terms $O(\lambda)$ and phase matching, the approximate boundary conditions become [19]

$$F_1(-\ell/2) = 1 \qquad F_1(\ell/2) = T_N$$
$$B_1(-\ell/2) = R_N \qquad B_1(\ell/2) = 0 \tag{6.A12}$$

The reflection and transmission coefficients are solved using the boundary conditions and the ECW equations. The details are carried out in Appendix C. We find

$$R_N = \frac{i\tilde{\chi}_{qp}}{D_N \coth D_N \ell - i\left(\frac{\tilde{\delta}_p + \tilde{\delta}_q}{2}\right)} \tag{6.A13}$$

$$T_N = \frac{D\, e^{i(\tilde{\delta}_p - \tilde{\delta}_q)\ell/2}}{D_N \cosh D_N \ell - i\left(\frac{\tilde{\delta}_p + \tilde{\delta}_q}{2}\right)\sinh D_N \ell} \tag{6.A14}$$

where $$D_N = \left[\tilde{\chi}_{pq}\tilde{\chi}_{qp} - \left(\frac{\tilde{\delta}_q + \tilde{\delta}_p}{2}\right)\right]^{\frac{1}{2}}$$

If the two coupled modes are identical, then $\tilde{\delta}_p = \tilde{\delta}_q = \tilde{\delta}$ and $\tilde{\chi}_{pq} = \tilde{\chi}_{qp} = \tilde{\chi}$. The subscript N has been dropped on $\tilde{\delta}$ and $\tilde{\chi}$ for convenience.

From the above equations for R_N and T_N we observe the following:

1. maximum reflection

$$R_N\Big|_{max} = i\tanh(\tilde{\chi}_{pq}\tilde{\chi}_{qp})^{\frac{1}{2}}\ell; \qquad (6.A15)$$

2. minimum transmission

$$T_N\Big|_{min} = 1/\cosh(\tilde{\chi}_{pq}\tilde{\chi}_{qp})^{\frac{1}{2}}\ell; \qquad (6.A16)$$

3. $R_N = 0$ and $T_N = 1$ for

$$\tilde{\delta}_p + \tilde{\delta}_q = 2[\tilde{\chi}_{pq}\tilde{\chi}_{qp} + (n\pi/\ell)^2]^{\frac{1}{2}} \quad (n = 1, 2, \ldots) \qquad (6.A17)$$

where the corresponding phase of R_N is $(2n-1)\pi/2$;

4. $|R_N|^2 + |T_N|^2 = 1$ for passive and lossless media.

These results are demonstrated in Figure 6.4 for the case $\chi\ell = 2$ where the boundary effects are neglected. The magnitudes of the reflection and transmission coefficients are shown as a function of $\delta\ell$ (i.e. frequency deviation from bandgap center). Note that the half-width of the main reflection maximum is equal to the bandgap width. Hence, there is significant reflection outside of the bandgap due to the deviation of $\mathrm{Re}\{\Delta\beta/K\}$ as well as $\mathrm{Im}\{\Delta\beta/K\}$ away from their

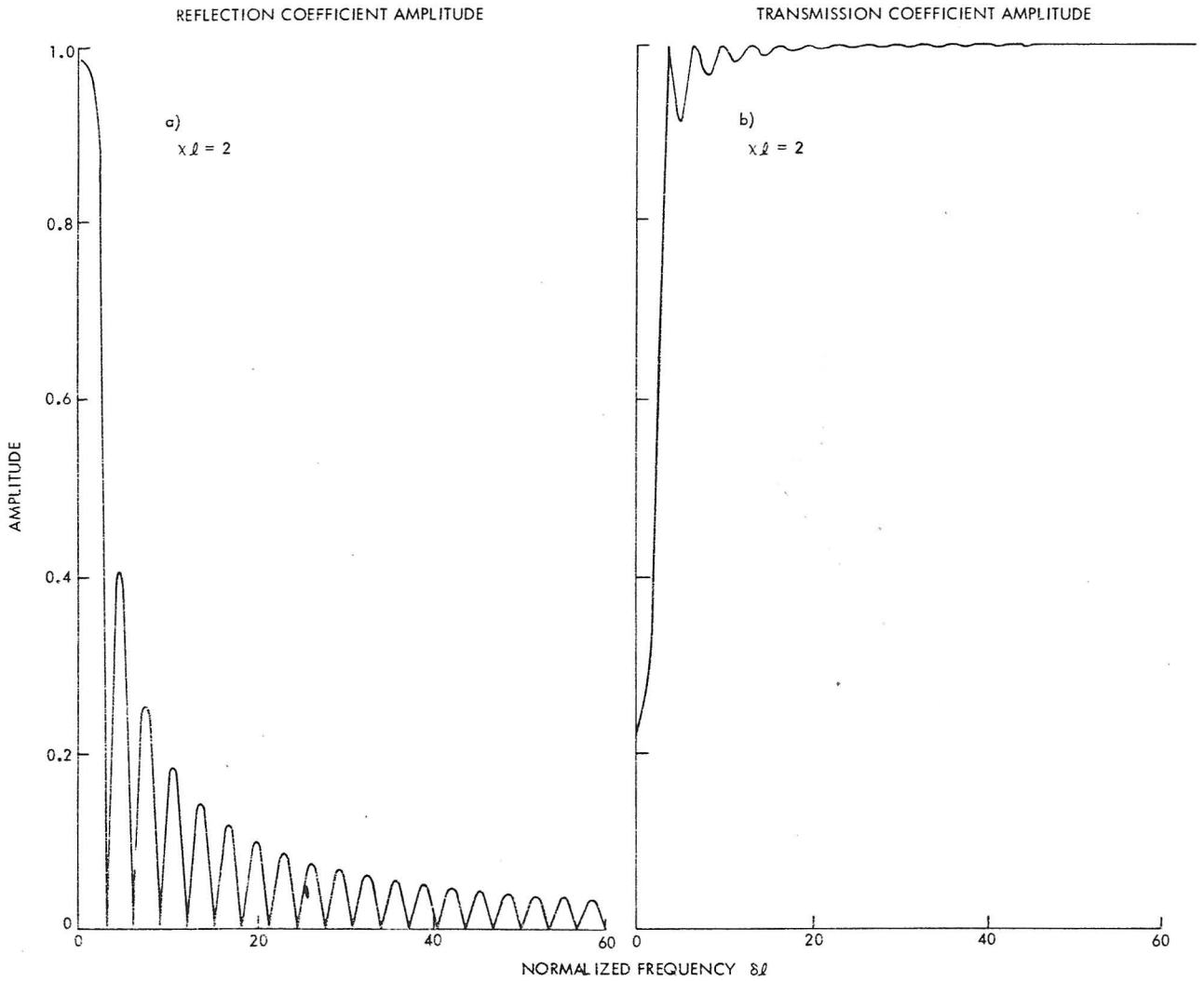

Fig. 6.4 Magnitude of reflection and transmission coefficients as a function of phase mismatch for fixed coupling. Boundary effects are neglected.

unperturbed values. Figure 6.5 shows the equimagnitude and equiphase curves of the reflection coefficient plotted as a function of $\chi\ell$ and $\delta\ell$ where again the boundary effects are neglected. Note that Figure 6.5a corresponds to a horizontal line ($\chi\ell = 2$) across Figure 6.4. If the coupled modes are different (i.e. $p \neq q$), the curves in Figure 6.4 and 6.5 are valid if δ is replaced by $(\delta_p + \delta_q)/2$ and χ by $(\chi_{pq}\,\chi_{qp})^{\frac{1}{2}}$. Similar results for media with average gain have been discussed for the first-order index coupling case when the modes are identical.[35]

It is of interest to note the change in the reflection coefficient with Bragg order. For small coupling $\tilde{\chi}_N \ell \ll 1$,

$$R_N\Big|_{\max} \simeq i\,\tilde{\chi}_N \ell \tag{6.A18}$$

Thus, the variation of R_N with N is

$$R_N\Big|_{\max} \propto i\left\{(\eta/2)^N K\ell + \eta \sin[(N\pm 1)K\ell/2]\right\} \tag{6.A19}$$

where the first term expresses the dependence upon the periodicity perturbation and the second term expresses the effect of the boundary perturbation.

For other typical periodicities, the results of Appendix B will provide appropriate coupling or phase mismatch. In particular, note that for thick slabs, the coupling is constant at odd Bragg orders for square-wave periodicities. This implies that the maximum reflection coefficient is also constant at odd Bragg orders. These results are in agreement with well-known exact results that use matrix calculations.[78] Figure 6.6 exemplifies these concepts for three typical

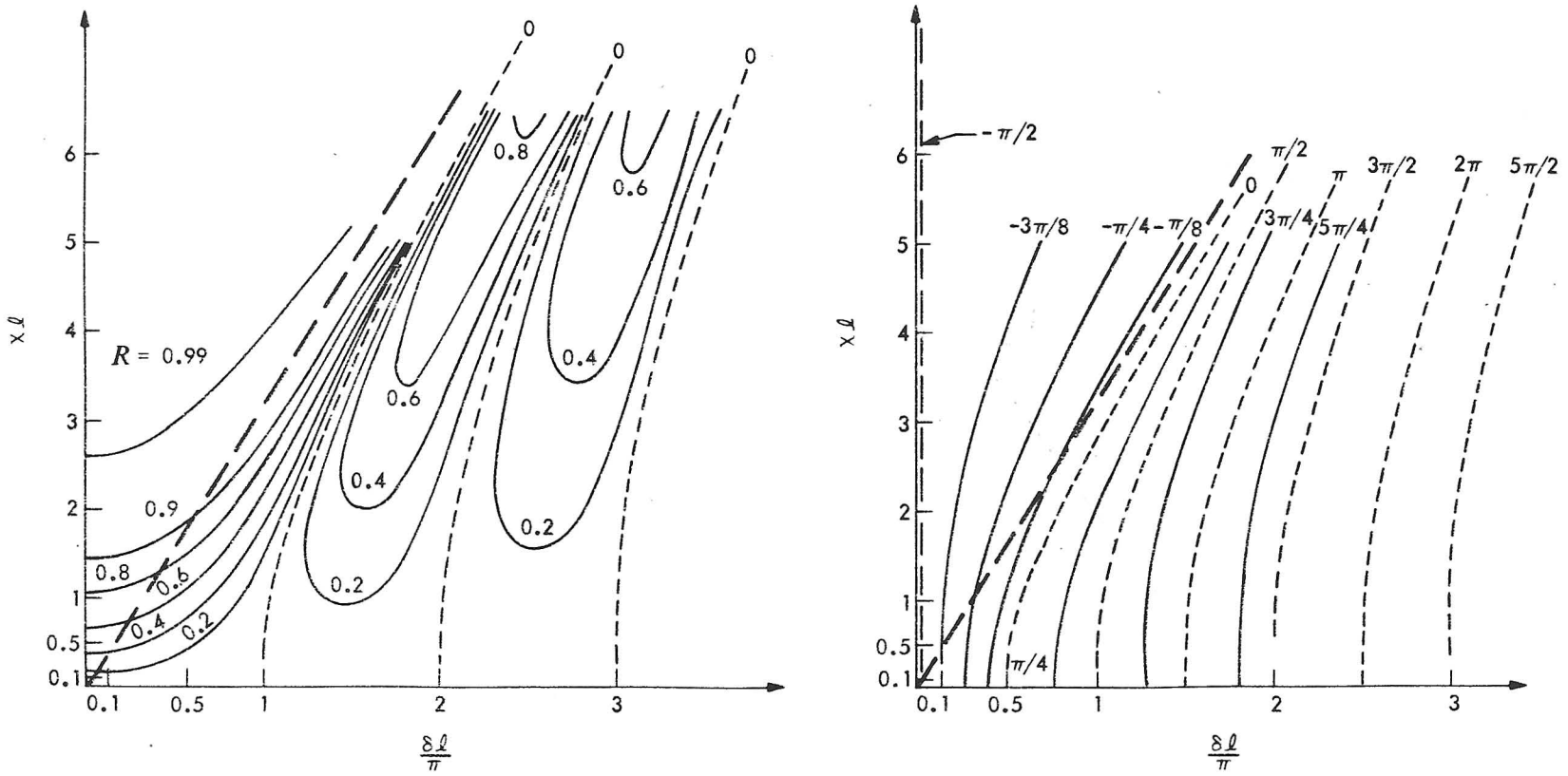

Fig. 6.5 Equimagnitude and equiphase curves of the reflection coefficient as a function of phase mismatch and coupling. Boundary effects are neglected.

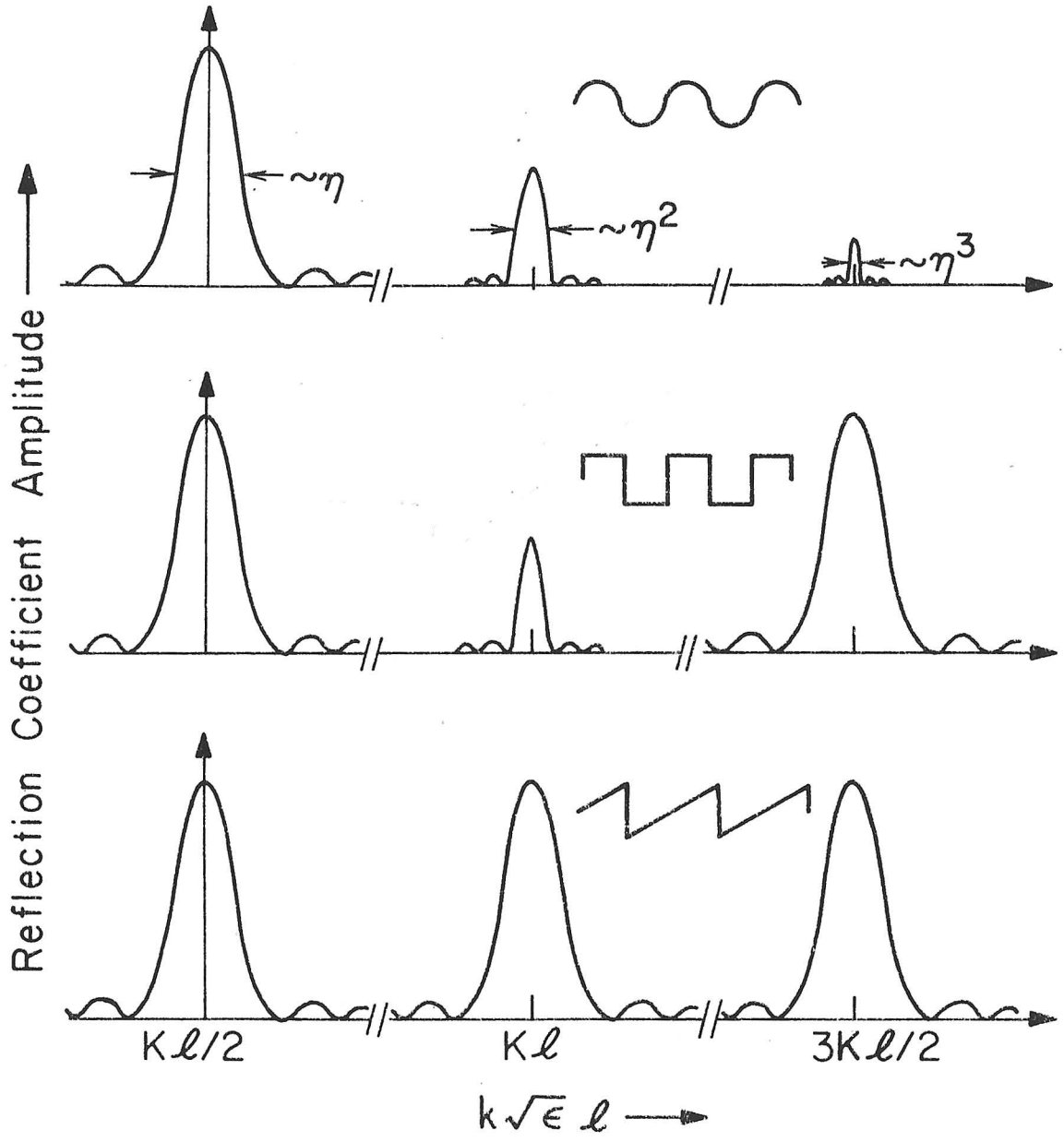

Fig. 6.6 Sketches of reflection coefficient amplitude for $\chi\ell \sim 0.5$ for a) sinusoidal, b) square-wave and c) sawtooth-wave periodicities. In all cases the boundary effects are neglected. Note small reflection at N^{th} Bragg order when $f_N = 0$. The bandgap shift is too small to observe on this scale.

periodicities with index coupling. Note that periodicities with large Fourier components f_N will have large coupling and reflection coefficients at the N^{th} Bragg order. Thus, periodicities with odd Fourier components (e.g. square- or triangular-wave) will have large reflection coefficients only at odd Bragg orders.

The use of dynamically generated (e.g. acoustic waves or electro-optic effect) multiharmonic periodicities opens up the possibility of controlling the feedback strength in DFB filters. This, in turn, varies the passband. From the results of chapter IV it is apparent that the passband could vary as $\sin(\theta/2)$ where θ is the relative phase between Fourier components of the periodicity at the second Bragg resonance (see Figure 4.5). If the boundary effects are significant or predominant, then the previous results will be modified. That is, for thin slabs, the reflection will be significantly increased at higher Bragg orders when $\{\eta\sin[(N\pm1)K + \Delta k\varepsilon_r^{\frac{1}{2}}]\ell/2\}$ is no longer negligible.

3. Born Approximation Reflection Coefficient

In order to summarize the properties of reflections from both thick and thin slabs, it is useful to find the Born approximation to the reflection coefficient. Consider the wave equation for some transverse component of the electric field E(z).

$$\left[\frac{d^2}{dz^2} + k^2\varepsilon_r\right]E(z) = -\lambda\eta k^2\varepsilon_r \cos Kz\, E(z) = -\lambda S(z)\, E(z) \qquad (6.A20)$$

where the ordering parameter λ has again been used to show the smallness of η. Assuming a solution

$$E(z) = E^{(0)}(z) + \lambda\, E^{(1)}(z) + \lambda^2 E^{(2)}(z) + \ldots$$

we find

$$E^{(n+1)}(z) = \int_{-\infty}^{\infty} S(z')\, g(z,z')\, E^{(n)}(z')\, dz' \qquad (6.A21)$$

where $E^{(0)}(z) = e^{i\beta z}$

$$g(z,z') = \frac{i\, e^{i\beta|z-z'|}}{2\beta}$$

and where $\beta = k\,\epsilon_r^{\frac{1}{2}}$ for this computation. A straightforward calculation shows,

$$E^{(1)}(z) = \frac{i\eta\beta\ell}{4}\, e^{-i\beta z}\left[\frac{\sin(\beta+K/2)\ell}{(\beta+K/2)\ell} + \frac{\sin(\beta-K/2)\ell}{(\beta-K/2)\ell}\right] \qquad (6.A22)$$

Thus $E^{(1)}$ represents a wave traveling to the left which is produced by the wave $E^{(0)}$ traveling to the right. The approximation which uses the terms $E^{(0)}$ and $E^{(1)}$ is known as the Born approximation. The Born reflection coefficient is then the coefficient of $e^{-i\beta z}$ in $E^{(1)}$, or

$$R^{(1)} = \frac{i\eta\beta\ell}{4}\left[\frac{\sin(\beta+K/2)\ell}{(\beta+K/2)\ell} + \frac{\sin(\beta-K/2)\ell}{(\beta-K/2)\ell}\right]$$

$$R^{(1)} = \frac{i\eta\, k\,\epsilon_r^{\frac{1}{2}}\,\ell}{4}\,\Phi \qquad (6.A23)$$

which is valid for $|\eta\, k\, \epsilon_r^{\frac{1}{2}}\, \ell|/4 \ll 1$ at the first Bragg resonance or for $|\eta/4| \ll 1$ at higher Bragg resonances.

At the first Bragg order, for $|\chi\ell| \ll 1$ and $|\eta| \ll 1$, the Born approximation and the modified ECW approximation become equal. Explicitly we find

$$R^{(1)}\Big|_{max} \simeq \frac{i\,\eta\, k\,\epsilon_r^{\frac{1}{2}}\,\ell}{4} \simeq R_1\Big|_{max} \qquad (6.A24)$$

at the bandgap center for $K\ell \geq 10$. For higher Bragg orders, the Born approximation produces a series in powers of η which accounts only for the depth of the perturbation (i.e. the end effects) and not the length over which it acts. A series in $\eta K\ell$ is needed to account for significant periodic effects. This latter series occurs through the modified ECW equations. Thus, the Born approximation is useful at the first Bragg order or at higher orders where the slab satisfies the relation $K\ell \ll \eta^{1-N}$. For thick slabs, the ECW theory provides the proper phase mismatch, coupling and reflection.

4. Transients in Periodic Slabs

Consider an incident pulse f(t) with frequency spectrum

$$F(\omega) = \int_{-\infty}^{\infty} f(t) e^{i\omega t}\, dt \tag{6.A25}$$

where the reflected and transmitted pulses are, respectively,

$$r(t) = \frac{1}{2\pi} \int_{-\infty}^{\infty} F(\omega)\, R_N(\omega) e^{-i\omega t}\, d\omega \tag{6.A26}$$

$$t(t) = \frac{1}{2\pi} \int_{-\infty}^{\infty} F(\omega)\, T_N(\omega) e^{-i\omega t}\, d\omega \tag{6.A27}$$

This case was shown in Figure 6.2. Numerical inversion has been used by a number of authors to obtain time response to radiation and scattering problems. The Cooley-Tukey fast Fourier transform (FFT)[80] has been used in the numerical examples with $2^{11} = 2048$ samples to calculate r(t) and t(t).

The cases of reflection and transmission of rectangular and Gaussian pulses of several center frequencies and widths have been carried out. Normalized pulse lengths τ were chosen to be 0.25

and 2.0 time units where each time unit corresponds to the transit time of the pulse across the slab length ℓ. As in previous sections, the numerical results are valid at the first Bragg order and all higher Bragg orders where the boundary effects can be ignored.

Figure 6.7 displays the envelopes of the reflected and transmitted pulses which result from an incident pulse of length $\tau = 0.25$. Several values of coupling are used and the carrier frequency is at the bandgap center ($\delta_N = 0$). In all the illustrations, the time value $t = 0$ corresponds to the instant when the center of the pulse is at the first boundary. For weak coupling, the reflected pulse is spread over 2.25 time units (Figure 6.7 a,c) because the energy is reflected from successive striations and the echo from the last boundary has a round trip time of 2 units. Since the successive reflections are relatively weak, the reflected pulse is quasi-rectangular while the transmitted pulse is similar to the time delayed incident pulse. As the coupling is increased, multiple interference leads to transients over a longer time period (Figure 6.7 i,j). The reflected pulse reaches a maximum at 0.25 units when the entire incident pulse has just entered the slab. The subsequent fall-off in the reflected pulse amplitude is due to the fact that a large portion of the signal has already been reflected due to the first few striations. For large coupling, the transmitted pulse consists mainly of two peaks, 0.25 units apart, which correspond to differentiation (i.e. high-pass filter) of the incident pulse.

The same coupling strength sequence is given in Figure 6.8 for a rectangular pulse of length $\tau = 2$. For weak coupling (Figure 6.8a), the reflected pulse is similar to the autocorrelation of the

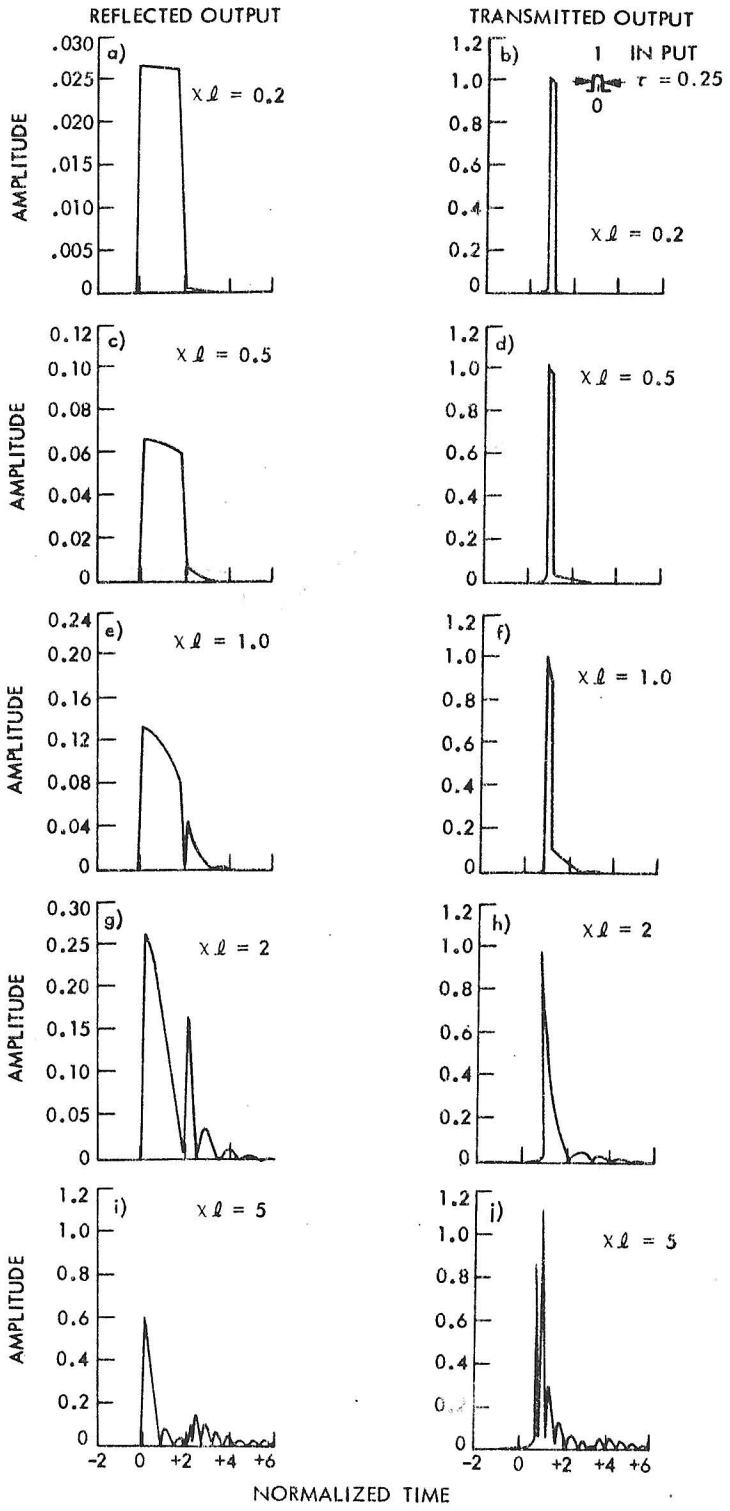

Fig. 6.7 Reflected and transmitted pulses for different values of coupling coefficient. Incident rectangular pulse has length 0.25 time units and a carrier frequency at $R_N|_{max}$. Note the difference in vertical scales.

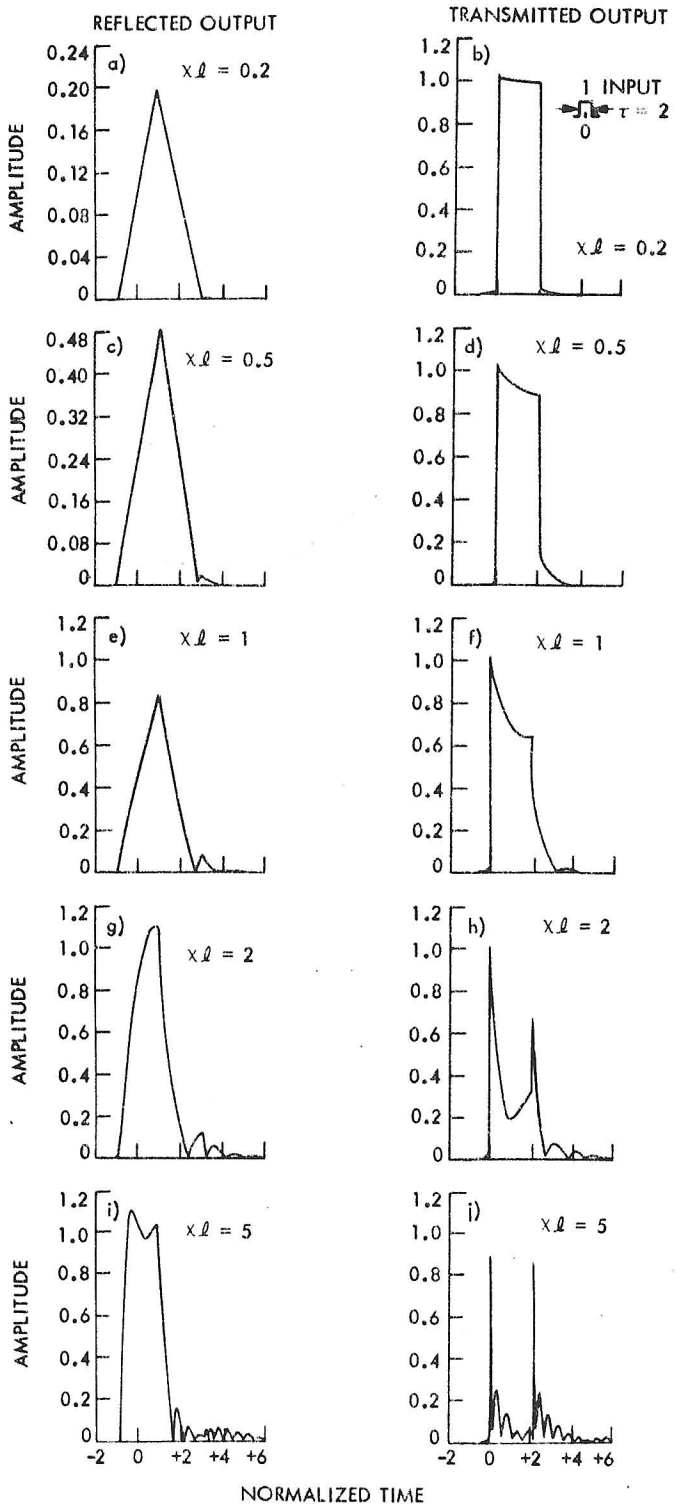

Fig. 6.8 Reflected and transmitted pulses for different values of coupling coefficient. Incident rectangular pulse has length 2.0 time units and a carrier frequency at $R_{N|max}$. Note the difference in vertical scales.

incident pulse. This indicates that the reflection coefficient is similar to the incident pulse spectrum. For strong coupling, the transmitted pulse is again similar to the absolute value of the derivative of the incident pulse with characteristic interfering echos. Note that the reflected pulse may have an amplitude larger than unity (Figure 6.8g,i) due to constructive addition of successive reflections.

Figure 6.9 displays the reflected and transmitted pulses for a Gaussian incident pulse of width $\tau = 2$ (width is taken at the 1/e values). Since a Gaussian pulse contains smaller higher frequency spectral components, the reflected and transmitted pulses are grossly similar to the incident pulse. For narrowed Gaussian pulses (not shown here), the results are somewhat similar to those obtained for a rectangular pulse of the same width.

Several examples of pulses with carrier frequencies at the first several zeros of the reflection coefficient have been given elsewhere.[29] In general, the transmitted pulse is similar to the incident pulse. However, the reflected pulse is broken up into a long pulse train which can be considerably longer than the incident pulse width.

5. Discussion of DFB Filters

In the preceding subsections, the ECW theory was applied to longitudinally bounded media. The ECW equations were modified to directly account for the coupling between $F_1(z)$ and $B_1(z)$ due to the boundary. This changed the coupling so that it consisted of two parts with the following physical meaning. One part of the coupling, due only to the perturbation is proportional to $\{\eta^N K\ell\}$ and hence increases

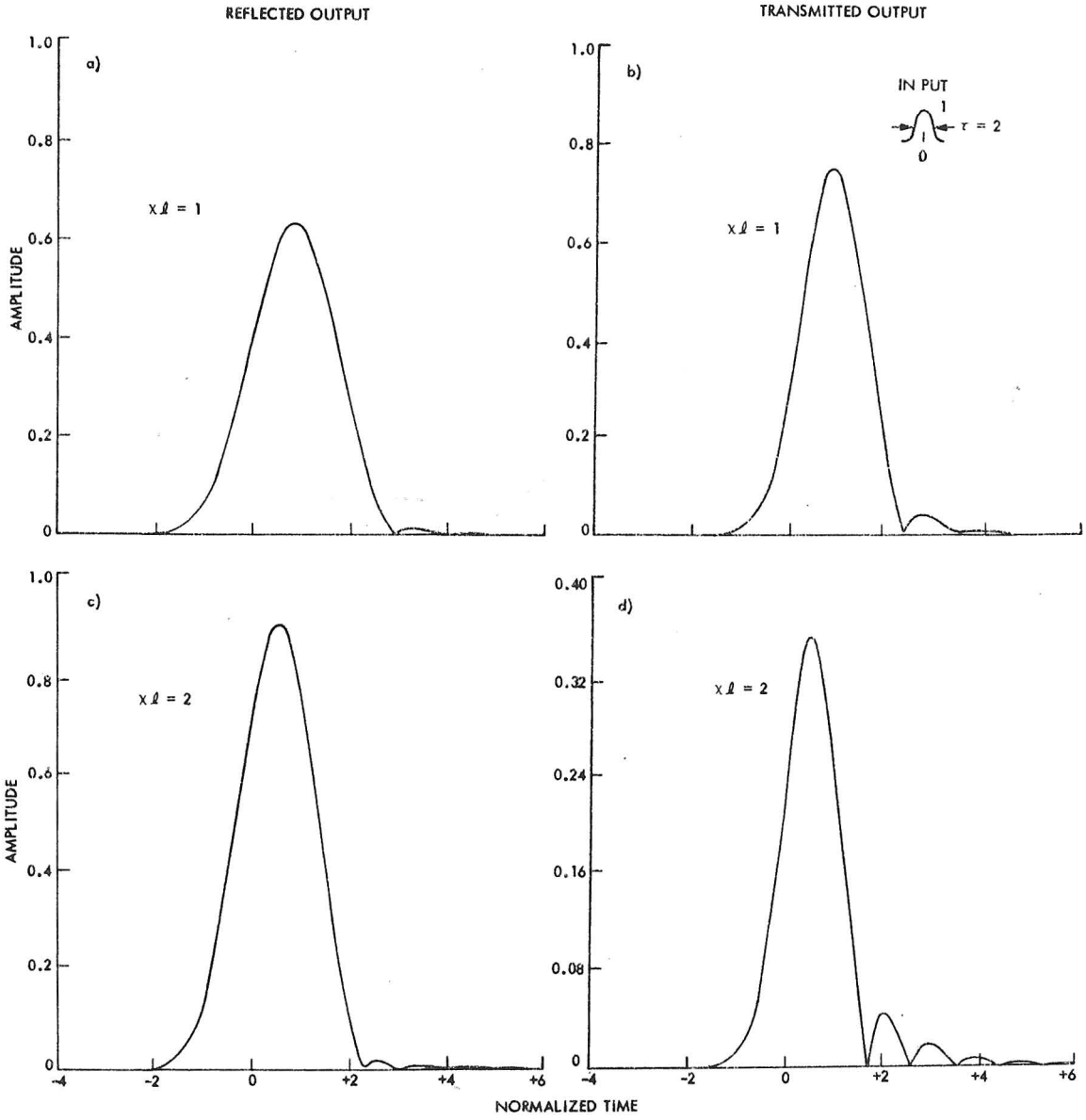

Fig. 6.9 Reflected and transmitted pulses for incident Gaussian pulse of width 2 time units and carrier frequency at $R_N|_{max}$. Note difference in vertical scales.

with slab thickness since it is due to repeated reflections in the dielectric. The second part of the coupling is due to the above mentioned boundary effects and is proportional to $\{\eta \sin[(N\pm1)K+\Delta k\epsilon_r^{\frac{1}{2}}]\ell/2\}$. This accounts only for the interference effects due to the periodicity truncation and may become zero for certain lengths at particular frequencies. The application of the boundary conditions was then introduced in such a way that end effects were not accounted for again.

The validity of this approach was tested by using the exact results of Bedrosian.[89,90] The comparison was made on periodic media of length $K\ell = 26\pi$ with $\eta = 0.05$. The ECW and exact invariant imbedding technique agreed to within 1% in the two cases where the boundary effect was insignificant ($R_2|_{max} = 2.55\times10^{-2}$) and where it had a large effect ($R_2|_{max} = 5.88\times10^{-2}$) at the second Bragg order.[90]

Comparisons to the Born approximation showed that at higher Bragg orders, the Born approximation ignored the $\eta^N K\ell$ term of the coupling. However, at the first Bragg order the Born and ECW approximations are in very close agreement. For cases where $\eta \to 1$, the full Floquet theory must be used. This is straightforward in principle but laborious to carry out. The disadvantage is that lengthy numerical calculations have to be carried out and the intuitive appeal of the ECW theory is lost.

We have shown that periodic slabs may be useful as edge differentiations or multiple pulse generators. The transient results may be useful in the fields of microwave and optical filters and for sounders of subsurface layers.

B. Higher-Order DFB Lasers

Ever since Kogelnik and Shank's demonstration[54] and description[23] of DFB lasers in the early 1970's there has been great interest in this field. Since then much work has been done at the first Bragg order.[14,24,25,30,35,36,58,70] In 1972 Bjorkholm and Shank[41] demonstrated the first higher-order DFB laser with output at the second and third Bragg resonances. More recently there has been further experimental work at the second Bragg resonance[71] and with multiple frequency DFB lasers.[70]

In this section the approximate mode spectrum and threshold gain are given as a function of Bragg order. The results, which use the ECW equations, are analogous to the coupled wave results of Kogelnik and Shank.[23] Hence, the derivation will be only briefly sketched here. The details are given in Appendix D.

1. ECW Result for Threshold Gains and Mode Spectra

Oscillation will take place when output occurs for zero input. This can be alternately stated as the condition where the reflection or transmission coefficient becomes infinite. We use the ECW reflection coefficient discussed in previous sections and set the denominator equal to zero or

$$D_N \coth D_N \ell = i\Delta\delta_N \tag{6.B1}$$

This can be put into the form

$$\left[\frac{D_N - i\,\delta_N}{D_N + i\,\delta_N}\right] e^{2D_N \ell} = -1 \qquad (6.B2)$$

The complex solution to the above transcendental equation produces the threshold gain and the mode spectrum when solved for amplitude and phase.

2. High-Gain Approximation

The high-gain approximation assumes that the periodicity has little effect on the propagation, or, for

$$\frac{\delta_N}{K} = \frac{\Delta k_N \sqrt{\epsilon_r}}{K} - \frac{\zeta_N \eta^3 N^3}{32(N^2-1)} + \frac{i\,\epsilon_i}{\epsilon_r} \frac{N}{4}\left[1 - \frac{\zeta_N \eta^2 N^2}{8(N^2-1)}\right] \qquad (6.B3)$$

$$\frac{\delta_N}{K} \triangleq \frac{\Delta_N}{K} - \frac{i\,g_N}{K} \qquad (6.B4)$$

the condition is

$$\chi_N \ll g_N \qquad (6.B5)$$

This is approximated for singly periodic media by the inequality

$$|\eta/2|^N \ll |\epsilon_i/\epsilon_r| \qquad (6.B6)$$

From Appendix D, the threshold gain approximation is given by

$$4(g_N^2 + \Delta_N^2) = \chi_N \chi_N^* e^{2g_N \ell} \qquad (6.B7)$$

and the longitudinal mode spectrum is given by

$$\tan^{-1}(\Delta_N/g_N) - \Delta_N \ell = (m+\tfrac{1}{2})\pi + \text{phase}(\chi_N) \quad m=0, \pm1, \pm2, \ldots \qquad (6.B8)$$

where the first term is usually small and can be neglected. These expressions neglect boundary effects which can be accounted for by a straightforward modification as in the previous section. Equation (6.B8) is first solved for Δ_N, the normalized frequency deviation from the bandgap center and then (6.B7) is solved for g_N, the normalized average gain. It is apparent that for singly periodic media, the average gain will increase drastically with Bragg order. However, boundary effects or multiharmonic periodicities may reduce the threshold gain by increasing the coupling.

The mode spectrum is asymmetric and is sketched in Figure 6.10 for higher Bragg orders. For index coupling (Figure 6.10a), the gain symmetrically pushes the modes outward from the usual two mirror cavity case (shown by dashed lines). However, the bandgap shift produces an asymmetry and shifts the entire spectrum toward higher wavenumbers. As in the first order case, no oscillation takes place at exact Bragg resonance. Figure 6.10b, c shows the analogous information for gain coupling at odd and even Bragg orders, respectively. For odd Bragg orders, oscillation is possible near Bragg resonance, but the bandgap shift prevents oscillation exactly at $\Delta k \epsilon_r^{\frac{1}{2}} \ell = 0$. As expected from the Brillouin diagrams, even-order gain/loss coupling is similar to even-order index coupling except for the sign of the bandgap shift.

3. Low-Gain Approximation

Low gain implies the inequality for singly periodic media

$$|\epsilon_i/\epsilon_r| \ll |\eta/2|^N \qquad (6.B9)$$

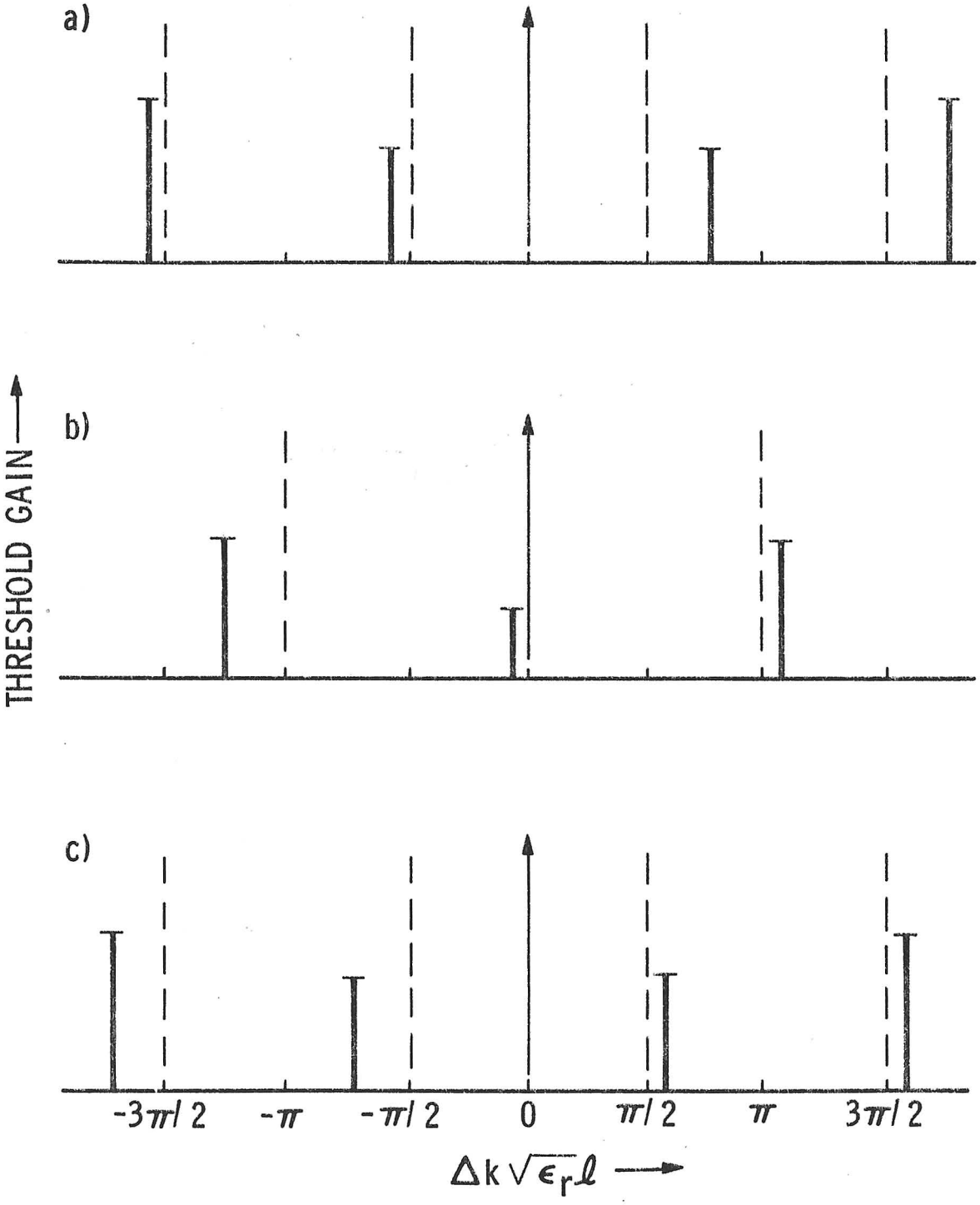

Fig. 6.10 Sketch of mode spectrum in higher-order ($N \geq 2$) DFB lasers for: a) index coupling ($N = 2, 3, 4, \ldots$); b) gain coupling ($N = 3, 5, 7, \ldots$); and c) gain coupling ($N = 2, 4, 6, \ldots$) in the high-gain approximation.

Again the details of the approximation are given in Appendix D. Boundary effects are neglected since low gain implies a large coupling-length product. Hence the boundary effects are small.

Consider first the case of index coupling. We find that the lowest-order longitudinal mode frequency is given by

$$\Delta_N^2 - \chi_N^2 = \frac{6}{\ell^2} \tag{6.B10}$$

which becomes

$$\Delta_N \simeq \pm \chi_N \tag{6.B11}$$

for long structures. Therefore, the oscillation takes place near the bandgap edges. This agrees with the stability analysis of the previous chapter as expected. Identical reasoning holds for the case of gain/loss coupling at even Bragg orders.

The threshold gain condition for index coupling and for even-order gain/loss coupling is given by

$$g_N \ell = \frac{3}{\Delta_N \ell \chi_N \ell} \simeq \frac{3}{(\chi_N \ell)^2} \tag{6.B12}$$

This is approximated by

$$\frac{\epsilon_i}{\epsilon_r} \simeq \frac{1}{(\eta/2)^{2N} (K\ell)^3} \tag{6.B13}$$

for singly periodic media. Hence the threshold gain varies inversely with $(\eta/2)^{2N}$ for singly periodic media and inversely with the length cubed. Thus the threshold gain condition predicts that the average gain approaches zero as the length becomes infinite. Again this is in agreement with the stability criteria results.

For gain/loss coupling at odd Bragg orders the lowest-order longitudinal oscillation takes place at the bandgap center

$$\Delta_N = 0 \tag{6.B14}$$

with the threshold condition on the perturbation

$$|\chi_N| \ell_c = \sqrt{3} \tag{6.B15}$$

for zero average gain. Thus for DFB oscillation to start with $\epsilon_i = 0$, the necessary critical length ℓ_c varies as

$$\ell_c \propto \frac{\sqrt{3}}{(|\eta|/2)^N} \tag{6.B16}$$

with Bragg order. The mode spectrum (6.B14) agrees with the stability prediction and (6.B15) implies that negative average gain can produce oscillation of $\ell > \ell_c$. This is verified by the approximate threshold gain condition on the average gain which is

$$\chi_N^2 + g_N^2 = \frac{\pm 6}{|\chi_N| \ell^3} \tag{6.B17}$$

and becomes

$$g_N \simeq |\chi_N| \tag{6.B18}$$

as the length increases. For singly periodic media the threshold gain varies as $(\eta/2)^N$. This also agrees with the stability criteria predictions since this condition is identical to equation (5.B3). Oscillation again takes place at the bandgap center given by

$$\Delta_N \simeq 0 \tag{6.B19}$$

Note that only the lowest-order (m = 0) longitudinal mode characteristics are given in the low-gain approximation.

4. Discussion of Higher-Order DFB Lasers

In all cases, the previous results are extensions of the well-known work of Kogelnik and Shank[23] to higher Bragg orders. The ECW theory gives the correct χ_N and δ_N to use in the theories. Numerical results have been given at the first Bragg order for both transversely unbounded[23, 35] and bounded[24, 30] media and so can be used at higher orders for guided modes.

The ECW theory shows that the mode spectrum is asymmetrically shifted from the exact Bragg resonance for high gain and has characteristic differences which depend upon coupling type and Bragg order. Note that in the low-gain case, the threshold gain and frequency of the lowest-order longitudinal mode is also predicted by the stability criteria without regard for the boundary conditions. In this case, enough coupling or feedback is available to produce oscillation without boundary coupling. In general, threshold gains increase drastically with Bragg order unless multiharmonic periodicities are used or unless boundary perturbations play a significant role. The low-gain threshold varies as $(\eta/2)^{-2N}$ or as $(\eta/2)^{N}$ for the case of index and even-order gain coupling or odd-order gain coupling, respectively, for singly periodic media.

C. Higher-Order Hologram Diffraction

There has been interest in transversely varying periodic media (Figure 6.11). This configuration represents electromagnetic

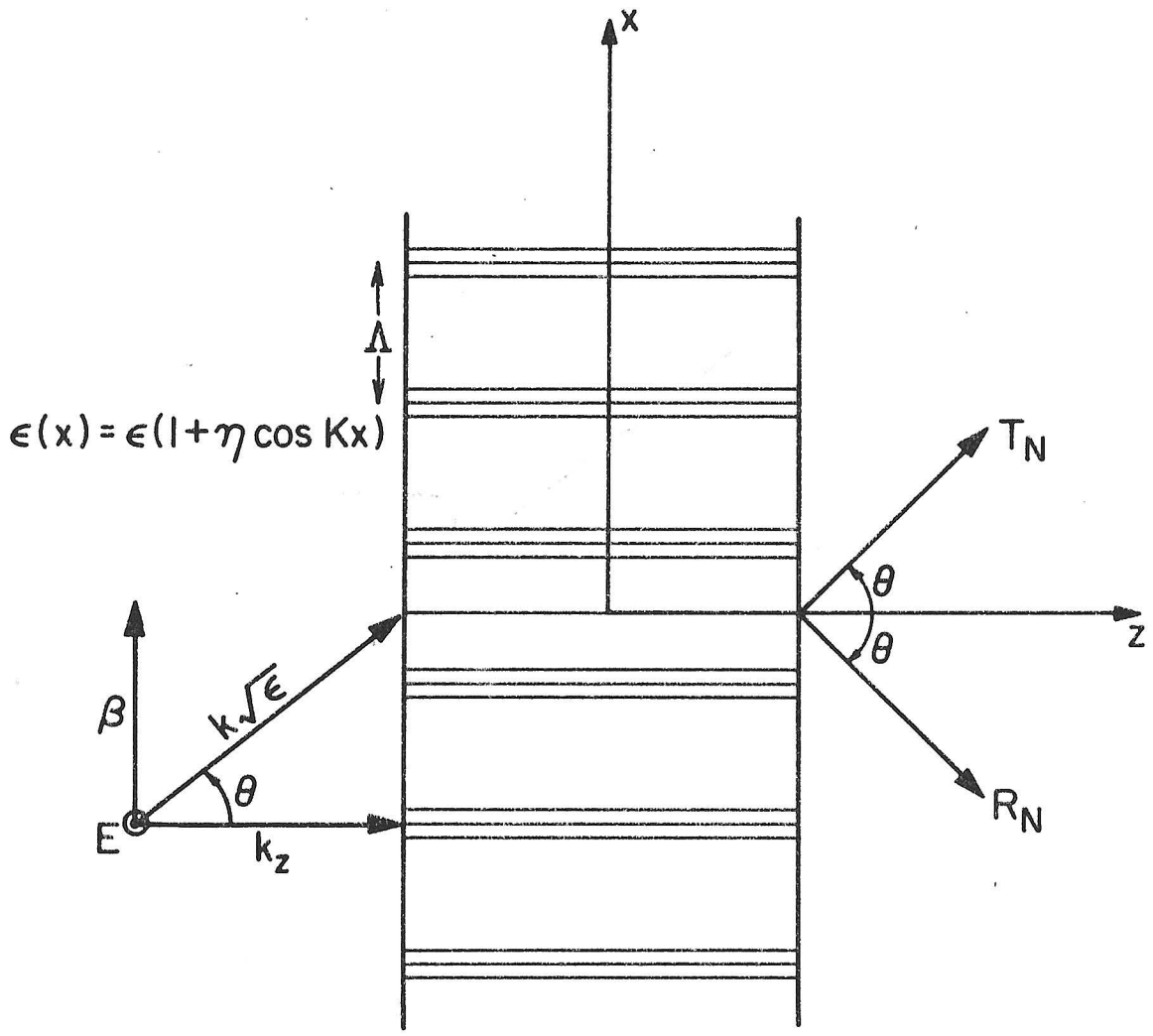

Fig. 6.11 Configuration of TE wave obliquely incident upon a holographic grating. The original wave and the Bragg reflected wave emerge as T_N and R_N respectively.

wave diffraction by acoustic waves or by holographic gratings. The former problem was solved by Chu and Tamir[22] who used both the Floquet and the coupled waves approach. The latter problem was dealt with exhaustively by Kogelnik[15] who developed a coupled waves approach that was valid near the first Bragg resonance. More recently variations of these problems have been investigated theoretically and experimentally by several authors.[68, 69, 81-84]

In this section the ECW equations are discussed for transversely periodic media. The derivation is similar to that of chapter III and the details are given in Appendix E. The approximate boundary conditions are applied and the results are given for the strengths of the undiffracted and Bragg diffracted waves in holographic gratings. As in previous chapters, the ECW results will hold for all Bragg orders.

1. ECW Equations for Transversely Periodic Media

Consider solutions to the wave equation for the transverse electric (TE) field

$$\left[\frac{\partial^2}{\partial z^2} + \frac{\partial^2}{\partial x^2} + k^2 \epsilon(x)\right] E(x, z) = 0 \qquad (6.C1)$$

where

$$\epsilon(x) = \epsilon_r + i\epsilon_i + \epsilon_r \sum_p (\eta_r + i\eta_i)_p f_p \cos pKz$$

is the periodic relative dielectric constant. Following the example of Kogelnik[15] we consider a wave of form $e^{i[\beta_x + k_z z]}$ which is successively scattered from the periodic dielectric to a wave of form $e^{i[(\beta - NK)x + k_z z]}$. The first wave is designated as $F_1(z)$ and the Bragg

scattered wave as $B_1(z)$. Using the same ECW assumptions as in chapter III we let

$$E(x,z) = \sum_{n=-1}^{N^*/2} \Big\{ F(z)_{1-2n/N}\, e^{i[(1-2n)/N)\beta_o x+\Delta\beta x+k_{z_o} z]} + B(z)_{1-2n/N}\, e^{-(1-2n/N)\beta_o x+\Delta\beta x+k_{z_o} z]} + \binom{1}{0} S(z)\, e^{i[\Delta\beta x+k_{z_o} z]} \Big\} \quad (6.C2)$$

be the assumed TE field. Substituting the above expression into the wave equation (6.C1) for singly periodic lossless media, we find the following ECW equations (see Appendix E).

$$\left.\begin{aligned} F_1'(z) - i\delta_N F_1(z) &= i\chi_N B_1(z) \\ B_1'(z) + i\delta_N B_1(z) &= i\chi_N F_1(z) \end{aligned}\right\} \quad (6.C3)$$

where

$$\delta_N = \frac{k^2\epsilon\left\{1-\zeta_N\left(\frac{\eta}{2\sin\theta_o}\right)^2\left[\frac{N^2}{2(N^2-1)}\right]\right\}-(\beta_o+\Delta\beta_N)^2-k_{z_o}^2}{2k_{z_o}} \quad (6.C4)$$

$$\chi_N = \frac{(-1)^{N+1} k^2\epsilon\,\eta^N}{2^{N+1} k_{z_o}(\sin^2\theta_o)^{N-1}} \frac{1}{\prod^*\{4n(n-N)/N^2\}^2} \quad (6.C5)$$

$$k = k_o + \Delta k_N$$

$$\beta = \beta_o + \Delta\beta_N$$

$$k_z = k_{z_o} + \Delta k_{z_N}$$

$$\beta_o = NK/2$$

$$k_o^2\epsilon = k_{z_o}^2 + \beta_o^2$$

$$\sin\theta_o = \beta_o/k_o\,\epsilon^{\frac{1}{2}}$$

Assuming a solution of the form $e^{i\Delta k_z z}$ gives the dispersion relation

$$\left(\frac{\Delta k_{z_N}}{K}\right)^2 = \left[\left(\frac{\delta_N}{K}\right)^2 + \left(\frac{\chi_N}{K}\right)^2\right] \qquad (6.C6)$$

The similarities and differences between the longitudinally periodic LP) and the transversely periodic (TP) case are given below.

1. The sign differences in the TP case cause the dispersion relation to be real for real periodicities and passive lossless dielectrics (i.e. $\eta_i = 0 = \epsilon_i$). Hence no bandgaps appear in the longitudinal wavenumber as in the LP case.
2. Maximum phase matching between $F_1(z)$ and $B_1(z)$ occurs slightly away from the exact Bragg condition for higher-order Bragg interactions in both the TP and LP cases.

The first Bragg order results are found from (6.C4-5) as

$$\frac{\delta_1}{K} \simeq \left[\frac{\Delta k_1 \sqrt{\epsilon}}{K} - \frac{\Delta\beta_1 \sin\theta_o}{K}\right] \frac{1}{\cos\theta_o} - \frac{\Delta\beta_1^2}{K^2} \qquad (6.C7)$$

$$\frac{\chi_1}{K} \simeq \frac{\eta}{8 \cos\theta_o \sin\theta_o} \qquad (6.C8)$$

Small changes in frequency or angle are accounted for by the first and second terms of the phase mismatch. The third term is negligible away from normal incidence. Results for other Bragg orders and for complex periodicities can be found easily from previous results. A similar derivation for TM waves can also be made.

2. ECW Reflection and Transmission Coefficients

The slab configuration of Fig. 6.11 shows the undiffracted wave proportional to T_N and the Bragg diffracted wave proportional

to R_N. The incident wave is of unit amplitude. The appropriate boundary conditions for the TP slab are approximately[15]

$$\left.\begin{aligned} F(-\ell/2) &= 1 & F(\ell/2) &= T_N \\ B(-\ell/2) &= 0 & B(\ell/2) &= R_N \end{aligned}\right\} \qquad (6.C9)$$

These equations indicate that the Bragg diffracted wave increases in value from zero to R_N while the undiffracted wave decreases from unity to T_N. Note that any reflected wave in the region $z < -\ell/2$ is ignored.

The ECW equations (6.C3) are solved with the boundary conditions imposed by (6.C9). The method of solution is analogous to that of the LP case (see Appendix C). The results are

$$R_N = \frac{i\,\chi_n \sin \Delta k_{z_N} \ell}{\Delta k_{z_N}} \qquad (6.C10)$$

$$T_N = \frac{\Delta k_{z_N} \cos \Delta k_{z_N} \ell + i\,\delta_N \sin \Delta k_{z_N} \ell}{\Delta k_{z_N}} \qquad (6.C11)$$

for coupling between identical modes (i.e. $\delta_p = \delta_q$, $\chi_{pq} = \chi_{qp} = \chi$). Note that for exact phase matching, the reflection and transmission coefficients vary as sines and cosines. Hence, the energy is alternately shifted between the undiffracted wave $F_1(z)$ and the Bragg diffracted wave $B_1(z)$, along the z coordinate. Away from exact phase match the energy transfer is incomplete.

3. Discussion of Holographic Gratings

We note that the development of the ECW equations for the TP case is identical to that of the LP case. The ECW equations are of the same form as that of several other authors.[19, 22, 69] The

advantage of the present derivation is the simplicity of the explicit expressions for phase mismatch and coupling. In particular the deviation from the exact Bragg condition that provides maximum coupling or highest diffraction efficiency is easily found.

In the preceding derivation we found coupling between the waves $F_1(z)$ and $B_1(z)$. This means that the diffracted and undiffracted waves, the amplitudes of which are given by R_N and T_N, are symmetric with respect to the z axis. A similar theory could be developed for coupling between any other set of two waves. For example, one could find a set of coupled equations for coupling between $F_1(z)$ and $B(z)_{1+2q/N}$ where $q = 0, 1, 2, \ldots$ represents different spectral orders. In this case the undiffracted wave propagates at the angle $\theta \simeq \arcsin(\beta_o/k_{z_o})$ whereas the diffracted wave propagates at the angle $\theta \simeq \arcsin[\beta_o(1+2q/N)/kz_o]$ with respect to the z axis. The diffraction efficiency DE is usually defined by the relation $DE = |T_N|^2$.

The theory is approximate since only a few space harmonics were used, only the approximate boundary conditions were applied and because the (assumed small) reflected wave for $z < -\ell/2$ was ignored.

D. Gaussian Beams in Periodic Media

With the advent of the laser, it is useful to consider Gaussian beam scattering from periodic structures. Several authors[85, 91-94] have considered Gaussian beam scattering at dielectric interfaces or in periodic media. The method of beam reflection at interfaces was developed by Brekhovskikh.[91] We will use this formulation and

a similar one used by Tamir and Bertoni.[92]

In this section, the formulation for Gaussian beam propagation in LP and TP slabs will be outlined. The previously derived ECW reflection and transmission coefficients will be used. Numerical examples will be given in a future report. However, the general characteristics may be determined from the previous transient analysis for certain cases.

Consider the aperture Gaussian beam $E_{ap}(x, -h)$ of Figure 6.12 that is formed at the plane $z = -h$.

$$E_{ap}(x', 0) = \frac{e^{-(x'/w)^2}}{\pi^{\frac{1}{2}} w} \tag{6.D1}$$

The propagating wave is given approximately by

$$E_{ap}(x, z)\Big|_{z=-h} = \frac{e^{-(x\cos\theta/w)^2} e^{ik\sqrt{\epsilon}\,[x\sin\theta+(z+h)\cos\theta]}}{\pi^{\frac{1}{2}} w}\Bigg|_{z=-h} \tag{6.D2}$$

The incident wave $E_{inc}(x, z)$ is given by the Fourier transform of the spectral amplitude $\Phi(k_x)$

$$E_{inc}(x, z) = \frac{1}{2\pi}\int_{-\infty}^{\infty} \Phi(k_x) e^{i[k_x x + k_z(z+h)]}\, dk_x \qquad -h < z < 0 \tag{6.D3}$$

where $k_z = (k^2\epsilon - k_x^2)^{\frac{1}{2}}$.

The spectral amplitude is given in terms of the aperture field by the relation

$$\Phi(k_x) = \int_{-\infty}^{\infty} E_{ap}(x, -h) e^{-ik_x x}\, dx \tag{6.D4}$$

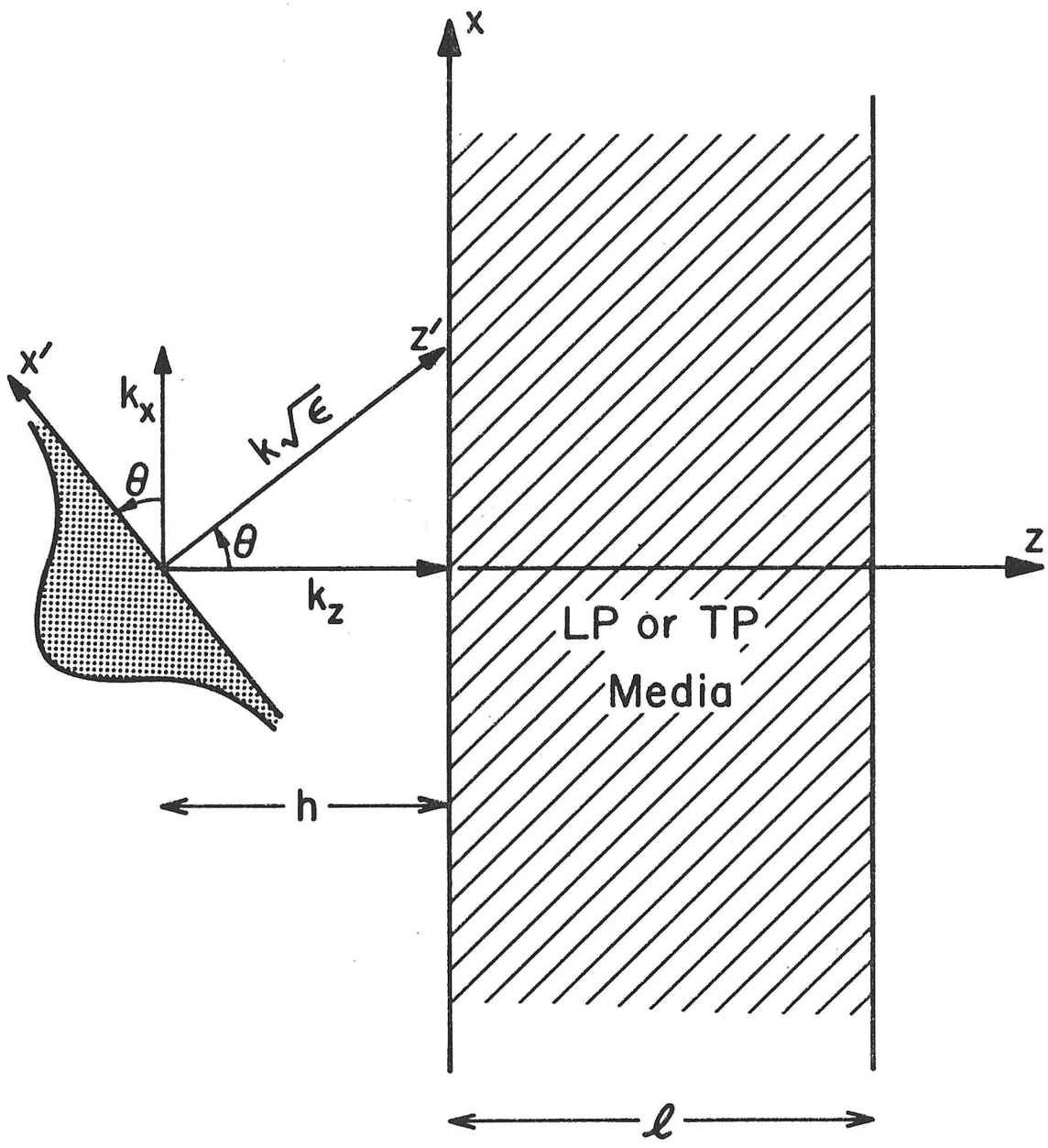

Fig. 6.12 Gaussian beam incident upon LP or TP slab near Bragg resonance.

$$\Phi(k_x) = \frac{e^{-[w(k_x - k\sqrt{\epsilon}\sin\theta_o)/2\cos\theta_o]^2}}{\cos\theta_o} \qquad (6.D5)$$

Two assumptions are made. First, assume that the beam is well-collimated, or

$$k\sqrt{\epsilon}\, w \gg 1 \qquad (6.D6)$$

where w represents the beam width. This limits significant spectral amplitude to values about $k_x = k\,\epsilon^{\frac{1}{2}}\sin\theta_o$. Hence, k_z is usually real and the contribution to surface or lateral waves can be ignored. This is also necessary for the ECW approximations. Second, the incident and scattered waves are near Bragg resonance, or

$$\beta_o/k_o\epsilon^{\frac{1}{2}} = N\,K/(2k_o\epsilon^{\frac{1}{2}}) \simeq \begin{cases} \cos\theta_o & \text{LP media} \\ \sin\theta_o & \text{TP media} \end{cases} \qquad (6.D7)$$

The transmitted and reflected fields $E_T(x, z)$ and $E_R(x, z)$ are found from the integral of the product of the spectral amplitude (at z = 0) and the appropriate coefficient;

$$E_T(x, z) = \frac{1}{2\pi}\int_{-\infty}^{\infty} T(k_x)\Phi(k_x)e^{+i[k_x x + k_z(z+h)]}\,dk_x \qquad (6.D8)$$

$$E_R(x, z) = \frac{1}{2\pi}\int_{-\infty}^{\infty} R(k_x)\Phi(k_x)e^{\pm i[k_x x - k_z(z+h)]}\,dk_x \qquad (6.D9)$$

where the $\left(\begin{smallmatrix}\text{upper}\\ \text{lower}\end{smallmatrix}\right)$ signs hold for $\left(\begin{smallmatrix}\text{LP}\\ \text{TP}\end{smallmatrix}\right)$ media.

The expressions for $R(k_x)$ and $T(k_x)$ can be found from equations (6.A13, 14) and (6.C10, 11) for LP and TP media, respectively. The values of phase mismatch and coupling have been derived for arbitrary angle of incidence in TP media and at normal incidence for

LP media. The extension of the LP results to arbitrary angles of incidence is a straightforward derivation and will not be given here. The explicit results near the first Bragg resonance are,

$$\frac{\delta_1}{K} \simeq \left[\frac{\Delta k_1 \sqrt{\epsilon}}{K} - \frac{\Delta k_x}{K} \sin\theta_o\right] \frac{1}{\cos\theta_o} - \frac{\Delta k_x^2}{K^2} \quad \text{for LP and TP media} \tag{6.D10}$$

$$\frac{\chi_1}{K} \simeq \frac{\eta}{8\cos\theta_o} \frac{1}{\begin{pmatrix}\cos\theta_o \\ \sin\theta_o\end{pmatrix}} \quad \text{for} \quad \begin{pmatrix}\text{LP} \\ \text{TP}\end{pmatrix} \text{ media} \tag{6.D11}$$

where

$$\sin\theta_o = \begin{cases} k_{xo}/k_o \epsilon^{\frac{1}{2}} & \text{for LP media} \\ \beta_o / k_o \epsilon^{\frac{1}{2}} & \text{for TP media} \end{cases}$$

$$\Delta k_x = k_x - k_{x_o}$$

$$k_{x_o} = \begin{cases} [k_o^2 \epsilon - \beta_o^2]^{\frac{1}{2}} & \text{for LP media} \\ \beta_o & \text{for TP media} \end{cases}$$

$$\beta_o = K/2$$

Note that for LP media the expressions for the transmitted and reflected fields are similar to the transient analysis if the time coordinate is replaced by the space coordinate. In particular, Figures 6.7-9 show the spatial dispersion of pulses in space for rectangular and Gaussian input beams at exact Bragg frequencies and non-normal incidence if the normalized time is replaced by normalized distance.

In this section the derivation for spatially bounded beams was given a form that is easy to compute under the ECW assumptions. It was shown that temporal and spatial dispersion are similar and that the results of the transient analysis could be extended to include beam propagation.

CHAPTER VII

CONCLUSIONS

This report establishes an approximate method of calculating the properties of the Brillouin diagram at all Bragg orders for waves in periodic media. The method is introduced in the second chapter where the connection between the Floquet and the coupled waves theory is shown and demonstrated with several numerical examples at the first Bragg resonance. In the third chapter, the idea of cross- and self-coupling helps to extend the coupled waves theory to all Bragg resonances by the use of coupling diagrams. These results explicitly show the dependence of the bandgap width, bandgap shift and coupling upon Bragg order. The results closely match the exact Floquet dispersion relations. Furthermore, the ECW theory accounts for multiharmonic periodicities and demonstrates the idea of disappearing bandgaps under certain conditions.

The fourth and fifth chapters deal with active or lossy dielectrics. Inverted bandgaps occur only for certain types of coupling and at certain Bragg orders. The stability of active periodic media has characteristics that depended on the nature (i.e. inverting or non-inverting) of these bandgaps. Absolute stabilities are found to occur under certain conditions and only at certain frequencies in active periodic media. These threshold conditions and mode spectra agree with results found from an entirely different analysis, in the appropriate limit, at the first Bragg order. The advantage of the stability analysis is that only the dispersion relation is needed to fully describe the stability characteristics.

The last chapter includes a few applications of the preceding theory to finite length media. The topics of reflection, transmission, transients, DFB lasers, holographic gratings and beams in periodic media are briefly discussed and illustrated.

The ECW theory demonstrates some of the power and versatility of the coupled waves formalism. It is anticipated that space-time periodic media and variable-frequency or almost-periodic media may be treated in a similar manner. The case of transversely bounded media can be treated using a previously developed approach[32] for the guided modes. The result is that each power of η will be multiplied by an overlap integral. Hence the coupling will be somewhat decreased.

Exact theories such as the Floquet theory, matrix theory or the method of invariant imbedding will be useful for specific cases where exact results are needed. However, the intuitively appealing ECW theory gives results explicitly without lengthy computations and is surprisingly accurate in the cases treated here.

APPENDIX A

ASYMPTOTIC FORM OF FIELDS FOR ABSOLUTE INSTABILITIES IN PERIODIC MEDIA

Consider the following equation for $F(z,t)$ which is proportional to the electric field

$$F(z,t) = \int_{-\infty}^{\infty} \int_{-\infty}^{\infty} \frac{S(\Delta\beta,\omega)e^{i(\Delta\beta z - \omega t)}}{D(\Delta\beta,\omega)} \frac{d(\Delta\beta)\,d\omega}{(2\pi)^2} \tag{A.1}$$

where $S(\Delta\beta,\omega)$ is the normalized source and $D(\Delta\beta,\omega)$ is the dispersion relation. We are interested in the asymptotic value of $F(z,t)$ for large times when an absolute instability occurs. This happens when the roots of $D(\Delta\beta,\omega)$ merge in the $\Delta\beta$ plane from opposite half-planes separated by the line $\mathrm{Im}\{\Delta\beta\} = 0$. We assume that the source is analytic in $\Delta\beta$ and that it is turned on at the time $t = 0$.

We follow the work of previous authors[73, 74] and expand the dispersion relation about the instability at $\omega = \omega'$ and $\Delta\beta = \Delta\beta'$ in a Taylor series. Then the integration is first carried out in the $\Delta\beta$ plane and finally in the ω plane.

The Taylor expansion of $D(\Delta\beta,\omega)/S(\Delta\beta,\omega)$ is,

$$\frac{D(\Delta\beta,\omega)}{S(\Delta\beta,\omega)} \simeq D_1^2 (\Delta\beta - \Delta\beta')^2 + D_2^2 (\omega - \omega') \tag{A.2}$$

where

$$D_1^2 = \frac{1}{2} \frac{\partial^2 (D/S)}{\partial (\Delta\beta)^2} \bigg|_{\Delta\beta=\Delta\beta'}$$

$$D_2^2 = \frac{\partial (D/S)}{\partial \omega} \bigg|_{\omega=\omega'}$$

We rearrange the dispersion relation to find

$$F(z,\omega) = \frac{1}{4\pi i D_1 D_2 (\omega-\omega')^{\frac{1}{2}}} \int_{C'} \left[\frac{e^{i\Delta\beta z}}{\Delta\beta-\Delta\beta'-iD_2(\omega-\omega')^{\frac{1}{2}}/D_1} - \frac{e^{i\Delta\beta z}}{\Delta\beta-\Delta\beta'+iD_2(\omega-\omega')^{\frac{1}{2}}/D_1} \right] d(\Delta\beta) \tag{A.3}$$

where

$$F(z,t) = \int_{-\infty}^{\infty} F(z,\omega)\, e^{-i\omega t}\, \frac{d\omega}{2\pi}$$

and the contour C' is shown in Figure A. 1a. The first pole of (A.3) is located in the upper half plane and contributes for $z > 0$ while the second pole is located in the lower half plane and contributes for $z < 0$. For $z > 0$, equation (A.3) becomes

$$F(z,\omega) = \frac{e^{i[\Delta\beta'+iD_2(\omega-\omega')^{\frac{1}{2}}/D_1]z}}{2i D_1 D_2 (\omega-\omega')^{\frac{1}{2}}} \tag{A.4}$$

To carry out the integration in ω, we depress the contour around the singularities down to the real ω axis. This contour C'' is shown in Figure A. 1b where two poles at $\omega = \pm \omega_s$ represent the harmonic source contributions. This second integral is

$$F(z,t) = \frac{e^{i\Delta\beta' z}}{2i D_1 D_2} \int_{C''} \frac{e^{-[D_2(\omega-\omega')^{\frac{1}{2}}/D_1]z}\, e^{-i\omega t}}{(\omega-\omega')^{\frac{1}{2}}}\, \frac{d\omega}{2\pi} \tag{A.5}$$

The branch cut of $(\omega-\omega')^{\frac{1}{2}}$ provides the major contribution. Hence, we approximate the integral (A.5) as $t \to \infty$ by

$$F(z,t) = \frac{e^{i\Delta\beta' z}}{2i D_1 D_2} \left\{ \int_o^{\sigma} \frac{e^{-[D_2(\omega-\omega')^{\frac{1}{2}}/D_1]}}{(\omega-\omega')^{\frac{1}{2}}} - \int_{\sigma}^{o} \frac{e^{+[D_2(\omega-\omega')^{\frac{1}{2}}/D]z}}{(\omega-\omega')^{\frac{1}{2}}} \right\} \times e^{-i\omega t}\, \frac{d\omega}{2\pi} \tag{A.6}$$

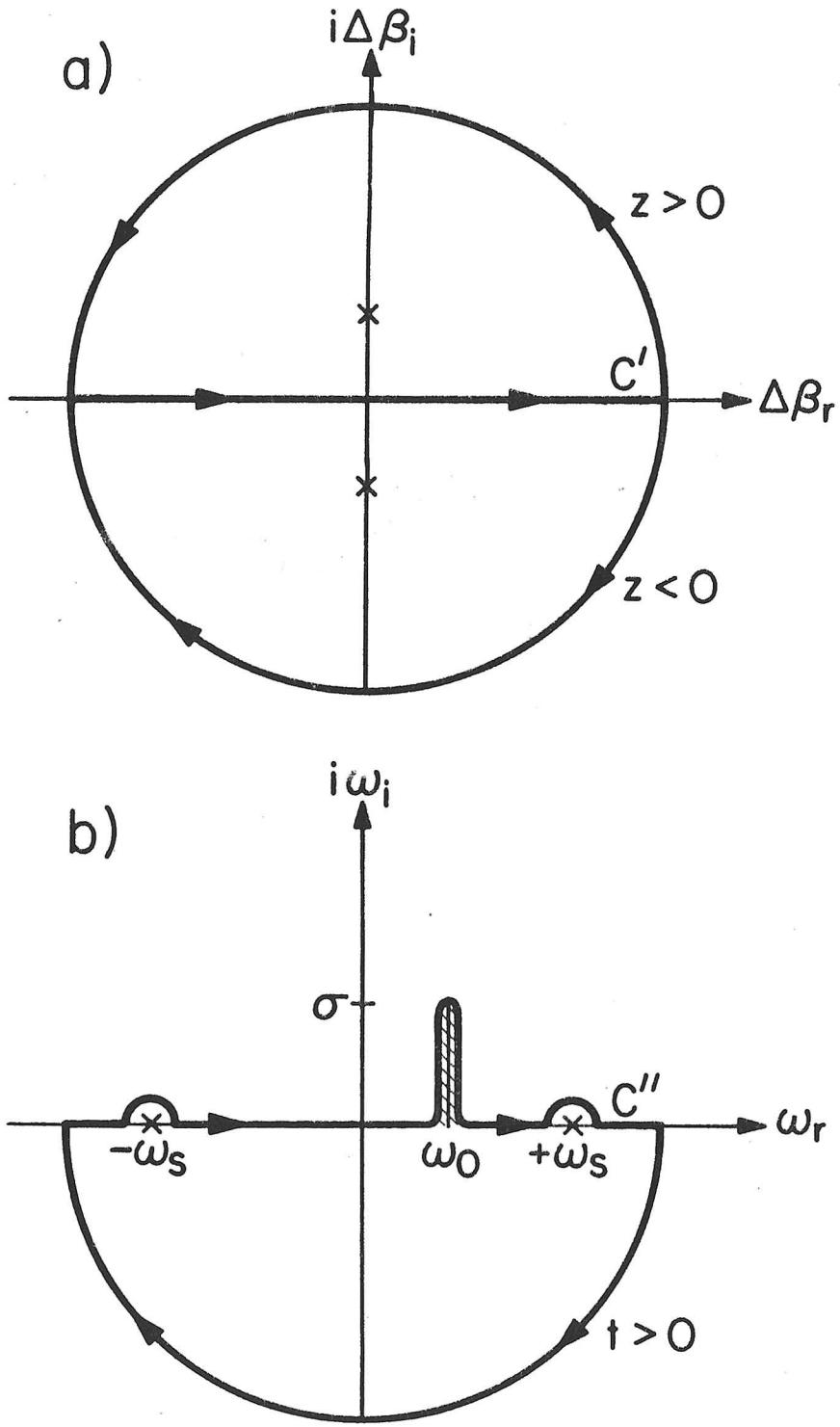

Fig. A.1 a) Contour C' in $\Delta\beta$-plane showing poles when $\Delta\beta' = 0$. b) Contour C'' in ω-plane showing 2 poles due to source at $\pm\omega_s$ and branch cut at instability frequency ω_o.

$$F(z,t) = \frac{e^{i\Delta\beta' z}\, e^{-i\omega_o t}}{i\, D_1\, D_2} \int_o^{\sigma} \frac{\cosh[D_2(i\omega_i - i\sigma)^{\frac{1}{2}}/D_1]z\; e^{\omega_i t}}{(i\,\omega_i - i\sigma)^{\frac{1}{2}}} \frac{id\omega_i}{2\pi} \quad (A.7)$$

where $\omega' = \omega_o + i\sigma$

Let $(\omega_i - \sigma) = -q$

$$F(z,t) = \frac{e^{i\Delta\beta' z}\, e^{-i\omega_o t}\, e^{\sigma t}}{2\pi\, D_1\, D_2} \int_o^{\sigma} \frac{e^{-qt} \cosh[D_1(-iq)^{\frac{1}{2}}/D_1]z dq}{(-i)^{\frac{1}{2}}\, q^{\frac{1}{2}}} \quad (A.8)$$

Letting the upper limit tend to infinity we get

$$F(z,t) \rightarrow \frac{e^{i(\Delta\beta' z - \omega_o t)}\, e^{\sigma t}}{2\pi^{\frac{1}{2}}\, D_1\, D_2 (-i)^{\frac{1}{2}}\, t^{\frac{1}{2}}} \qquad \text{as} \qquad t \rightarrow \infty \quad (A.9)$$

Thus, the electric field is time-growing with the wavenumber and frequency of the absolute instability. For two instabilities at different frequencies, there will be two branch cuts in Figure A.1b and the $F(z,t)$ will have two similar contributions, each of the form of (A.9).

APPENDIX B

ECW PARAMETERS FOR SQUARE-WAVE, TRIANGULAR-WAVE AND SAWTOOTH PERIODICITIES

For applications to instabilities and DFB filters and oscillators it is convenient to have the phase mismatch δ_N and the coupling χ_N at the first three Bragg orders for square-wave, triangular-wave and sawtooth periodicities.

It has been shown that the major contribution to N^{th} order coupling is from the Fourier component f_N of the periodicity. Hence for the three periodicities under consideration, the results at first and third orders are a straightforward application of the results of chapter III since each wave contains odd harmonics. In addition the sawtooth wave contains both even and odd harmonics so previous results can be used at all Bragg orders for this periodicity. The computation that needs to be carried out is for parameters at even-order resonances with odd-order Fourier components. We will carry out these computations for N = 2 in the lossless case ($\epsilon = \epsilon_r$).

The three periodicities have the following Fourier decomposition:

$$\text{Square-wave} \quad f_p = \begin{cases} \frac{1}{p} & p \text{ odd} \\ 0 & p \text{ even} \end{cases} \tag{B.1}$$

$$\text{Triangular-wave} \quad f_p = \begin{cases} (-1)^{(p-1)/2}/p^2 & p \text{ odd} \\ 0 & p \text{ even} \end{cases} \tag{B.2}$$

$$\text{Sawtooth} \quad f_p = (-1)^{(p+1)}/p \tag{B.3}$$

with the normalization $f_1 = 1$. An appropriate sine or cosine Fourier

series is used for periodicities that are odd or even in z, respectively.

At the first Bragg resonance, we find that $\chi_1/K = \eta/8$ and $\delta_1/K = \Delta k\, \epsilon^{\frac{1}{2}}/K$ by the use of (3.A24, 3.A25) for all three periodicities. This is identical to the sinusoidal case.

At the second Bragg resonance, we find $\chi_2/K = -\eta^2/8$ and $\delta_2/K = \Delta k \epsilon^{\frac{1}{2}}/K - \eta^2/12$ for sinusoidal periodicities. The other periodicities present need to be calculated. We consider the seventeen waves B_8, B_7, ..., S, ..., F_7, F_8 for periodicities with $f_p = 0$ for p even and N = 2. Thus, we need only the eleven waves B_8, B_6, ..., S, ... F_6, F_8 since no significant coupling can take place through B_q, F_q with q odd. Using the ECW approximations, we need to solve the following equations.

$$-63\, F_8 = -\frac{\eta}{2} f_7 F_1$$

$$-35\, F_6 = -\frac{\eta}{2} (f_5 F_1 + f_7 B_1)$$

$$-15\, F_4 = -\frac{\eta}{2} (f_3 F_1 + f_5 B_1)$$

$$-3\, F_2 = -\frac{\eta}{2} (f_1 F_1 + f_3 B_1)$$

$$\frac{2\Delta k}{k} F_1 + \frac{2i F_1'}{k \epsilon^{\frac{1}{2}}} = -\frac{\eta}{2} [f_5(B_6+F_4) + f_7(F_8+B_6) + f_3(F_4+B_2) + f_1(F_2+S)]$$

$$S = -\frac{\eta}{2} [f_1(B_1+F_1)]$$

$$\frac{2\Delta k}{k} B_1 + \frac{2i B_1'}{k \epsilon^{\frac{1}{2}}} = -\frac{\eta}{2} [f_5(B_6+F_4) + f_7(B_8+F_6) + f_3(B_4+F_2) + f_1(B_2+S)]$$

$$-3\, B_2 = -\frac{\eta}{2} (f_1 B_1 + f_3 F_1)$$

(continued on next page)

$$-15\ B_4 = -\frac{\eta}{2}(f_3 B_1 + f_5 F_1)$$

$$-35\ B_6 = -\frac{\eta}{2}(f_5 B_1 + f_7 F_2)$$

$$-63\ B_8 = -\frac{\eta}{2} f_7 B_1 \qquad \text{(B.4)}$$

where self- and cross-coupling $O(\eta^2)$ has been included. The equations (B.4) are solved to give the usual coupled equations for F_1 and B_1 with

$$\frac{\chi_2}{K} = \frac{\eta^2}{8}\left[-f_1^2 + \frac{2f_1 f_3}{3} + \frac{2}{15} f_3 f_5 + \frac{2}{35} f_5 f_7 + \ldots\right] \qquad \text{(B.5)}$$

$$\frac{\delta_2}{K} = \frac{\Delta k\, \epsilon^{\frac{1}{2}}}{K} - \frac{\eta^2}{12}\left[f_1^2 - \frac{4}{5} f_3^2 - \frac{1}{7} f_5^2 - \frac{13 f_7^2}{210} - \ldots\right] \qquad \text{(B.6)}$$

In (3.B6), if the terms drop off as $f_p \propto 1/p$ or faster, only the first two terms need to be kept in the series for accuracies of order 1% in phase mismatch. In (3.B5) the series can be summed explicitly by using Schläfli's Polynomials[98] S_n of order n for the square- and triangular-wave. Two terms will again give accuracies of order 1%. For square-waves we find

$$\frac{\chi_2}{K} = \frac{\eta^2}{8}[-1+2S_2], \quad \frac{\delta_2}{K} = \frac{\Delta k \epsilon^{\frac{1}{2}}}{\eta} - \frac{\eta^2}{12}(.911) \qquad \text{(B.7)}$$

while for triangular waves

$$\frac{\chi_2}{K} = \frac{\eta^2}{8}[-1+2S_3], \quad \frac{\delta_2}{K} = \frac{\Delta k \epsilon^{\frac{1}{2}}}{\eta} - \frac{\eta^2}{12}(.990) \qquad \text{(B.8)}$$

where $S_2 = \frac{\pi^2 - 8}{16} \simeq 0.1168\ldots$

$S_3 = \frac{32 - 3\pi^2}{64} \simeq 0.3736\ldots$

Thus, we have accounted for the major self- and cross-coupling terms $O(\eta^2)$ which can be approximated by only considering the seven waves B_4, B_2, B_1, S F_1, F_2, F_4 for periodicities with odd Fourier components f_p.

The case of the sawtooth-wave must be treated separately since it contains both even and odd Fourier components and must be expanded in a sine series. To consider the correction to the self-coupling from ηf_1 and to the cross-coupling from ηf_2 we consider only the first three Fourier components f_1, f_2, f_3 and the waves B_3, B_2, B_1, S, F_1, F_2, F_3 for simplicity. The equations for N = 2 in the ECW approximation are then,

$$\left.\begin{aligned}
-15\, F_4 &= -\frac{\eta}{2i} f_3\, F_1 \\
-8 F_3 &= -\frac{\eta}{2i} f_2\, F_1 \\
-3\, F_2 &= -\frac{\eta}{2i} f_1\, F_1 \\
\frac{2\,\Delta k}{k} F_1 + \frac{2i\, F_1'}{k\, \epsilon^{\frac{1}{2}}} &= -\frac{\eta}{2i}\left[f_1(S-F_2)+f_2(B_1-F_3)+f_3(B_2-F_4)\right] \\
S &= -\frac{\eta}{2i}\left[f_1(B_1-F_1)\right] \\
\frac{2\,\Delta k}{k} F_1 + \frac{2i\, F_1'}{k\, \epsilon^{\frac{1}{2}}} &= -\frac{\eta}{2i}\left[f_1(B_2-S)+f_2(B_3-F_1)+f_3(B_4-F_2)\right] \\
-3\, B_2 &= +\frac{\eta}{2i} f_1\, B_1 \\
-8\, B_3 &= +\frac{\eta}{2i} f_2\, B_1 \\
-15\, B_4 &= +\frac{\eta}{2i} f_3\, B_1
\end{aligned}\right\} \qquad \text{(B.9)}$$

The solution for the coupling and phase mismatch are

$$\frac{\chi_2}{K} = \frac{\eta}{4}\left[f_2 + O(\eta f_p)\right] \qquad (B.10)$$

$$\frac{\delta_2}{K} = \frac{\Delta k \epsilon^{\frac{1}{2}}}{K} - \frac{\eta^2}{12}\left[f_1^2 - \frac{3f_2^2}{16} - \frac{f_3^2}{10} - \ldots\right] \qquad (B.11)$$

where it is understood that $\chi^{\pm} = \pm i\,\chi$. The approximations to 1% involves keeping only the first term in (B. 10) for $\eta \ll 1$) and the first two terms in the series in (B. 11). Thus, for the sawtooth-wave,

$$\frac{\chi_2}{K} = \frac{\eta}{8}, \qquad \frac{\delta_2}{K} = \frac{\Delta k \epsilon^{\frac{1}{2}}}{K} - \frac{\eta^2}{12}\ (0.953) \qquad (B.12)$$

The approximation that uses only the first term in both (B. 10) and (B. 11) can be gotten directly from (3. A24, 3. A25) with $\sim$ 5% accuracy.

At the third Bragg order all three of the periodicities considered here contain the Fourier component f_3. Hence, the major cross-coupling will be due to ηf_3 and the major self-coupling will be due to ηf_1. The phase mismatch and coupling from (3. A24, 3. A25) are

$$\frac{\delta_3}{K} = \frac{\Delta k \epsilon^{\frac{1}{2}}}{K} - \frac{27\,\eta_2 f_1^2}{256} \qquad (B.13)$$

$$\frac{\chi_3}{K} = \frac{3\eta f_3}{8} \qquad (B.14)$$

The error is again on the order of 1% except for the phase mismatch of the sawtooth-wave where the error $\sim$ 5%.

The results of this appendix and comparisons to the sine wave are found in Tables B. 1 and B. 2.

	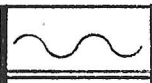	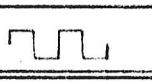	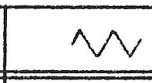	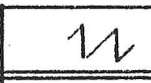
N = 1	$\frac{\eta}{8}$	$\frac{\eta}{8}$	$\frac{\eta}{8}$	$\frac{\eta}{8}$
N = 2	$\frac{-\eta^2}{8}$	$\frac{-\eta^2}{8}(0.77)$	$\frac{-\eta^2}{8}(0.93)$	$\frac{\eta}{8}$
N = 3	$\frac{243\,\eta^3}{2048}$	$\frac{\eta}{8}$	$\frac{\eta}{24}$	$\frac{\eta}{8}$

Table B.1 Normalized coupling coefficient χ_N/K for sine-, square-, triangular- and sawtooth-wave periodicities. For the sawtooth-wave the coupling is $\chi^{\pm} = \pm i\chi$.

	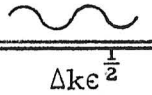	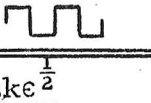	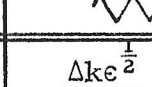	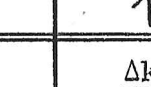
N = 1	$\frac{\Delta k\epsilon^{\frac{1}{2}}}{K}$	$\frac{\Delta k\epsilon^{\frac{1}{2}}}{K}$	$\frac{\Delta k\epsilon^{\frac{1}{2}}}{K}$	$\frac{\Delta k\epsilon^{\frac{1}{2}}}{K}$
N = 2	$\frac{\Delta k\epsilon^{\frac{1}{2}}}{K} - \frac{\eta^2}{12}$	$\frac{\Delta k\epsilon^{\frac{1}{2}}}{K} - \frac{\eta^2}{12}(0.91)$	$\frac{\Delta k\epsilon^{\frac{1}{2}}}{K} - \frac{\eta^2}{12}(0.99)$	$\frac{\Delta k\epsilon^{\frac{1}{2}}}{K} - \frac{\eta^2}{12}(0.95)$
N = 3	$\frac{\Delta k\epsilon^{\frac{1}{2}}}{K} - \frac{27\eta^2}{256}$	$\frac{\Delta k\epsilon^{\frac{1}{2}}}{K} - \frac{27\eta^2}{256}$	$\frac{\Delta k\epsilon^{\frac{1}{2}}}{K} - \frac{27\eta^2}{256}$	$\frac{\Delta k\epsilon^{\frac{1}{2}}}{K} - \frac{\eta^2}{12}$

Table B.2 Normalized phase mismatch δ_N/K for sine-, square-, triangular- and sawtooth-wave periodicities.

APPENDIX C

REFLECTION AND TRANSMISSION COEFFICIENTS OF DFB FILTER

Consider the following coupled equations

$$\left.\begin{aligned} F_1'(z) - i\,\delta_p\, F_1(z) &= i\,\chi_{pq}\, B_1(z) \\ -B_1'(z) - i\,\delta_q\, B_1(z) &= i\,\chi_{qp}\, F_1(z) \end{aligned}\right\} \qquad \text{(C. 1)}$$

which describe waves in a DFB filter. The primes denote differentiation with respect to the coordinate z. Differentiating (C. 1) and eliminating $B_1(z)$ and $F_1(z)$ respectively, produces

$$\begin{pmatrix} F \\ B \end{pmatrix}'' - i(\delta_p - \delta_q)\begin{pmatrix} F \\ B \end{pmatrix}' + (\delta_q\,\delta_p - \chi_{pq}\,\chi_{qp})\begin{pmatrix} F \\ B \end{pmatrix} = 0 \qquad \text{(C. 2)}$$

where the subscripts and arguments have been dropped for simplicity and the primes denote differentiation with respect to the coordinate z. The solutions to (C. 2) are

$$F\, e^{-i\left(\frac{\delta_p - \delta_q}{2}\right)z} = f_1\, e^{Dz} + f_2\, e^{-Dz} \qquad \text{(C. 3)}$$

$$B\, e^{-i\left(\frac{\delta_p - \delta_q}{2}\right)z} = b_1\, e^{Dz} + b_2\, e^{-Dz} \qquad \text{(C. 4)}$$

where $$D = + \left[\chi_{pq}\,\chi_{qp} - \left(\frac{\delta_p + \delta_q}{2}\right)\right]^{\frac{1}{2}} \qquad \text{(C. 5)}$$

Apply the boundary conditions

$$\left.\begin{aligned} F(\ell/2) &= 1 & F(\ell/2) &= T \\ B(-\ell/2) &= R & B(\ell/2) &= 0 \end{aligned}\right\} \qquad \text{(C. 6)}$$

to find the following equations

$$1 = \left[f_1 e^{-D\ell/2} + f_2 e^{D\ell/2}\right] e^{-i\left(\frac{\delta_p - \delta_q}{2}\right)\ell/2} \tag{C.7}$$

$$T = \left[f_1 e^{D\ell/2} + f_2 e^{-D\ell/2}\right] e^{i\left(\frac{\delta_p - \delta_q}{2}\right)\ell/2} \tag{C.8}$$

$$R = \left[b_1 e^{-D\ell/2} + b_2 e^{D\ell/2}\right] e^{-i\left(\frac{\delta_p - \delta_q}{2}\right)\ell/2} \tag{C.9}$$

$$O = \left[b_1 e^{D\ell/2} + b_2 e^{-D\ell/2}\right] e^{i\left(\frac{\delta_p - \delta_q}{2}\right)\ell/2} \tag{C.10}$$

Use (C. 7-8) to solve for $f_{\frac{1}{2}}$ and use (C. 9-10) to solve for $b_{\frac{1}{2}}$.

$$f_{\frac{1}{2}} = \mp\left[\frac{e^{(i\hat{\delta}\ell/2 \mp D\ell/2)} - T\, e^{(-i\hat{\delta}\ell/2 \pm D\ell/2)}}{e^{D\ell} - e^{-D\ell}}\right] \tag{C.11}$$

$$b_{\frac{1}{2}} = \mp\left[\frac{Re^{(i\hat{\delta}\ell/2 \mp D\ell/2)}}{e^{D\ell} - e^{-D\ell}}\right] \tag{C.12}$$

where $\hat{\delta} = (\delta_p - \delta_q)/2$

Two other equations for f_1 and b_1 can be found by substituting (C. 3, 4) into the coupled equations (C. 1). This produces the coupled equations

$$(i\hat{\delta} \pm D) f_{\frac{1}{2}} - i\delta_p f_{\frac{1}{2}} = i\chi_{pq} b_{\frac{1}{2}} \tag{C.13}$$

$$-(i\hat{\delta} \pm D) b_{\frac{1}{2}} - i\delta_q b_{\frac{1}{2}} = i\chi_{qp} f_{\frac{1}{2}} \tag{C.14}$$

Equations (C. 11-14) provide the necessary relations to solve for T and R, the transmission and reflection coefficients. After algebraic manipulations, the results are,

$$R = \frac{i\chi_{qp}}{D \coth D\ell - i\left(\frac{\delta_p + \delta_q}{2}\right)} \qquad (C.15)$$

$$T = \frac{D\, e^{i(\delta_p - \delta_q)\ell/2}}{D \cosh D\ell - i \frac{(\delta_p + \delta_q)}{2} \sinh D\ell} \qquad (C.16)$$

Note that the equations hold for all Bragg orders when the proper δ and χ are used. Also the equations hold for coupling between waves of different transverse modes, or in general for any coupled system where the phase mismatch and coupling might be different for the waves F(z) and B(z).

APPENDIX D

APPROXIMATIONS FOR DFB THRESHOLD AND SPECTRUM

1. High-Gain Approximation

Oscillation will occur in a DFB laser when the reflection or transmission coefficient becomes infinite. This implies the condition

$$D_N \coth D_N \ell = i \delta_N \tag{D.1}$$

where

$$D_N = [\chi_N^2 - \delta_N^2]^2$$

$$\delta_N = \Delta_N - i g_N$$

Equation (D.1) can be written in exponential form

$$\left[\frac{D_N - i \delta_N}{D_N + i \delta_N}\right] e^{2D_N \ell} = -1 \tag{D.2}$$

which is a complex equation. Under the high-gain approximation $g_N >> \chi_N$ and expanding the expression for D_N we find

$$D_N \mp i \delta_N = D_N \mp i \Delta_N \mp g_N \tag{D.3}$$

Either root of (D.3) when substituted into (D.2) yields

$$(g_N + i \Delta_N) e^{-(g_N + i\Delta_N)\ell} = \mp \frac{i \chi_N}{2} \tag{D.4}$$

Taking the amplitude of (D.4) we find the threshold gain condition for g_N

$$4(g_N^2 + \Delta_N^2) = \chi_N \chi_N^* e^{2g_N \ell} \tag{D.5}$$

where the value Δ_N is found from equating the phase of (D.4), or,

$$\tan^{-1}(\Delta_N/g_N) - \Delta_N \ell = (m + \tfrac{1}{2})\pi + \text{phase}(\chi) \quad (m=0, \pm1, \pm2, \ldots) \quad (D.6)$$

This latter result produces multiple values for the spectrum or oscillation frequencies which are called longitudinal modes. Since $\tan^{-1}(\Delta_N/g_N) \ll 1$, the mode spectrum can be further approximated by

$$\frac{\Delta k \sqrt{\epsilon_r}}{K} \simeq - (m+\tfrac{1}{2})\pi - \begin{pmatrix} 0 \\ \pi/2 \end{pmatrix} + \frac{\zeta_N \eta^2 N^3}{32(N^2-1)} \quad (D.7)$$

where $\begin{pmatrix} 0 \\ \pi/2 \end{pmatrix} = \begin{cases} 0 & \text{index coupling (all N), gain coupling (N even)} \\ \pi/2 & \text{gain coupling (N odd)} \end{cases}$

for index or gain coupling and singly periodic media.

The high-gain approximation yields the entire spectrum and a transcendental equation for the threshold gain of each longitudinal mode.

2. Low-Gain Approximation

It is more convenient to start with an alternative expression for index coupling or even-order gain coupling. Consider the solutions

$$F_1 = f_1 e^{D\ell} + f_2 e^{-D\ell} \quad (D.8)$$

$$B_1 = b_1 e^{D\ell} + b_2 e^{-D\ell} \quad (D.9)$$

to the coupled equations

$$\left.\begin{aligned} F_1' - i \delta_N F_1 &= i \chi_N B_1 \\ -B_1' - i \delta_N B_1 &= i \chi_N F_1 \end{aligned}\right\} \quad (D.10)$$

where $D_N = [\chi_N^2 - \delta_N^2]^{\frac{1}{2}}$

Since there are no outside sources for DFB lasers, we may use the boundary conditions

$$B(-\ell/2) = 0 = F(\ell/2) \tag{D.11}$$

This implies the relation

$$f_1/f_2 = b_2/b_1 = -e^{-D_N \ell} \tag{D.12}$$

When (D.12) is substituted into the coupled equations (D.10) along with expressions (D.8,9), the following equation can be derived.

$$\chi_N \sinh D_N \ell = \pm i D_N \tag{D.13}$$

Either of the exact equations (D.1) or (D.13) may be used for threshold calculations.

Consider the low-gain approximation where $g_N \ll \chi_N$ for index coupling and even-order gain coupling. Expand the hyperbolic function in (D.13) to obtain

$$\chi_N \left[D_N \ell + \frac{(D_N \ell)^3}{3!} \right] \simeq i D_N \tag{D.14}$$

where $$D_N^2 \simeq \chi_N^2 - \Delta_N^2 + 2i \Delta_N g_N \ .$$

From the real part of the above equation,

$$\Delta_N^2 - \chi_N^2 = 6/\ell^2 \tag{D.15}$$

For ℓ large, oscillation takes place just outside the bandgap edges given by

$$\Delta_N \simeq \pm \chi_N \tag{D.16}$$

From the imaginary part of (D. 14) the gain condition becomes

$$g_N \ell = 3/(\chi_N \ell)^2 \qquad \text{(D. 17)}$$

The low-gain approximation for odd-order gain coupling is most easily derived from equation (D. 1). First consider the necessary condition on the perturbation for no average gain (i. e. $g_N = 0$). An expansion of the hyperbolic function in (D. 1) produces

$$D_N \left[\frac{1}{D_N \ell} + \frac{D_N \ell}{3} \right] \simeq i \delta_N \qquad \text{(D. 18)}$$

Equating the real and imaginary parts produces the results

$$\Delta_N = 0 \qquad \text{(D. 19)}$$

$$\left| \chi_N \ell_c \right|^2 = 3 \qquad \text{(D. 20)}$$

Thus oscillation takes place at the bandgap center. The necessary length ℓ_c for a given perturbation, is the critical length

$$\ell_c = \sqrt{3} \, / \, |\chi_N| \qquad \text{(D. 21)}$$

For gain perturbations or lengths less than those given by (D. 20), no oscillation takes place.

To find the threshold condition on the average gain, equation (D. 13) can be expanded to yield

$$\chi_N \ell \left[D_N \ell + \frac{(D_N \ell)^3}{3!} \right] \simeq \pm i \, D_N \ell \qquad \text{(D. 22)}$$

Keep all terms in D_N^2 to get

$$- |\chi_N| + g_N^2 = \pm \frac{6}{|\chi_N| \ell} \tag{D.23}$$

and

$$\Delta_N = 0 \tag{D.24}$$

Hence oscillation takes place at the bandgap center with the approximate gain condition

$$g_N \simeq - |\chi_N| \tag{D.25}$$

when ℓ is large.

Note that the low-gain approximation gives explicit values for the spectrum and thresholds of the average gain and perturbation for the lowest order (m=0) longitudinal mode only.

All previous results match those of Kogelnik and Shank[23] at the first Bragg order. This appendix extends their results to all Bragg orders.

APPENDIX E

ECW EQUATIONS FOR TRANSVERSELY PERIODIC MEDIA

Consider the wave equation

$$\left[\frac{d^2}{dz^2} + \frac{d^2}{dx^2} + k^2\epsilon(x)\right] E(x, z) = 0 \qquad \text{(E. 1)}$$

where $\epsilon(x) = \epsilon\,(1+\eta\cos Kz)$ for transverse singly periodic media.

Assume a TE field of the form

$$E(x, z) = \sum_{n=-1}^{N^*/2} \Big\{ F(z)_{1-2n/N}\, e^{i[(1-2n/N)\beta_o x + \Delta\beta x + k_{z_o} z]} + B(z)_{1-2n/N}\, e^{i[-(1-2n/N)\beta_o x + \Delta\beta x + k_{z_o} z]} \Big\} + \binom{1}{0} S(z)\, e^{i(\Delta\beta x + k_{z_o} z)} \qquad \text{(E. 2)}$$

where

$$N^*/2 = \begin{cases} \dfrac{N-2}{2} & \text{for N even} \\ \dfrac{N-1}{2} & \text{for N odd} \\ -1 & \text{for N = 1} \end{cases}$$

$$\binom{1}{0} = \begin{cases} 1 & \text{for N even} \\ 0 & \text{for N odd} \end{cases}$$

This accounts for positive group velocity space harmonics involved in cross- and self-coupling of $F_1(z)$ and $B_1(z)$. A similar expression exists for negative group velocity space harmonics.

The following set of N+3 coupled equations exist when (E. 2) is substituted into (E. 1) for higher-order Bragg interactions.

$$
\left.
\begin{aligned}
&\{k^2\epsilon - k_{z_o}^2 - [(1+2/N)\beta_o + \Delta\beta]^2\} F_{1+2/N} + 2ik_{z_o} F'_{1+2/N} = -\frac{k^2\epsilon\eta}{2} F_1 \\
&\{k^2\epsilon - k_{z_o}^2 - (\beta_o + \Delta\beta)^2\} F_1 + 2ik_{z_o} F_1' = -\frac{k^2\epsilon\eta}{2}(F_{1+2/N} + F_{1-2/N}) \\
&\qquad\qquad \vdots \\
&\binom{1}{0}\{k^2\epsilon - k_{z_o}^2 - \Delta\beta^2\} S = -\binom{1}{0}\frac{k^2\epsilon\eta}{2}(F_{2/N} + B_{2/N}) \\
&\qquad\qquad \vdots \\
&\{k^2\epsilon - k_{z_o}^2 - (-\beta_o + \Delta\beta)^2\} B_1 + 2ik_{z_o} B_1' = -\frac{k^2\epsilon\eta}{2}(B_{1+2/N} + B_{1-2/N}) \\
&\{k^2\epsilon - k_{z_o}^2 - [-(1+2/N)\beta_o + \Delta\beta]\} B_{1+2/N} + 2ik_{z_o} B'_{1+2/N} = -\frac{k^2\epsilon\eta}{2} B_1
\end{aligned}
\right\} \quad \text{(E.3)}
$$

where $k_z = k_{z_o} + \Delta k_z$

$\beta = \beta_o + \Delta\beta = NK/2 + \Delta\beta$

$k = k_o + \Delta k$

$k_o^2 \epsilon = k_{z_o}^2 + \beta_o^2$

The primes denote differentiation with respect to the coordinate z and the arguments with respect to z have been dropped for simplicity. The above equations are solved using the ECW assumptions and approximations of chapter III.

First, solve for $F(z)_{1-2/N}$ and $B(z)_{1-2/N}$. The result is similar to (3.A16-17) with the change $\eta \to \eta/\sin^2\theta_o$ where $\sin\theta_o = \beta_o/k_o\epsilon^{\frac{1}{2}}$. Hence,

$$
F(z)_{1-2/N} = \frac{-\zeta_N \eta N F_1(z)}{8(1-1/N)\sin^2\theta_o} + \frac{(-1)^{N+1}\left(\frac{\eta}{2\sin^2\theta_o}\right)^{N-1} B_1(z)}{\prod^{*} \{4n(n-N)/N^2\}^2} \qquad \text{(E.4)}
$$

$$B(z)_{1-2/N} = \frac{-\zeta_N \eta N B_1(z)}{8(1-1/N)\sin^2\theta_o} + \frac{(-1)^{N+1}\left(\frac{\eta}{2\sin^2\theta_o}\right)^{N-1} F_1(z)}{\prod^* \{4n(n-N/N^2\}^2} \qquad \text{(E.5)}$$

where $\zeta_N = \begin{cases} 0 & N = 1 \\ 1 & N \geq 2 \end{cases}$

$$\prod^* f^2(n) = \begin{cases} \prod_{n=1}^{(N-1)/2} {}^* f^2(n) & \text{for N odd} \\ \prod_{n=1}^{N/2} f(n) & \text{for N even} \\ 1 & \text{for N = 1} \end{cases}$$

Second, trivially solve for $F(z)_{1+2/N}$ and $B(z)_{1+2/N}$. The result is again identical to the previous results of (3.A18-19) with the change $\eta \rightarrow \eta/\sin^2\theta_o$.

$$F(z)_{1+2/N} = \frac{\zeta_N \eta N F_1(z)}{8(1+1/N)\sin^2\theta_o} \qquad \text{(E.6)}$$

$$B(z)_{1+2/N} = \frac{\zeta_N \eta N B_1(z)}{8(1+1/N)\sin^2\theta_o} \qquad \text{(E.7)}$$

Substituting (E.4-7) into the equations for $F_1(z)$ and $B_1(z)$ in (E.3) produces the ECW coupled equations for TP media.

$$\left.\begin{aligned} F_1'(z) - i\,\delta_N F_1(z) &= i\,\chi_N B_1(z) \\ B_1'(z) + i\,\delta_N B_1(z) &= i\,\chi_N F_1(z) \end{aligned}\right\} \qquad \text{(E.8)}$$

where

$$\delta_N = \frac{k^2\epsilon\left\{1-\zeta_N\left(\frac{\eta}{2\sin\theta_o}\right)^2\left[\frac{N^2}{2(N^2-1)}\right]\right\}-(\beta_o+\Delta\beta_N)^2-k_{z_o}^2}{2k_{z_o}} \qquad \text{(E.9)}$$

$$\chi_N = \frac{(-1)^{N+1}\,k^2\epsilon\,\eta^N}{2^{N+1}k_{z_o}(\sin^2\theta_o)^{N-1}} \quad \frac{1}{\prod^*\{4n(n-N)/N^2\}^2} \qquad \text{(E.10)}$$

The expressions can be further simplified by noting the equality $k_o^2\,\epsilon = \beta_o^2 + k_{z_o}^2$ and the relations $k\,\epsilon^{\frac{1}{2}}/k_{z_o} \simeq k_o\epsilon^{\frac{1}{2}}/k_{z_o} = 1/\cos\theta_o$ and $k_o\epsilon^{\frac{1}{2}}/\beta_o = 1/\sin\theta_o$. The deviation from $k_o\epsilon^{\frac{1}{2}}$ and β_o represent the changes in frequency and angle from the exact Bragg condition.

REFERENCES

1. E. Mathieu, "Memoire sur le Mouvement Vibratoire d'une Membrane de Forme Elliptique," Jour. de Math. Pures et Appliqués, (Jour. de Liouville) 13, 137 (1868).

2. M. Floquet, "Sur Les Équations Différentielles Linéaires a Coefficients Périodiques," Ann. de l'École Normale Superieure 12, 47 (1883).

3. G. Hill, "On the Part of the Motion of the Lunar Paragee which is a Function of the Mean Motions of the Sun and Moon," Acta Mathematica VIII, 1 (1886).

4. Lord Rayleigh, "On the Maintenance of Vibrations by Forces of Double Frequency, and on Propagation of Waves through a Medium Endowed with Periodic Structures," Phil. Mag. 24, 145 (1887).

5. N. McLachlan, Theory and Application of Mathieu Functions, Dover Publications, New York (1964).

6. Brillouin, Wave Propagation in Periodic Structures, Dover Publications, New York (1953).

7. J. Pierce, private communication and Cutler, "Mechanical Traveling-Wave Oscillator," Bell Laboratories Record (April 1954).

8. D. Tseng, "Guiding and Scattering of Electromagnetic Fields by Corrugated Structures," Ph.D. thesis, Polytechnic Institute of Brooklyn (July 1967).

9. J. Pierce, "Coupling of Modes of Propagation," J. Appl. Phys. 25, 179 (1954).

10. J. Pierce, Almost all About Waves, MIT Press, Cambridge, Mass. (1974).

11. C. Elachi, "Electromagnetic Wave Propagation and Source Radiation in Space-Time Periodic Media," Caltech Ant. Lab. Tech. Report No. 61, California Institute of Technology, Pasadena, Ca. (Nov. 1971).

12. D. Marcuse, Theory of Dielectric Optical Waveguides, Academic Press, New York (1974).

13. A. Yariv, Introduction to Optical Electronics, Holt, Rinehart and Winston, New York (1971).

References (Cont'd)

14. A. Yariv, Quantum Electronics, 2nd ed., John Wiley and Sons, New York (1975).

15. H. Kogelnik, "Coupled Wave Theory for Thick Hologram Gratings," Bell Syst. Tech. J. 48, 2909 (1969).

16. S. Miller, "Coupled Wave Theory and Waveguide Applications," Bell Syst. Tech. J. 33, 661 (1954).

17. J. Pierce, Traveling Wave Tubes, Van Nostrand, Princeton (1950).

18. W. Louisell, Coupled Mode and Parametric Electronics, John Wiley and Sons, New York (1960).

19. D. Marcuse, Light Transmission Optics, Van Nostrand, New York (1972).

20. A. Yariv, "Coupled-Mode Theory for Guided-Wave Optics," IEEE J. QE-9, 919 (1973).

21. B. Batterman and H. Cole, "Dynamical Diffraction of X-Rays by Perfect Crystals, Rev. Mod. Phys. 36, 681 (1964).

22. R. Chu and T. Tamir, "Guided-Wave Theory of Light Diffraction by Acoustic Microwaves," IEEE Trans. MTT-17, 1002 (1969).

23. H. Kogelnik and C. Shank, "Coupled-Wave Theory of Distributed Feedback Lasers," J. Appl. Phys. 43, 2327 (1972).

24. C. Elachi and G. Evans, "Transversely Bounded DFB Lasers," J. Opt. Soc. Am. 65, 404 (1975).

25. S. Wang, "Principles of Distributed Feedback and Distributed Bragg-Reflector Lasers," IEEE J. QE-10, 413 (1974).

26. E. Denman, Coupled Modes in Plasmas, Elastic Media, and Parametric Amplifiers, American Elsevier, New York (1970).

27. C. Kittle, Introduction to Solid State Physics, 4th ed., John Wiley and Sons, New York (1971).

28. E. Bahar, "Radio Wave Propagation over a Rough Variable Impedance Boundary: Part I--Full-Wave Analysis, Part II--Application of Full-Wave Analysis," IEEE Tran. AP-20, 354 (1972).

References (Cont'd)

29. C. Elachi, D. Jaggard, and C. Yeh, "Transients in a Periodic Slab: Coupled Waves Approach," IEEE Trans AP-23, 352 (1975).

30. G. Evans, "Electromagnetic Theory of Distributed Feedback Lasers and Periodic Dielectric Waveguides," Caltech Ant. Lab. Tech. Report No. 71, California Institute of Technology, Pasadena, Ca. (Sept. 1974).

31. C. Elachi and C. Yeh, "Mode Conversion in Periodically Distributed Thin Film Waveguides," J. Appl. Phys. 45, 3494 (1974).

32. C. Elachi and C. Yeh, "Periodic Structures in Integrated Optics," J. Appl. Phys. 44, 3146 (1973).

33. R. Millar, "On the Rayleigh Assumption in Scattering by a Periodic Surface," Proc. Camb. Phil. Soc. 65, 773 (1969) and "On the Rayleigh Assumption in Scattering by a Periodic Surface II," Proc. Camb. Phil. Soc. 69, 217 (1971).

34. D. Flanders, H. Kogelnik, R. Schmidt and C. Shank, "Grating Filters for Thin-Film Optical Waveguides," Appl. Phys. Lett. 24, 194 (1974).

35. A. Yariv and H. Yen, "Bragg Amplification and Oscillation in Periodic Optical Media," Opt. Comm. 10, 120 (1974).

36. S. Chinn and P. Kelley, "Analysis of the Transmission Reflection and Noise Properties of Distributed Feedback Laser Amplifiers," Opt. Comm. 10, 123 (1974).

37. H. Jones, Theory of Brillouin Zones and Electronic States in Crystals, North-Holland, Amsterdam (1960).

38. R. Collin, Field Theory of Guided Waves, McGraw-Hill, New York (1960).

39. N. Kapeney and J. Burke, Optical Waveguides, Academic Press, New York (1973).

40. F. Borgnis and C. Papas, "Electromagnetic Waveguides and Resonators," Appearing in Hanbuch der Physik, Vol. 16: Elektrische Felder und Wellen, edited by S. Flügge, Springer-Verlag, Berlin (1958).

41. J. Bjorkholm and C. Shank, "Higher-Order Distributed Feedback Oscillators," Appl. Phys. Lett. 20, 306 (1972).

References (Cont'd)

42. D. Jaggard and G. Evans, "Coupled Waves and Floquet Approach to Periodic Structures," Caltech Ant. Lab. Tech. Report No. 73, California Institute of Technology, Pasadena, California (Aug. 1975).

43. E. Cassedy and A. Oliver, "Dispersion Relations in Time-Space Periodic Media: Part I - Stable Interactions," Proc. IEEE, 51, 1342 (1963).

44. F. Bloch, "Über die Quantenmechanik der Elektronen in Kristallgittern," Z. Physik 52, 555 (1928).

45. F. Odeh and J. Keller, "Partial Differential Equations with Periodic Coefficients and Bloch Waves in Crystals," J. Math. Phys. 5, 1499 (1964).

46. E. Ince, Ordinary Differential Equations, Dover Publications, New York (1944).

47. E. Whittaker and G. Watson, A Course in Modern Analysis, 4th ed., Cambridge University Press, London (1935).

48. A. Hessel, "General Characteristics of Traveling-Wave Antennas," appearing in Antenna Theory, Part II, edited by R. Collin and F. Zucker, McGraw-Hill, New York (1969).

49. T. Tamir and H. Wang, "Characteristic Relations for Non-periodic Solutions of Mathieu's Equation," J. of Res. of N.B.S., sec. B 69B, 101 (1965).

50. G. Blanck, "Mathieu Functions" appearing in Handbook of Mathematical Functions, edited by M. Abramowitz and I. Stegun, Dover Publications, New York (1965).

51. A. Yariv and A. Gover, "The Equivalence of Coupled Mode and Floquet-Bloch Formalism in Periodic Optical Waveguides," Appl. Phys. Lett. 26, 537 (1975).

52. G. Evans and D. Jaggard, unpublished report.

53. D. Jaggard and C. Elachi, "Higher Order Interactions in Periodic Media: Floquet and Coupled Waves Approach," presented at 1975 USNC/URSI-IEEE meeting, Boulder, Colorado (Oct. 20-23, 1975), also "Floquet and Coupled Waves Analysis of Higher Order Bragg Coupling in a Periodic Medium," J. Opt. Soc. Am. 66, 674 (1976).

References (Cont'd)

54. H. Kogelnik and C. Shank, "Stimulated Emission in a Periodic Structure," Appl. Phys. Lett. 18, 152 (1971).

55. C. Elachi, G. Evans and F. Grunthauer, "Proposed Distributed Feedback Crystal Cavities for X-Ray Lasers," Appl. Optics 14, 14 (1975).

56. E. Cassedy, "Dispersion Relations in Time-Space Periodic Media: Part II - Stable Interactions," Proceedings IEEE 55, 1154 (1967).

57. C. Yeh, K. Casey and Z. Kaprielian, "Transverse Magnetic Wave Propagation in Sinusoidally Stratified Dielectric Media," IEEE Trans. MTT-13, 297 (1965).

58. S. Wang, "Thin-Film Bragg Lasers for Integrated Optics," Wave Electronics 1, 31 (1974/75).

59. E. Cassedy, "Waves Guided by a Boundary with Time-Space Periodic Modulation," Proc. IEE 112, 269 (1965).

60. R. Hurd, "The Propagation of an Electromagnetic Wave along an Infinite Corrugated Surface," Can. J. Phys. 32, 727 (1954).

61. K. Casey, J. Matthes and C. Yeh, "Wave Propagation in Sinusoidally Stratified Plasma Media," J. Math. Phys. 10, 891 (1969).

62. K. Casey and C. Yeh, "Transition Radiation in a Periodically Stratified Plasma," Phys. Rev. A 2, 810 (1970).

63. S. Peng, H. Bertoni and T. Tamir, "Analysis of Periodic Thin-Film Structures with Rectangular Profiles," Opt. Comm. 10, 91 (1974).

64. S. Peng, T. Tamir and H. Bertoni, "Theory of Periodic Dielectric Waveguides," IEEE Trans. MTT-23, 123 (1975).

65. B. Tong, "Electronic Structure of One-Dimensional Binary Alloys," Phys. Rev. 175, 710 (1961).

66. P. Sah and K. Srivastava, "A Generalized Diatonic Kronig-Penney Model," Physica 43, 528 (1969).

67. C. Papas, Theory of Electromagnetic Wave Propagation, McGraw-Hill, New York (1965).

References (Cont'd)

68. S. Case, "Coupled-Wave Theory for Multiply Exposed Thick Holographic Gratings," J. Opt. Soc. Am. 65, 724 (1975).

69. S. Su and T. Gaylord, "Calculation of Arbitrary-Order Diffraction Efficiencies of Thick Gratings with Arbitrary Grating Shape," J. Opt. Soc. Am. 65, 59 (1965).

70. H. Stoll and D. Seib, "Multiply-Resonant Distributed Feedback Lasers," Proc. Integrated Optics Conference, Salt Lake City, Utah (Jan. 12-14, 1976), also in IEEE J. QE-12, 53 (1976).

71. Zh. Alferov, S. Gurevich, V. Kuchinsky, M. Mizerov, E. Portnoy and M. Reich, "Investigations of Ga As/Ga AlAs Waveguide Lasers with Second Order Distributed Feedback," Proc. Integrated Optics Conference, Salt Lake City, Utah (Jan. 12-14, 1976).

72. P. Sturrock "Kinematics of Growing Waves," Phys. Rev. 112, 1488 (1958).

73. R. Briggs, Electron-Stream Interaction with Plasmas, MIT Press, Cambridge, Mass. (1964).

74. A. Scott, Active and Nonlinear Wave Propagation in Electronics, Wiley-Interscience, New York (1970).

75. S. Peng and E. Cassedy, "Scattering of Light Waves at Boundaries to Parametrically Modulated Media," appearing in Modern Optics, Polytechnic Press, New York (1967).

76. B. Minakovic and J. Gokgor, "Attenuation and Phase-Shift Coefficients in Dielectric-Loaded Periodic Waveguides," IEEE Trans. MTT-21, 568 (1973).

77. A. Neyfeh, Perturbation Methods, John Wiley and Sons, New York (1973).

78. M. Born and E. Wolf, Principles of Optics, 4th ed., Pergamon Press, Oxford (1970).

79. R. Feynman and A. Hibbs, Quantum Mechanics and Path Integrals, McGraw-Hill, New York (1965).

80. J. Cooley, P. Lewis and P. Welch, The Fast Fourier Transform Algorithm, Yorktown Heights, N. Y., IBM Watson Research Center (1969).

References (Cont'd)

81. R. Alferness, "Equivalence of the Thin-Grating Decomposition and Coupled Wave Analysis of Thick Holographic Gratings," Opt. Comm. 15, 209 (1975).

82. R. Alferness, "Analysis of Optical Propagation in Thick Holographic Gratings," Appl. Phys. 7, 29 (1975).

83. R. Alferness and S. Case, "Coupling in Doubly Exposed, Thick Holographic Gratings," J. Opt. Soc. Am. 65, 730 (1975).

84. R. Alferness, "Analysis of Propagation at the Second-Order Bragg Angle of a Thick Holographic Grating," J. Opt. Soc. Am. 66, 353 (1976).

85. R. Chu and T. Tamir. "Bragg Diffraction of Gaussian Beams by Periodically Modulated Media," J. Opt. Soc. Am. 66, 220 (1976).

86. G. Allen, "Band Structures of One-Dimensional Crystals with Square Wells," Phys. Rev. 91, 531 (1953).

87. C. Elachi, "Waves in Active and Passive Periodic Structures," to appear in Proc. IEEE.

88. R. Bellman and G. Wing, An Introduction to Invariant Imbedding, Wiley-Interscience, New York, (1975).

89. G. Bedrosian, "The Invariant Imbedding Solution for Electromagnetic Wave Propagation in Periodic, Almost Homogeneous and Almost Periodic Media," Ph.D. thesis, California Institute of Technology, Pasadena, California (1977).

90. G. Bedrosian, private communication.

91. L. Brekhovskikh, Waves in Lanyard Media, Academic Press, New York (1960).

92. T. Tamir and H. Bertoni, "Lateral Displacement of Optical Beams at Multilayered and Periodic Structures," J. Opt. Soc. Am. 61, 1397 (1971).

93. T. Ooya, M. Tateiba, and O. Fukumitsu, "Transmission and Reflection of a Gaussian Beam at Normal Incidence on a Dielectric Slab," J. Opt. Soc. Am. 65, 537 (1975).

94. J. Ra, H. Bertoni and L. Felsen, "Reflection and Transmission of Beams at a Dielectric Interface," SIAM J. Appl. Math. 24, 396 (1973).

References (Cont'd)

95. S. Seshadri, "Higher Order Wave Interactions in a Periodic Media," Appl. Phys. 10, 165 (1976).

96. D. Jaggard and C. Elachi, "Higher-Order Bragg Coupling in Periodic Media with Gain or Loss," submitted for publication.

97. D. Jaggard, "Stability of Higher-Order Bragg Interactions in Active Periodic Media," submitted for publication.

98. I. Gradshteyn and I. Ryzhik, Table of Integrals, Series and Products, Academic Press, New York (1965).